SELECTED SCIENTIFIC RESULTS OBTAINED IN 2017–2023 AT THE JOINT INSTITUTE FOR NUCLEAR RESEARCH

Dubna 2024

CONTENTS

PREFACE 3
NICA ACCELERATOR COMPLEX 4
SUPERHEAVY ELEMENT FACTORY 8
U-400M CYCLOTRON COMPLEX 11
RECONSTRUCTION OF THE U-400(R) CYCLOTRON COMPLEX 12
THEORETICAL PHYSICS 14
HIGH-ENERGY HEAVY-ION PHYSICS 21
PARTICLE PHYSICS 24
LOW-ENERGY HEAVY-ION PHYSICS 28
NEUTRINO PHYSICS AND ASTROPHYSICS 29
NEUTRON NUCLEAR PHYSICS 34
CONDENSED MATTER PHYSICS 37
DEVELOPMENT OF THE IBR-2 SPECTROMETER COMPLEX 40
RADIATION AND RADIOBIOLOGICAL RESEARCH 42
APPLIED RESEARCH AND LIFE SCIENCE 48
NETWORKS, INFORMATION TECHNOLOGY AND COMPUTER PHYSICS 51
JINR EDUCATIONAL PROGRAMME 59
REFERENCES 66

PREFACE

At the 134th session of the JINR Scientific Council (21–23 September 2023), the results of implementation the Seven-Year Plan for the Development of JINR for 2017–2023 were summarized. The adopted resolution emphasized that during this period JINR achieved impressive results both in development of a vast research infrastructure and in scientific research on its basis. Despite the working conditions complicated by COVID-19 and the sharp deterioration of geopolitical situation, there is much to be proud of. The incontestable achievements opening a new stage in the organization of scientific research in Dubna are: the creation of the Superheavy Element Factory, the commissioning of the Govorun supercomputer, the increase in the Baikal-GVD neutrino telescope effective performance to a record high, entering the final stage of the NICA megaproject and using it as a basis for extensive international experimental collaborations BM@N, MPD, SPD and ARIADNA based on JINR's large research infrastructure.

We offer you the key achievements of JINR in 2017–2023. Along with the development of its own infrastructure and information, network and computing technologies, JINR took an active part in international collaborations at CERN and a number of other centres around the world, building up its intellectual potential, which made it possible to obtain significant scientific results in a wide range of areas.

The Institute has substantially expanded its international partner network. In 2021, the community of legitimate JINR Member States welcomed a new country — the Arab Republic of Egypt. Ties with China, Mexico, India, and Brazil are flourishing. Important steps have been taken to develop and strengthen international cooperation with Armenia, Cuba, Egypt, Kazakhstan, Serbia, South Africa, and Vietnam.

A landmark event was the signing of the Sofia Declaration, a document that contains an appeal to the states and organizations concerned to join the multilateral scientific cooperation implemented under the auspices of JINR.

The Institute was deeply involved in the International Year of Basic Sciences declared by the UN, and actively participated in the Decade of Science and Technology in the JINR host country.

Regulations on the JINR flag, as well as on the associate membership in the Institute, were adopted; work was completed on the new outline of the Topical Plan for JINR Research and International Cooperation, which gives a clear idea of the structure of the Institute's scientific projects.

Our educational programmes are being enhanced, new formats of cooperation and attracting young people are being introduced, and the social infrastructure is being vigorously updated.

Overall, these achievements have built a solid foundation for the further growth of the Institute in the coming seven years. Our scientists, engineers and specialists managed to achieve brilliant results by doing their best to reach our goals, which has helped the Institute to secure its role as one of the leaders in the world scientific community. All the Institute's activities are drenched with the principle "Science Brings Nations Together". All this enables us to look confidently into the future.

The November (2023) session of the JINR Committee of Plenipotentiaries held in Kazakhstan approved the new ambitious Seven-Year Plan for the Development of JINR for 2024–2030. It covers a wide range of projects and scientific areas. The main goal of the new Seven-Year Plan is implementing a bright and appealing scientific research programme, as well as accumulation of intellectual capital, provided with infrastructural and financial resources. The new stage involves conducting intensive scientific research on the base already created. We open this page full of anticipation of new accomplishments and the excitement of pioneers at the forefront of science.

G.TRUBNIKOV
Director
Joint Institute for Nuclear Research

NICA ACCELERATOR COMPLEX

During the implementation of the **NICA** megascience project at JINR, the acceleration mode of polarized protons was implemented for the first time in the JINR Nuclotron accelerator in 2017, which is a fundamental step in the realization of the spin physics programme at the NICA complex. The main scientific task of this programme is to study the spin quark–parton structure of the proton. This was preceded by the construction (together with INR RAS) of a high-intensity source of polarized protons and deuterons, the commissioning of a new high-frequency section of the pre-accelerator, developed in cooperation between JINR, MEPhI and ITEP NRC KI, and manufactured at the enterprise in Snezhinsk. The complex problem of maintaining the polarization of proton beams in a hard-focusing superconducting synchrotron was solved, and the possibility of using the Nuclotron at an extremely low proton injection energy of 5 MeV was considered. The measurements showed that the source parameters will ensure the production of beams of polarized protons and deuterons with an intensity of 10^{11} particles per cycle and a degree of polarization of more than 90%.

Intense work was carried out on the installation, step-by-step verification and commissioning of a superconducting ring accelerator (with a perimeter of 210 m) — a booster for the NICA research complex.

NICA collider

NICA Complex Development in 2017–2023

2017

The construction site of the NICA complex

2018

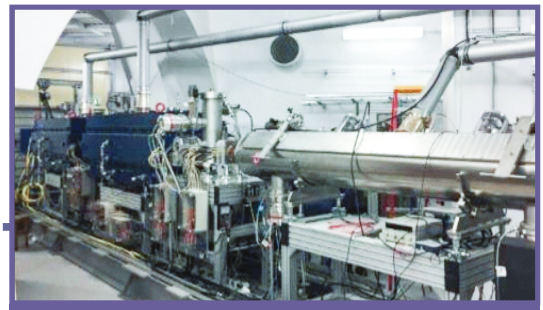

HILac commissioning

2019

Booster commissioning with beam

2020

NICA collider tunnel

2021

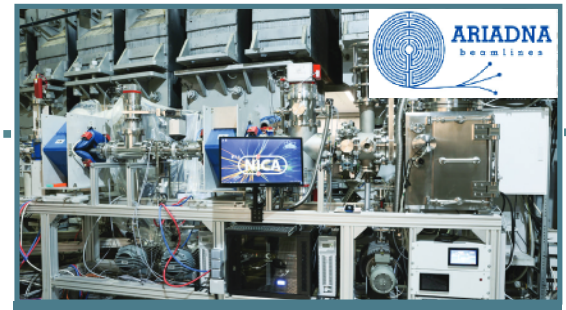

ARIADNA — applied researches

4th Technical Run
(2022–2023):
HILac + Booster + Nuclotron

2022

Commissioning of the
NICA injector complex

2023

40 MW — now available

Successful 5th commissioning run
at NICA in 2023 (4 months)

- **490 scientific papers**
- **240 reports at conferences**
- **students practice**

All elements of the magnetic cryostat system of the booster (the basis of the accelerator) were manufactured at JINR using original technology that has received recognition in Europe. The technological start-up of the superconducting booster synchrotron was carried out by the Prime Minister of the Russian Federation on 20 November 2020, after the completion of commissioning of all objects of the injection complex of the project, including sources of polarized, light and heavy ions and a linear accelerator of heavy ions — the basis for obtaining the required beams and their input into the booster. Superconducting structural magnets of the booster were also manufactured, and the built-in systems of the booster ring, namely, a high-frequency accelerating system, an electronic cooling system for the circulating beam, and beam injection and extraction devices, were mounted and tested. The booster cycle-setting equipment, diagnostic and thermometry equipment, power supply systems, transition detection and protection of the magnetic cryostat system were manufactured.

In strict accordance with the schedule, on 19 December 2020, singly charged helium ions were injected into the booster and stable beam circulation was obtained. A beam of singly charged He ions with an energy of 3.2 MeV/amu circulated in the accelerator channel with an intensity of about 10^9 ions/revolution. The high quality of manufacturing and assembly of all elements of the magnetic system of the booster synchrotron made it possible to begin work without the use of a leading magnetic field correction system.

The achieved bright result summed up the many years of well-coordinated work of a team of accelerator physicists and engineers at JINR in collaboration with partners from INP SB RAS, INR RAS, ITEP, IHEP NRC KI, and many other Russian and foreign organizations.

In September 2021, the booster synchrotron systems were brought to their design parameters. During the run, a beam of iron ions was accelerated in the booster ring for the first time to a design energy of 578 MeV/nucleon. The run also included a full launch of the booster electron cooling system equipment and, for the first time in Russia, electronic cooling of a heavy-ion beam was achieved. The beam cooling experiment was carried out with $^{56}Fe^{14+}$ ions at an injection energy of 3.2 MeV/nucleon.

An important result of the run was the successful completion of joint work by specialists from JINR and the Institute of Nuclear Physics of SB RAS to create systems for beam extraction from the booster and a beam transport channel to the Nuclotron. A unique impact magnet was successfully launched to extract the beam from the booster with a record magnetic field level of 2 kG, and the extraction of beams of two types of ions — helium and iron — was obtained at an energy of 240 MeV/nucleon with further transportation through the channel, at the final section of which the ion beams were detected by current and beam position sensors.

By autumn 2022, the most important stage of the NICA project was completed — a heavy-ion chain was created and the collider injection complex was put into operation, which includes unique facilities that have no analogues in the world: a cryogenic source and linear accelerator of heavy ions, cryogenic synchrotrons booster and Nuclotron, as well

Cycle of the Nuclotron magnetic field and the intensity of the beam of xenon nuclei, measured by a parametric current transformer, during setup tuning for the BM@N experiment. The intensity of the accelerated beam is approximately 10^7 particles

as a system of beam transportation channels. It was possible to obtain the required parameters and ensure stable operation of the complex for 4 months. At the same time, commissioning of the electron cooling of ion beams made it possible to double the number of particles accelerated in the Nuclotron. The run showed the high performance of the injection complex and confirmed the correctness of the design decisions taken for its construction. A record intensity was obtained for extracted beams of accelerated xenon ions. In addition to injecting ion beams up to gold and bismuth into the collider, the injection complex provides solutions to many physical and applied problems.

In the 2022–2023 run, the BM@N international collaboration conducted research using extracted beams, recording more than half a billion collisions of xenon ions with a nuclear target. The accumulated data is being analysed.

Participants in the ARIADNA collaboration have carried out a number of experiments within the framework of the applied research programme implemented at JINR, for which the necessary infrastructure is being created.

To modernize the Nuclotron superconducting synchrotron, a setup for the production of a hollow cable from a high-temperature superconductor was developed, manufactured and put into operation. A model fast-cycling quadrupole magnet was manufactured from this cable and successfully tested at 25 K [1–6].

Installation of the HTS magnets winding

SUPERHEAVY ELEMENT FACTORY

The priority task in 2017–2023 was the construction and commissioning of the Superheavy Element Factory based on the DC-280 cyclotron and the construction of a complex of cutting-edge experimental setups for synthesizing superheavy elements and studying their properties. In 2018, the construction of the experimental building of the SHE Factory was completed. The required approval documents were received. The experimental complex was put into operation.

The SHE Factory was created on the basis of the new DC-280 heavy-ion accelerator, the world leader among accelerators of this type. The accelerator was designed at JINR. Its components were manufactured in JINR Member States. The designed intensity of calcium-48 ion beams delivered by the DC-280 accelerator is 10 pμA, which is 10 times higher than the intensities provided by its predecessors.

Two gas-filled separators, DGFRS-2 and GRAND, were constructed and put into operation. The main tasks that will be performed at DGFRS-2 are related to the synthesis of new superheavy elements 119 and 120, the synthesis of new SHE isotopes, and study of their radioactive decay properties. Research at the GRAND separator will focus on studies of the structure of superheavy nuclei (nuclear spectroscopy) and the chemical properties of SHE.

In 2017–2023, the construction of two promising setups of the SHE Factory has begun: the multiple-reflection time-of-flight mass spectrometer for the precision measurement of the masses of heaviest nuclei and the novel GASSOL separator based on a superconducting gas-filled solenoid for studies of the chemical properties of SHE with lifetimes of up to tens of milliseconds.

The synthesis of new elements with atomic numbers 119 and 120 is one of the key objectives to be fulfilled at the SHE Factory. One of the promising reactions for synthesizing element 120 is $^{54}Cr + ^{248}Cm$.

With a view to preparing for experiments aimed at synthesizing new SHE, the fusion reaction $^{48}Ca + ^{232}Th$ leading to the isotopes of element 110

Experimental building of the SHE Factory

was studied. The major goal of the experiment was to verify the record low fission stability predicted by theory for the region under consideration, which should thus result in the low survival probability of the excited compound nucleus. Experiments carried out at an extremely low cross section, 70 fb, were shown to be feasible, which is of fundamental significance for launching experiments aimed at the synthesis of new elements.

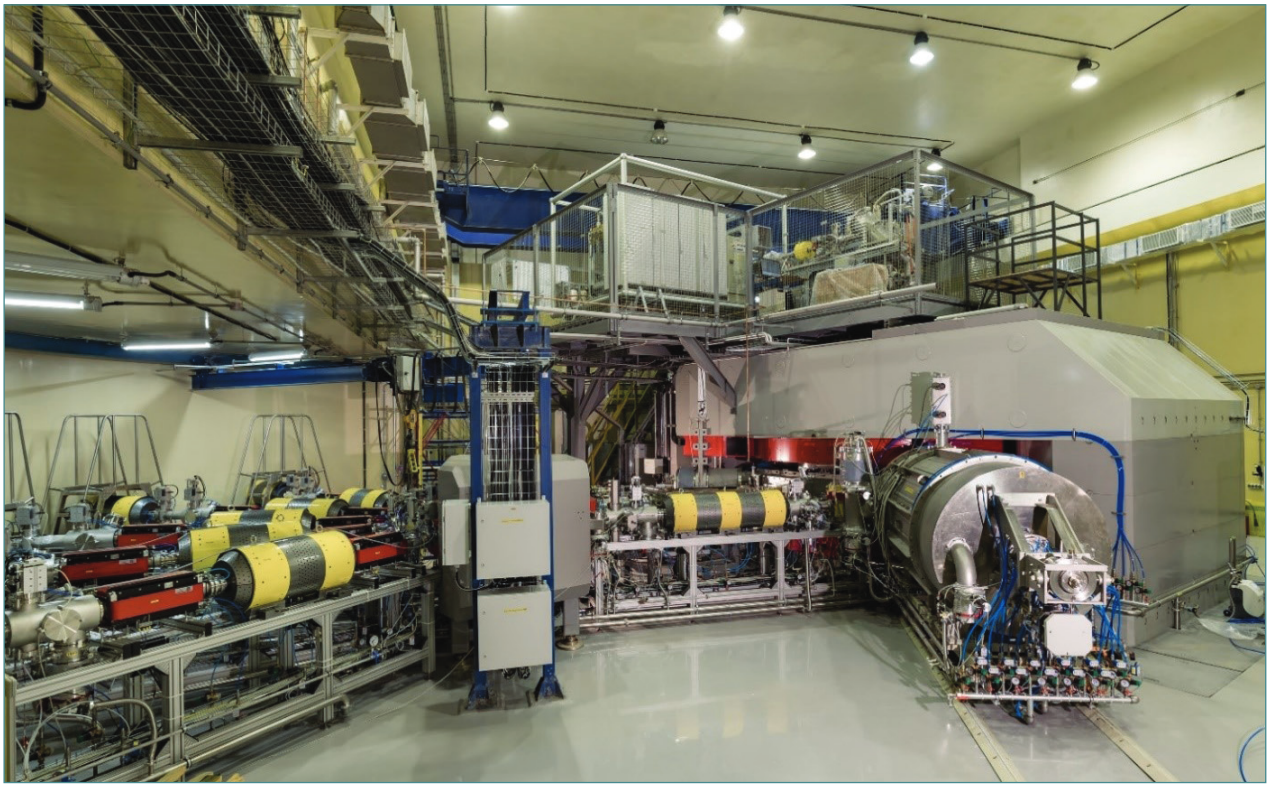

DC-280 cyclotron, SHE Factory

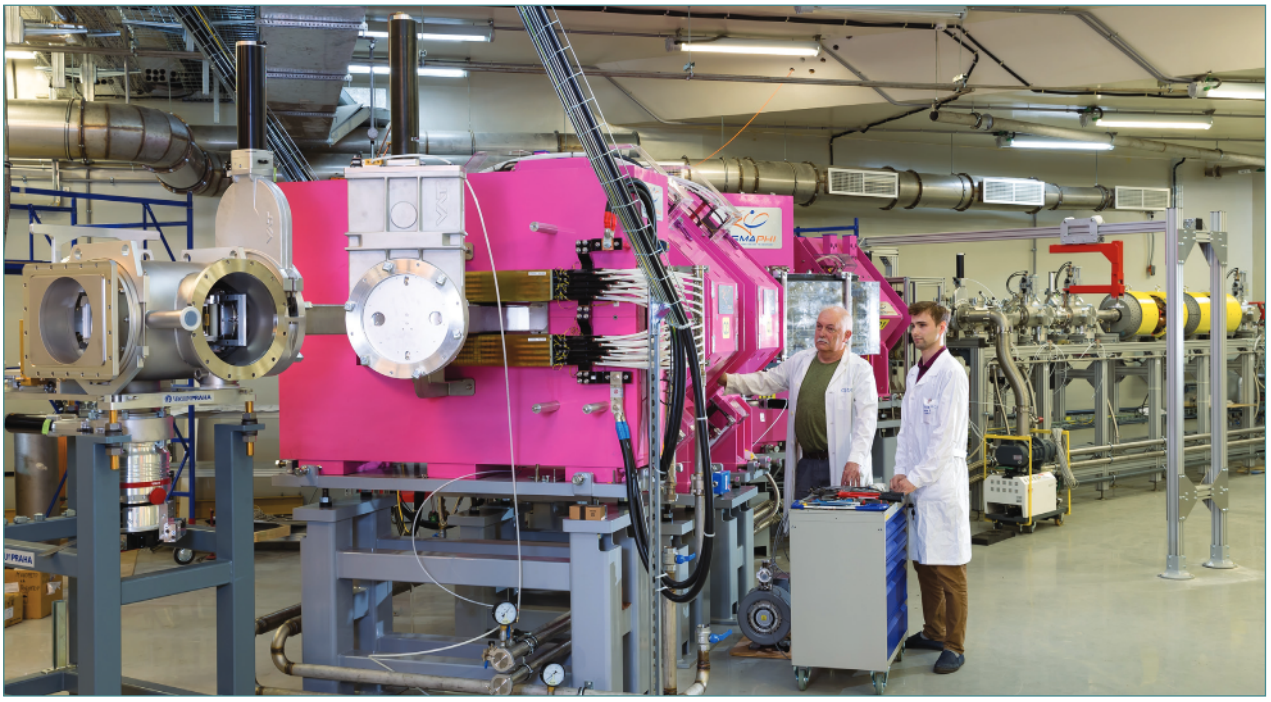

Gas-filled separator GRAND, SHE Factory

Commissioned FLNR Setups

2017

RIBs at the U400M cyclotron (Under modernization. Scheduled to be back in operation in 2024)

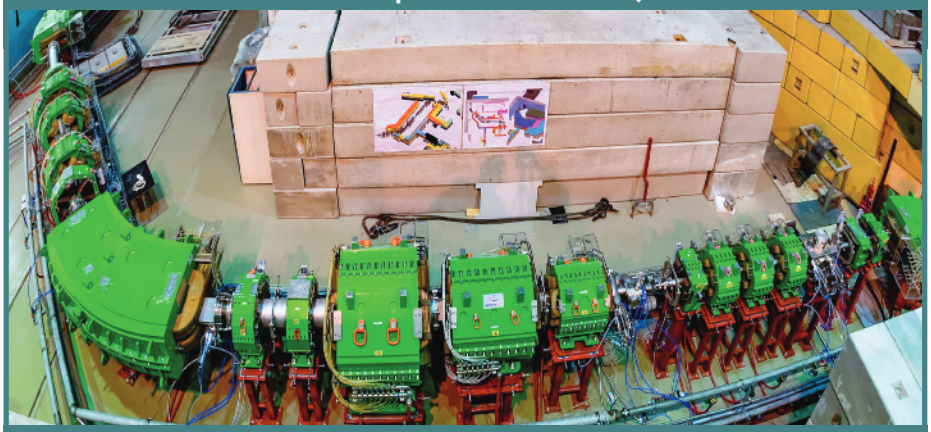

Main areas of research:
study of the structure of exotic nuclei near and beyond the neutron drip-line in the direct reactions

2020

Gas-filled recoil separator DGFRS-2

Main areas of research:
· detailed study of already known superheavy elements;
· synthesis of elements 119 and 120

2022

Gas-filled recoil separator GRAND (DGFRS-3)

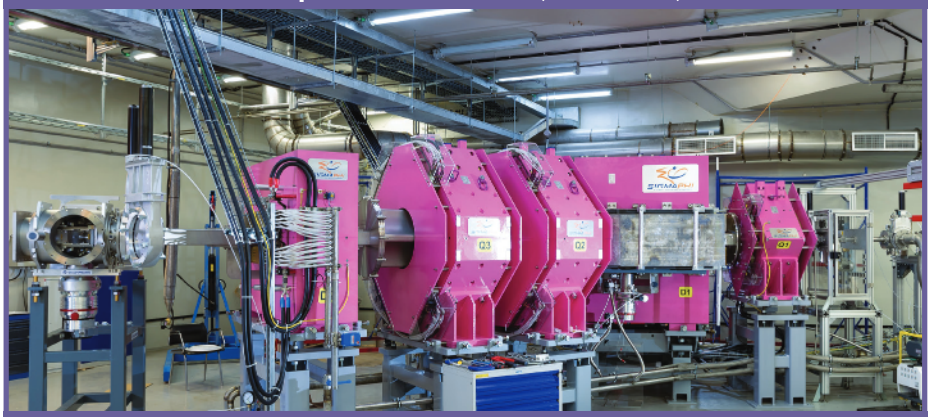

Main areas of research:
· experiments on nuclear and mass spectroscopy of SHE;
· studying their chemical properties

U-400M CYCLOTRON COMPLEX

The new fragment separator ACCULINNA-2 designed for producing beams of radioactive nuclei was commissioned at the U-400M accelerator in 2017. The separator was manufactured in cooperation with the SigmaPhi company and installed at the primary beam line of the U-400M accelerator. The ACCULINNA-2 separator is equipped with a radio-frequency filter for additional purification of secondary beams, a magnetic spectrometer for reaction product separation, a cryogenic target complex of hydrogen and helium isotopes, an array of neutron detectors based on stilbene crystals, and systems for the registration of charged particles. Test experiments confirmed the main projected ion-optical parameters of the setup for certain radioactive beams (^{14}B, ^{12}Be, ^{9,11}Li, ^{6,8}He, etc.). The yields of these isotopes were, on average, higher by a factor of 25 than those produced at ACCULINNA-1, which has been operating at FLNR since 1996.

First experiments at the novel ACCULINNA-2 fragment separator in 2018–2020 were of decisive importance in that they resulted in the detection of the superheavy ^{6}H and ^{7}H isotopes, thereby resolving one of the key issues that has long been posing challenges to nuclear physics experimentalists. The experiments also allowed advances in exploring a new mode of spontaneous decay accompanied by a simultaneous emission of four neutrons.

The upgrade of the U-400M cyclotron began in July 2020. This effort is aimed at enhancing the reliability and stability of the accelerator (by replacing the main magnet coils and the components of the accelerator vacuum system, control system, and radiation control system), as well as at increasing the intensity of heavy-ion beams. The accelerator commissioning is scheduled for spring 2024.

In combination with the capabilities of the upgraded U-400M accelerator complex of FLNR JINR, the fragment separator ACCULINNA-2 is the basic facility for studying light exotic nuclei near the borders of nucleon stability and will enable for the first time the search for an investigation of exotic nuclear systems, such as $^{5-7}$H, $^{8-10}$He, $^{24-26}$O, etc., as well as new types of radioactive decay.

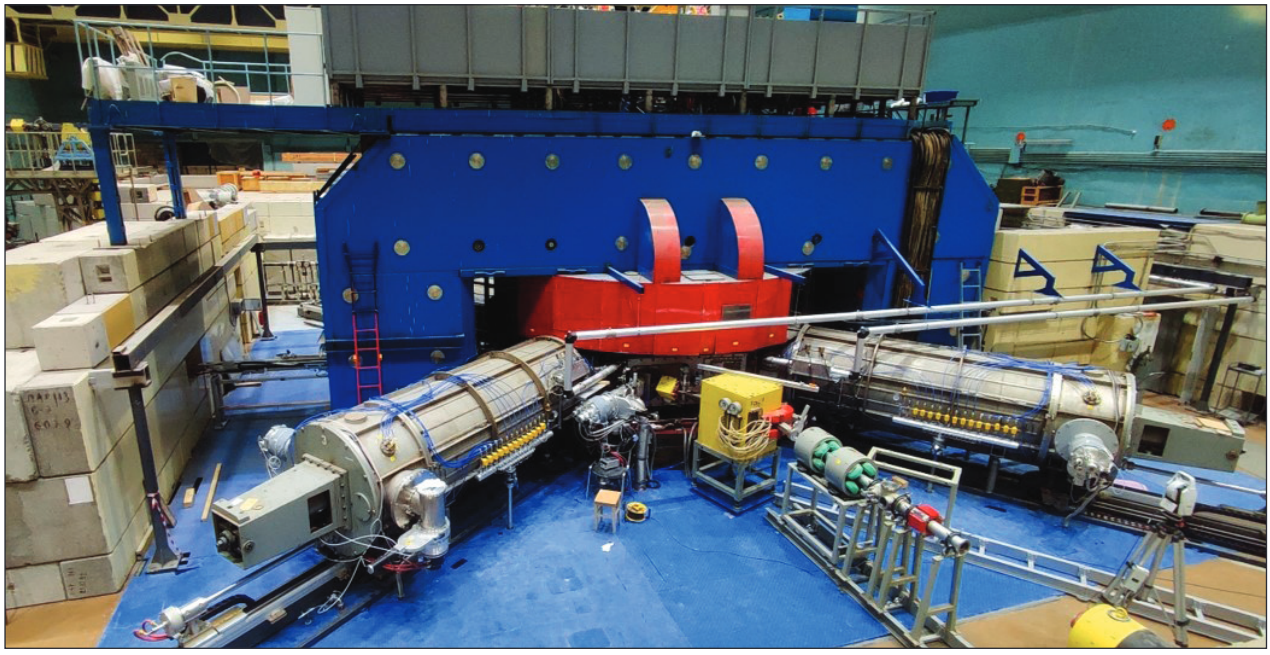

U-400M accelerator

RECONSTRUCTION OF THE U-400(R) CYCLOTRON COMPLEX

The main goal of the reconstruction of the U-400 complex, converting it to U-400R, is to expand the range of accelerated ions from helium to uranium, decrease the energy spread of accelerated ions, enable smooth ion energy variation within a range of 0.8–25 MeV/nucleon, reduce electric power consumption, and to increase the cyclotron long-term operation stability.

27 July 2023. The first pile was driven into the construction site of the experimental building of the U-400R cyclotron

21 December 2023. Pouring the first cubic meters of concrete into the foundation of the U-400R experimental building

Installation of the DC-140 cyclotron

In addition to upgrading the accelerator, the U-400(R) reconstruction project involves the construction of a new experimental building and the development of novel experimental setups. Owing to the construction of the new building that has been underway since the middle of 2023, the total area of experimental halls will be expanded up to 1500 m^2, enabling work in several radiation-shielded caves. The completion of the construction and the final phase of the U-400(R) cyclotron upgrade are scheduled for 2026.

The **DC-140** accelerator complex is being created for fundamental research and application of heavy-ion beams in the field of solid state physics, surface modification of materials, in the production of track membranes, as well as in testing the electronic component base for resistance to single radiation effects. The DC-140 accelerator complex project is in its final stage.

The DC-140 cyclotron is designed for producing beams of ions from oxygen to bismuth accelerated up to 4.8 and 2.1 MeV/nucleon. The 4.8-MeV/nucleon beams will enable ion penetration in Si up to 55 μm and linear energy transfer in Si up to 100 MeV·cm^2/mg for ensuring efficient testing of electronics. The 2.1-MeV/nucleon beams will allow the production of track membranes using polymer films up to 30 μm in thickness [7–15].

In 2017–2023, studies were carried out in the traditional areas: Fundamental Interactions of Fields and Particles; Theory of Nuclear Systems; Theory of Complex Systems and Advanced Materials; Modern Mathematical Physics: Gravity, Supersymmetry and Strings. New projects were opened and actively developed: "Theory of Hadronic Matter under Extreme Conditions" and "Quantum Field Theory Methods in Complex Systems". An important component of the BLTP activities was the theoretical support of experimental research at JINR and other research centres with JINR's participation. The 7 years of research resulted in more than 3200 publications in peer-reviewed journals and proceedings of international conferences. A number of studies have been carried out in collaboration with scientists from JINR Member States and other countries. In this period, more 58 international conferences and 17 schools were organized by BLTP in Dubna and in Member States. The international cooperation of BLTP was supported by special programmes and international agreements. The international collaboration in research areas was supported by grants of Plenipotentiaries of the Governments of the JINR Member States, as well as of the JINR Directorate. Many research projects and conferences were supported by the RFBR, RSF and BASIS Foundation grants. Special attention was paid to recruiting young researchers, students, and post-graduate students to the Laboratory within the research and education project "Dubna International Advanced School of Theoretical Physics" (DIAS-TH). Currently, about one third of the scientific personnel are young scientists and PhD students. Below are a few of the many striking results obtained over these years.

A new approach to the theory of nonrenormalized interactions is developed. Generalizations of the renormalization group equations are obtained, which make it possible to sum up the leading asymptotics in all orders of the perturbation theory. The ultraviolet behavior of a number of supersymmetric gauge models of quantum field theory is found [16, 17].

In the framework of the most general renormalizable theory in four dimensions, the expressions are derived for the first time for the beta functions of gauge and Yukawa coupling constants at four and three loops, respectively. The main feature of the utilized approach lies in the fact that tedious and cumbersome calculations are avoided by considering simple "toy" models and fixing unknown model-independent coefficients in general expressions for the renormalization group (RG) functions. Thanks to the obtained results, it became possible to carry out precision RG analysis of an arbitrary New Physics model without the need for explicit diagrammatic calculation and renormalization. As an application, the four-loop beta functions of all gauge couplings in the Standard Model and its generalization with several Higgs doublets are derived [18, 19].

The transition frequency of $(n, l) = (17, 16) \to (16, 15)$ in pionic helium-4 is calculated to an accuracy of 4 ppb (parts per billion), including relativistic and quantum electrodynamic corrections up to $O(R \infty \alpha^5)$. New calculations significantly improve our previous theoretical values (*Hori M., Soter A., Korobov V. I.* // Phys. Rev. A. 2014. V. 89. 042515). In addition, collisional effects between pionic heli-

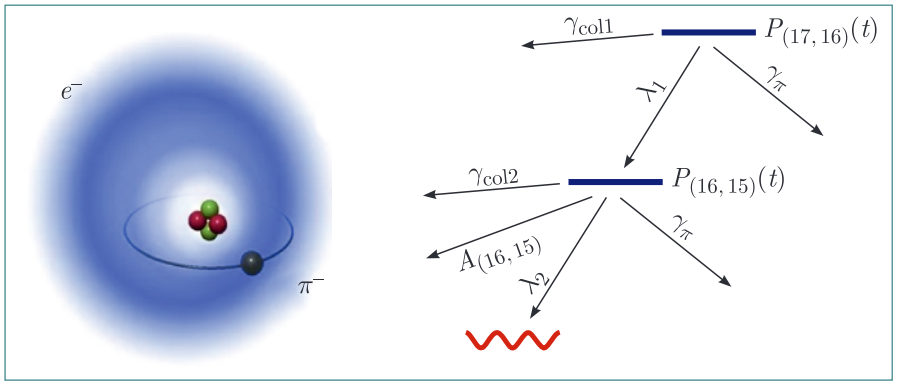

Pionic helium and a diagram of two-photon experiment on precision measurement of the $(17, 16) \to (16, 15)$ transition frequency

um and target helium on transition frequencies are estimated. Once measurements reach the ppb level, then the accuracy of determining the pionic mass will increase by 2–3 orders of magnitude. Such a high precision value of m_π can impose direct experimental constraints on the mass of the antineutrino of muon flavor [20].

A generalized renormalization group equation summing up all leading logarithms is obtained for the effective potential in the scalar theory with an arbitrary form of the potential. The equation was applied to inflationary cosmology in the slow-roll attractor T-model: conservation of the asymptotic behavior of the corresponding effective potentials was shown, cosmological observables were calculated, and spontaneous symmetry breaking in the effective potential due to quantum corrections was discovered (Coleman–Weinberg mechanism) [21].

The transport properties of quark–gluon plasma were studied. Shear and bulk viscosities were calculated. Conductivity in an external magnetic field and at nonzero baryon density was calculated for the first time [22–24].

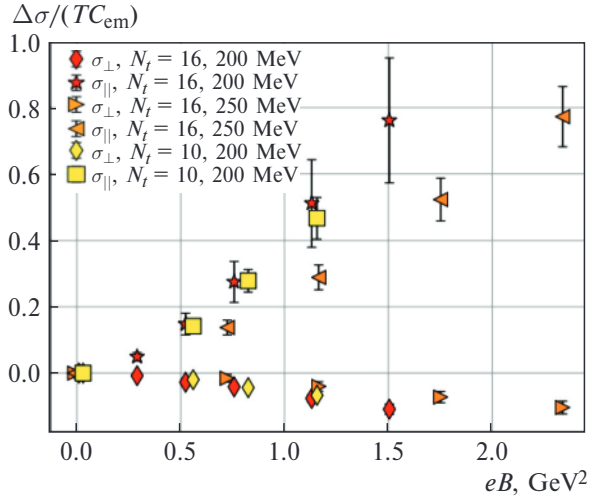

Longitudinal and transverse conductivities of quark–gluon plasma as a function of magnetic field at temperatures $T = 200$ and 250 MeV

The properties of dense two-color QCD at nonzero baryon density were studied. The interaction potential of static quarks in dense baryon matter, gluon propagator and equation of state were studied. Deconfinement in low-temperature dense baryon matter was observed [25–28].

The influence of relativistic rotation on QCD properties has been studied for the first time. We studied how rotation affects phase transitions in QCD, calculated the equation of state of rotating gluodynamics and the moment of inertia of the gluon plasma. A number of new phenomena have been discovered that can occur in rotating QCD. In particular, a state was discovered in which two different spatially separated phases of confinement and deconfinement can coexist [29–31].

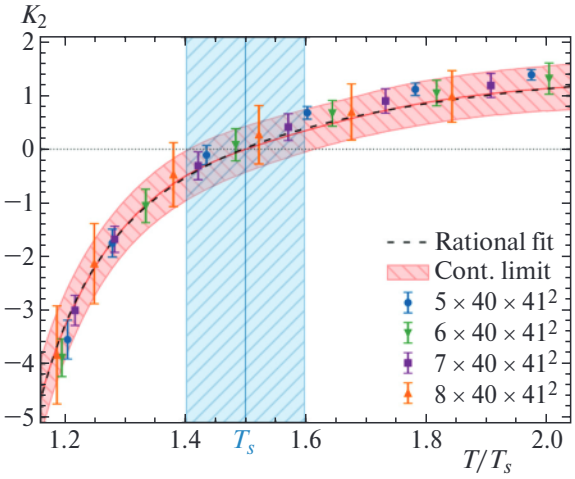

Coefficient K_2 for gluodynamics, which is proportional to the moment of inertia of the quark–gluon plasma, as a function of temperature

The three-fluid model has been developed, which is used to describe Au + Au collisions at energies of the RHIC beam energy scan program. From calculations it becomes evident that the satisfactory description of the bulk observables like particle yields, spectra, etc. can be achieved for the EoS with the deconfinement phase transition. This proliferates the baryon stopping so that its efficiency being of

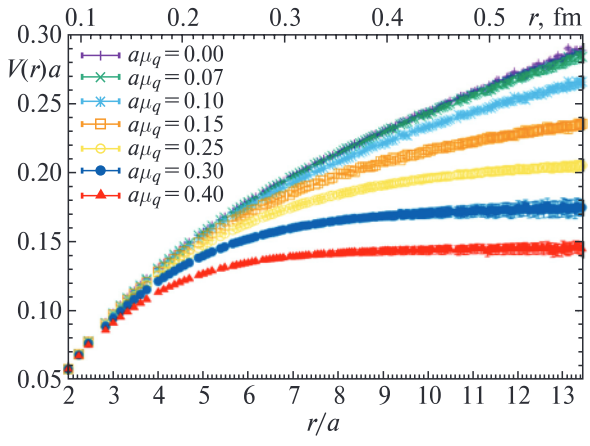

Interaction potential of static quarks for various baryon chemical potentials

100% at 7.7 GeV (centre-of-mass energy) decreases only to ≈40% at 62 GeV. The highest initial baryon densities of the equilibrated matter are reached in the central region of colliding nuclei at $\sqrt{s_{NN}}$ = = 20–40 GeV [32–34].

For the first time, the hydrodynamical model was used to investigate cluster production. The light-nuclei production is treated within the thermodynamic approach on an equal basis with hadrons. It is found that the late freeze-out is preferable for deuterons, tritons, and ^{3}He. Remarkably, the ^{4}He observables are better reproduced with the standard freeze-out [35].

The hybrid model connecting the parton–hadron–string dynamic model (PHSD) and a hydrodynamic model is developed that considers the shear viscosity within the Israel–Stewart approach. The performance of the code is tested on the pion and proton rapidity and transverse mass distributions calculated for Au + Au and Pb + Pb collisions at AGS–SPS energies. Despite the overall good agreement with the data, it is realized that it is not easy to reproduce simultaneously pion and proton rapidity distributions [36].

Vorticity generated in HICs and its influence on the hyperon polarization are studied within hydrodynamics and transport approaches. Analyses of experiments show that the description of momentum distributions of pion produced in heavy-ion collision at RHIC and LHC energies could require a large value of the pion chemical potential being close to the critical one for a Bose–Einstein condensation (BEC) in an ideal pion gas. The proximity of the system to the BEC critical point would manifest itself through a growth of fluctuations [37–40].

The influence of the pion interaction on the particle number fluctuations is considered. The normalized variance of the total particle number and the relative number of charged and neutral pions increases with a temperature decrease but remains finite in the critical point of the Bose–Einstein condensation, whereas the charge fluctuations diverge [41, 42].

A broad range of problems is associated with phase transitions in systems characterized by the strong interaction between particles and with formation of structures. A general phenomenological mean-field model is proposed in describing phase transitions of the first and the second order to the homogeneous and inhomogeneous states, and the latter may occur even when the interaction is translation-invariant. The theory is applicable to the description of pasta phases in neutron stars and cluster formations [43–45].

The production cross sections of the heaviest unknown isotopes ^{283,284}Rg, $^{287-290}$Nh, $^{291-294}$Mc, ^{294}Lv, and $^{295-297}$Ts in the *pxn* channels and ^{286,287}Cn, ^{290,291}Fl, ^{291,292}Mc, and ^{294}Lv in the αxn channels of the hot-fusion reactions were calculated for the first time. It is shown that the use of charged particle evaporation channels makes it possible to increase the mass number of the heaviest isotopes of nuclei with $Z = 111-117$ by a few units. The proton evaporation channels are more effective to approach $N = 184$ than the α-emission channels. The *pxn* and αxn evaporation channels allow us to obtain an access to those isotopes that are unreachable in the *xn* channels due to the lack of proper projectile–target combination. The production cross sections of new isotopes ^{261,263,264}No, $^{263-265}$Lr, ^{263,264,266,268}Rf, ^{264,265,269}Db and ^{267,268,270,272}Sg in the αxn and *xn* evaporation channels of the asymmetric hot-fusion reactions with the radioactive beams were estimated. It is shown that the charged particle evaporation channels are suitable for producing these unknown isotopes with cross sections of about 0.1–300 nb [46, 47].

The effect of finite temperature on electron captures by nuclei near the $N = 50$ closed shell which dominate the composition of core-collapse supernova is studied. Applying thermodynamically consistent approach, it is shown that thermal effects unblock Gamow–Teller (GT) transitions at astrophysically relevant temperatures $T \approx 10^{10}$ K. Comparison of electron capture rates on nuclei ground and thermal excited states for ^{78}Ni, ^{82}Ge, ^{86}Kr, and ^{88}Sr indicates that thermal effects are crucial for core-collapse supernova modeling. The results obtained contribute to solving the long-standing problem of explaining core-collapse supernova explosions [48].

The $\gamma\gamma$ decay of the low-energy quadrupole state of an even-even nucleus was studied. Choosing the first excited state of ^{48}Ca as an example, its $\gamma\gamma/\gamma$ branching ratio of $3 \cdot 10^{-8}$ was computed for the first time for an even-even nucleus. By making use of the energy density functional, it is shown that the $\gamma\gamma$-decay width is sensitive to the mixing of the simple and complex configurations in the giant dipole resonance region. This work elucidates a new way to test our understanding of collective modes of nuclei and opens a perspective area of research [49].

On the basis of the geometric collective model and the quasiparticle-phonon model, a microscopic version of the phenomenological Grodzins relation

is derived. This relation is used to predict the excitation energy of the first 2^+ states in nuclei with charge $Z \geqslant 100$ in order to analyze the α-decay spectra. It was found that at the beginning of the chain of nuclei under study at $Z = 100-110$, where the quadrupole deformation is high, the excitation energy of the first 2^+ states does not exceed 100 keV; i.e., it corresponds to rotational states. Then, with decreasing deformation, $E(2^+_1)$ increases sharply and reaches a maximum value in ^{284}Fl or ^{292}Og, i.e., in nuclei with minimal values of β_2 [50].

The new mechanism of incomplete fusion was explored as a very mass-asymmetric quasi-fission of a dinuclear system formed in the entrance reaction channel. It was shown that the incomplete fusion occurs due to the strong increase in the intrinsic fusion barrier along mass and charge transfer degrees of freedom, causing a hindrance of complete fusion in very asymmetric systems; as a result, the α-particle formation probability increases. The centrifugal force causes a breakup of that asymmetric system (for example, with α particle). The residue nucleus formed in the incomplete fusion is less heated than the compound nucleus formed in the complete fusion. The suggested mechanism can be useful to produce new isotopes in incomplete fusion reactions [51].

It is shown that the unexpected behavior of the Fermi surface of high-temperature superconducting cuprates can be explained in the framework of the $t-J$ model due to strong electron correlations resulting in charge density wave instability. Thus, for the first time, an explanation of experimental data on the charge ordering in the hole-doped cuprates was obtained within the microscopic model [52].

The effect of coupling between the superconducting current and magnetization in the superconductor–ferromagnet–superconductor Josephson junction under an applied circularly polarized magnetic field is studied. Manifestation of ferromagnetic resonance in the frequency dependence of the amplitude of the magnetization and the average critical current density is demonstrated. The IV characteris-

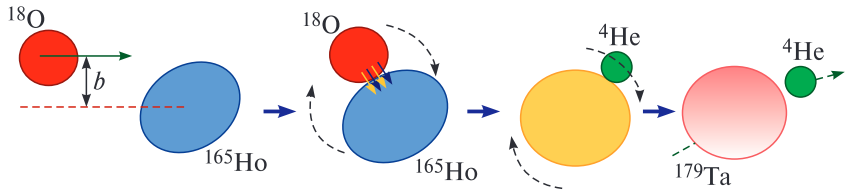

The sketch of the incomplete fusion mechanism as a very asymmetric quasi-fission in the case of the ^{18}O + ^{93}Nb reaction

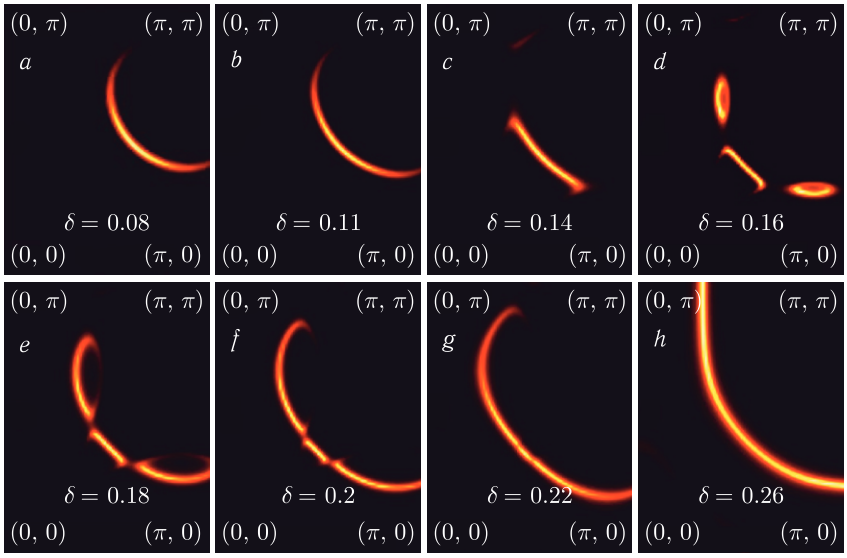

The spectral function at the Fermi level in the first quadrant of the Brillouin zone is calculated for different doping levels, δ. The observed Fermi surface reconstruction: pseudogap phase (a–c) ↔ charge density wave (d–f) ↔ pseudogap (g) ↔ Fermi liquid (h)

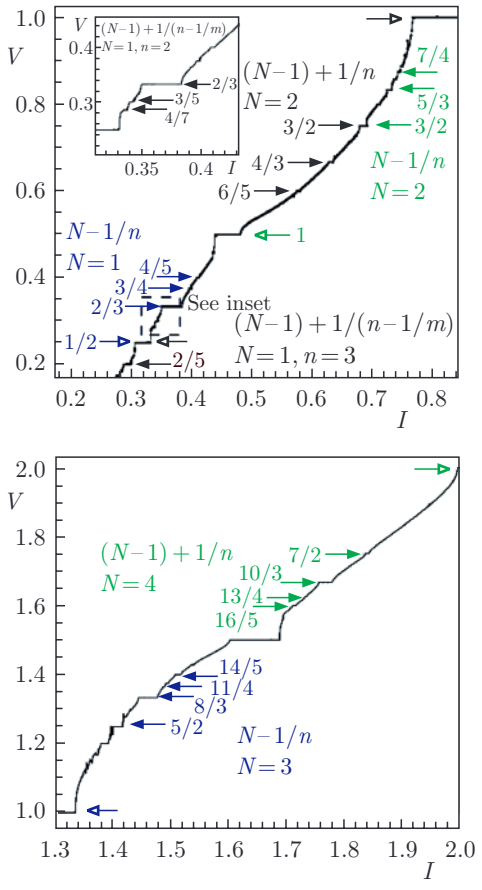

Subharmonic steps that form devil's staircases in different parts of IV characteristic at ferromagnetic resonance

tics show subharmonic steps that form devil's staircases, following a continued fraction algorithm. The origin of the found steps relates to the effect of the magnetization dynamics on the phase difference in the Josephson junction [53].

A statistical method for generating fluorinated graphene structures with desirable fluorine distribution is developed within the framework of stochastic reactive molecular dynamics simulations. Electronic transport properties of fluorinated graphene are investigated in a wide range of functionalization degrees and system ordering. A strong correlation is found between irregularities in fluorine distribution and electronic properties. The proposed consideration allows for the reproduction of both the experimentally observed electron-hole asymmetry in transport properties of fluorinated graphene and a recently revealed conductivity peak at 10% fluoride content [54].

A model is formulated that makes it possible to describe interactions of excitons in single-layer transition metal dichalcogenides (SLTMDs) with both

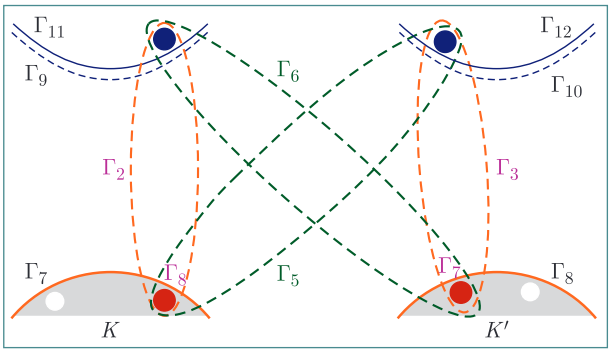

Band structure of single-layer tungsten dichalcogenides at the K and K' valleys and related excitons

intravalley and intervalley excitons taken into account. It is found that the correct consideration of two-pair correlations between Fermi charge carriers constituting two excitons and the symmetry of interacting excitons has a decisive influence on the character of the exciton–exciton interaction: the interaction is generally repulsive, except the case of excitons from different valleys, which are attracted and form an intervalley biexciton. Thus, we revealed the physical nature of biexciton in SLTMDs and for the first time explained the experimentally observed wide spread of biexciton energies in various SLTMDs, including those during their encapsulation. The results obtained are of obvious practical interest for the development of semiconductor nanotechnologies, primarily in optoelectronics [55].

The properties of new materials in solid state physics were studied using lattice simulation methods. In particular, graphene and Dirac semimetals have been studied. For these materials, the static potential of electric charges, conductivity and the influence of the chiral chemical potential on phase transitions were studied [56–59].

The general theory of spinning particles with electric and magnetic dipole moments moving in arbitrary electromagnetic, inertial, and gravitational fields is presented. Both the quantum mechanical and classical dynamics are investigated. The complete agreement between the quantum mechanics and the classical theory is proven in the general case. As an application of the results obtained, the dynamics of a spinning particle in the gravitational wave is considered, and the prospects of the use of the magnetic resonance setup for the registration of the gravitational wave via its impact on the spin dynamics are analyzed [60].

$SU(2|1)$ supersymmetric multiparticle quantum mechanics with additional semidynamical spin de-

grees of freedom is considered. In particular, an $N=4$ supersymmetrization of the quantum $U(2)$ spin Calogero–Moser model is provided, with an intrinsic mass parameter coming from the centrally extended superalgebra $SU(2|1)$. The full system admits an $SU(2|1)$ covariant separation into the centre-of-mass sector and the quotient. Explicit expressions for the classical and quantum $SU(2|1)$ generators in both sectors as well as for the total system are derived, and the relevant energy spectra, degeneracies, and the sets of physical states are determined [61].

A new effect of staggered radiative decay of long-lived oscillating states is discovered. It is related to a series of transitions, during which higher harmonics are released as short, staccato bursts of radiation [62].

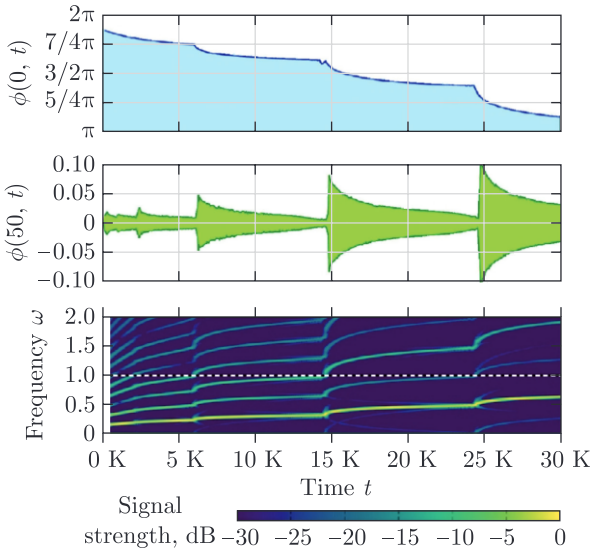

Power spectrum of the radiation flux of the quasi-breather in the deformed sine-Gordon theory

The exact densities ν_c and ν_{nc} of contractible and noncontractible loops in the $O(1)$ model on a strip of the square lattice rolled into an infinite cylinder of finite even circumference $L=2N$ were obtained. These densities are also equal to the densities of critical percolation clusters on 45° rotated square lattice rolled into a cylinder, which do not or do wrap around the cylinder respectively. The results are presented as explicit rational functions of N taking rational values for any N. Their asymptotic expansions in the large N limit have irrational coefficients reproducing the earlier results in the leading orders. This result gives a unique example of exact calculation of an observable in a confined system that approaches a critical state in the infinite size limit. Studies of its universal scaling behavior are useful for understanding the physics of critical phenomena in two-dimensional systems [63].

The method to parameterize all simple complex Lie algebras by three parameters, which are defined up to a common factor and permutations, proposed by Vogel, was investigated. It was shown how this description arises when considering the split (polarized) Casimir operators — the main building blocks used in calculating of the color factors in the amplitudes in the non-Abelian gauge field theories. The characteristic identities were constructed for the split Casimir operators of all simple complex Lie algebras in the defining and adjoint representations. Using these identities, the explicit formulas were obtained for the projectors onto invariant subspaces of the representation $T\otimes T$ in two cases, when T is the defining and when T is the adjoint representation. In the adjoint representation, the constructed characteristic identities and the corresponding projectors were investigated from the standpoint of a univer-

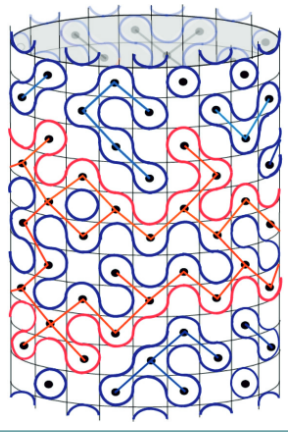

$$\nu_c(2N)=\frac{3\Gamma\left(\frac{N}{2}\right)\Gamma\left(\frac{3N}{2}+\frac{1}{2}\right)}{4\Gamma\left(\frac{3N}{2}\right)\Gamma\left(\frac{N+1}{2}\right)}+\frac{\pi_2^2-2N_3^2-3N_{\Gamma(3N)}}{\Gamma\left(\frac{N}{2}+\frac{1}{6}\right)^2\Gamma\left(\frac{N}{2}+\frac{5}{6}\right)^2\Gamma(N)}-\frac{5}{2}=$$

$$=\frac{1}{8},\frac{17}{160},\frac{913}{8960},\frac{3953}{39424},\frac{14569}{146432},\frac{3945737}{39829504},\cdots$$

$$\nu_{nc}(2N)=\frac{2^{2(N-2)}\Gamma(N)}{N\pi^2\Gamma(3N)}\left(3^{3N}\Gamma\left(\frac{N}{2}+\frac{1}{6}\right)^2\Gamma\left(\frac{N}{2}+\frac{5}{6}\right)^2-\frac{12\pi^2\Gamma\left(\frac{3N}{2}\right)^2}{\Gamma\left(\frac{N}{2}\right)^2}\right)=$$

$$=\frac{1}{8},\frac{11}{320},\frac{421}{26880},\frac{1403}{157696},\frac{4189}{732160},\frac{952067}{238977024},\cdots$$

Contractible (blue) and noncontractible (red) loops of the $O(1)$ loop model on the cylinder and corresponding percolation clusters (on the left); their exact densities (on the right)

sal description of all simple complex Lie algebras in terms of the Vogel parameters [64].

Electrodynamics in space-time with a straight null cosmic string was studied. Two kinds of point-like sources crossing the string horizon were considered: sources with an electric charge and sources with a magnetic moment. It was shown that null cosmic strings disturb electric fields of charged sources and produce electromagnetic (EM) pulses. An analytic approximation was developed for the asymptotic of EM waves at future null infinity, and radiation fluxes for sources of both types were calculated. The estimates show that the peak power of the radiation can be quite large for null strings moving near pulsars and considerably large in the case of magnetars. In gravity, it was shown that perturbations of gravitational fields of massive sources caused by null cosmic strings are radiated away in the form of gravitational wave pulses. Near the future null infinity, the resulting geometry, sourced by the string and point-like mass, belongs to the class of so-called polyhomogeneous space-times [65, 66].

HIGH-ENERGY HEAVY-ION PHYSICS

In 2018, the **BM@N** (Baryonic Matter at the Nuclotron) collaboration conducted the first run of the physical experiment programme. More than 2 million events were recorded in the interaction of a beam of carbon ions with an energy of 4 GeV/c per nucleon with a liquid hydrogen target as part of the short-range correlation research programme. In addition, the BM@N collaboration detected almost 200 million events in beams of argon and krypton ions with kinetic energies of 3.2A and 2.3A GeV, respectively.

Trigger detectors of the target area and the central tracking system inside the BM@N spectrometric magnet

Participants of the BM@N collaboration meeting

Participants of the MPD collaboration meeting

A technological transfer of the 800-ton MPD detector solenoid

Participants of the SPD collaboration meeting

During the long run in 2022–2023, 508 million interactions of ^{124}Xe ions with CsI target at an energy of 3.8A GeV and 48 million at an energy of 3.0A GeV were recorded in the experiment using the extracted Nuclotron beams. Based on the results of processing the collected statistics, the registration of $4 \cdot 10^6$ Λ hyperons, $1.2 \cdot 10^6$ K^0_S mesons and 8000 Ξ hyperons is expected. Together with identified charged particles, they are the main tool for studying the properties of nuclear matter formed during Xe + CsI interactions.

The experiment involves an international collaboration that includes 240 physicists and engineers from 21 research institutes in 11 countries.

Intensive work is nearing completion on the creation of the **MPD** (Multi-Purpose Detector) facility, designed to study the properties of dense baryonic matter formed in collisions of heavy ions at the NICA collider. The international MPD collaboration brings together over 500 participants from 38 institutions in 12 countries.

The Spin Physics Detector (**SPD**) is the second facility at the NICA collider, built by 300 collaboration members from 35 institutions in 15 countries. The participants' efforts are currently focused on preparing TDR and testing detector prototypes. The SPD detector is expected to begin operation in 2028 [67–70].

In 2017, the **STAR** collaboration at RHIC (USA), with the active participation of a group from JINR, reported the first observation of the effect of collective polarization of Λ hyperons in heavy-ion collisions. It was found that the direction of polarization of Λ hyperons correlates with the direction of the angular momentum of the system at a level of several percent in non-central collisions with energy $\sqrt{s_{NN}} = 7.7-32$ GeV. It has also been established that a hot system arising in the region of intermediate velocities can be considered as a liquid, and hydrodynamic calculations directly relate the polarization of emitted particles to the so-called vorticity (swirling of the flow) of the liquid. Using this relationship, the vorticity of the fluid generated at RHIC was estimated to be on the order of $9 \cdot 10^{21}$ s^{-1}, which is 14 orders of magnitude higher than that of any previously observed fluid. Previous results showed that the system at RHIC is the hottest and least viscous (relative to entropy density) ever created [71].

JINR physicists in the **COMPASS** experiment (CERN) initiated a programme to search for a new possible mechanism for the production of exotic charmoniums — photoproduction on a nuclear target. As a result of a search for $X(3872)$ with a statistical significance of 4.1σ, a signal of a particle whose mass and width are consistent with those expected for $X(3872)$ was discovered in the invariant mass spectrum of the $J/\psi\pi^+\pi^-$ final state subsystem. A detailed analysis of the decay kinematics of the observed particle showed a complete discrepancy with the well-known decay kinematics of $X(3872)$. This unexpected observation suggested that the detected signal may belong to a new particle, which is a partner particle of $X(3872)$, has a similar mass, but differs from $X(3872)$ in a set of quantum numbers. The existence of such a partner particle is predicted by some theoretical models, which describe $X(3872)$ as a state of two quarks and two antiquarks, tightly coupled by the strong interaction (tetraquark). The mass of the new state is (3860.1 ± 10.0) MeV/c^2, and the Breit–Wigner width with a 90% probability is less than 51 MeV/c^2 [72].

A number of interesting results were obtained by the JINR group in the **ALICE** experiment at the LHC (CERN). A new analysis of femtoscopic correlations for pairs of identical charged pions and kaons in pp collisions at 13 TeV was performed separately for spherical ($S_T > 0.7$) and jet-like ($S_T < 0.3$) events, where S_T is the transverse sphericity of the event. A decrease in source radii with increasing transverse momentum of the pair was observed not only for jet-like events, but also for spherical events, which demonstrate non-trivial behavior of collective-like particles, expected only in collisions of heavy ions with the possible formation of quark–gluon plasma [73].

In the **ATLAS** experiment at the LHC (CERN), with the active participation of JINR employees, studies were carried out to search for decays of the Higgs boson of the Standard Model into a pair of b quarks produced in association with a W or Z boson. The analysed data, corresponding to an integral luminosity of 79.8 fb^{-1}, were obtained in proton–proton collisions at $\sqrt{s} = 13$ TeV. The measured excess of observed events over expected background events in the associative production channel with only a vector boson corresponds to a significance of 5.3σ, which is comparable to the significance of 4.8σ predicted within the SM. The statistical significance of the results was significantly improved after all data were processed.

JINR team took part in the search for potential $cccc$ tetraquarks decaying into a pair of charmonium states in the four-muon final state, using pp collisions at 13 TeV and an integral luminosity of 139 fb^{-1}. Statistically significant excesses of the

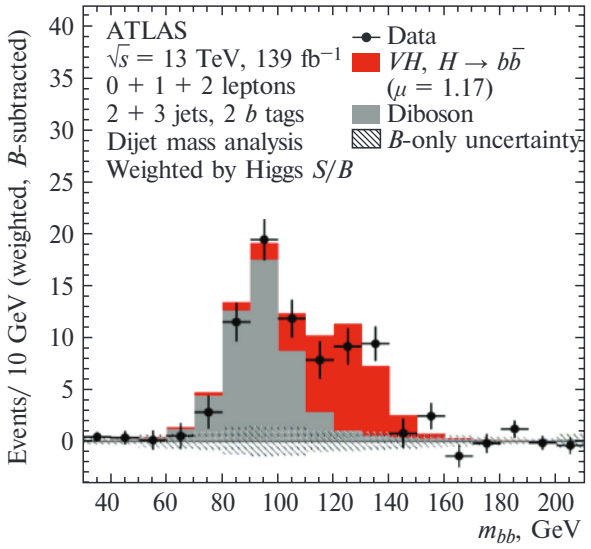

Distribution over the invariant mass of a pair of b jets formed in the WH and ZH reactions, after subtracting the contribution of all backgrounds, except for the WZ and ZZ diboson processes

signal above background were found in the channel with two J/ψ mesons, consistent with a narrow resonance at 6.9 GeV and a broader structure at lower masses. In addition, a statistically significant excess of the signal above the background in the channel with $J/\psi + J/\psi(2S)$ mesons was discovered. Estimates of the corresponding masses and widths of the decays were made [74–77].

In 2023, within the ATLAS project, a search for quantum black holes (QBH) in the lepton+jet invariant mass spectrum was performed with 140 fb^{-1} of the data collected from $\sqrt{s} = 13$ TeV pp collisions at the LHC. The observed invariant mass spectrum of lepton+jet pairs is consistent with the Standard Model expectations. Upper limits are set at 95% confidence level on the production cross-sections times branching fractions for the QBH decaying into a lepton and a quark in a search region with the invariant mass above 2 TeV. The resulting lower QBH mass threshold limit is 9.2 TeV in the ADD model and 6.8 TeV in the RS model [78].

In the **CMS** experiment at the LHC, with the participation of JINR physicists, a search for so-called quantum black holes (QBHs) with a characteristic experimental signature of flavor violation $e\mu$, $e\tau$, $\mu\tau$ was carried out. The resulting restrictions on the minimum permissible values of the mass of quantum black holes range from 3.6 to 5.6 TeV/c^2, depending on the model and the number n of additional dimensions.

In collisions of protons with an energy of 13 TeV in the centre-of-mass system in a channel with a pair of electrons and muons of high energies, using a data set of a total integrated luminosity of 140 fb^{-1}, upper limits were measured of the ratio of the cross sections for the production of new narrow resonances with spin 1 and spin 2 and the gauge Z boson. This made it possible to establish the strongest global restrictions on the masses of graviton states in the Randall–Sundrum model, carriers of interaction between SM particles and the dark matter sector, and new heavy gauge bosons of the Grand Unified models. As part of the search for non-resonant signals of new physics, a lower limit was established

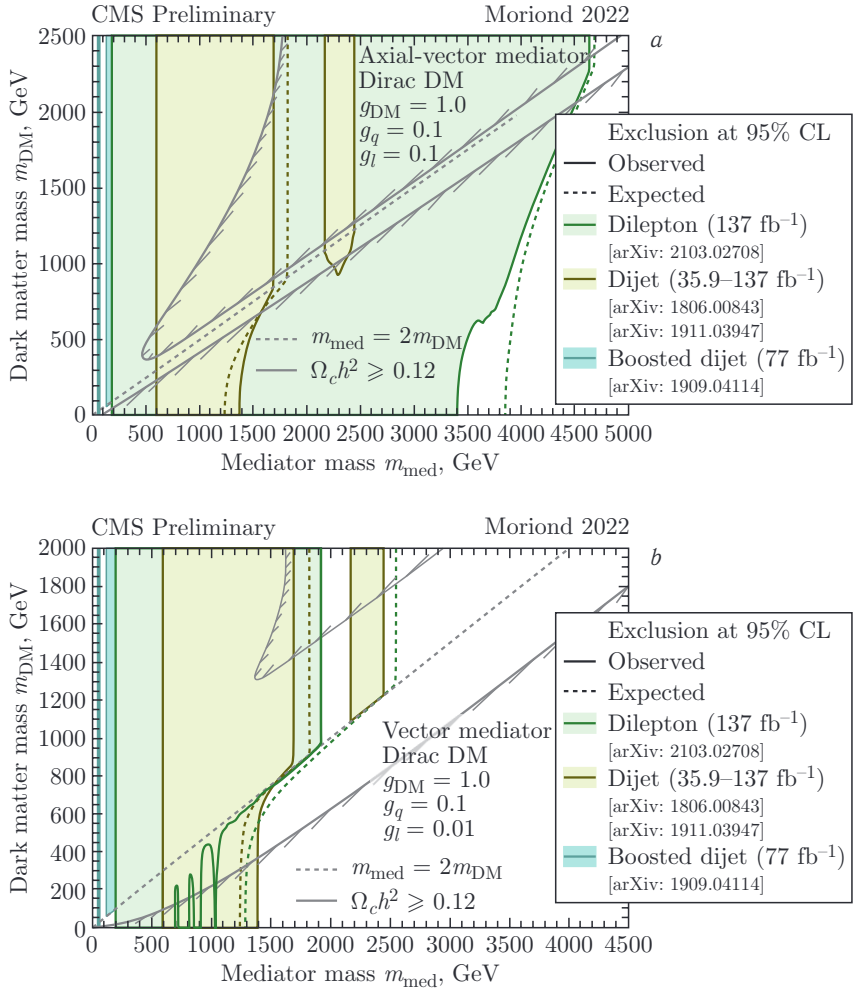

Limits (95% CL) on the masses of candidate particles for the role of dark matter particles m_{DM} and the particle carrier of interaction with the dark sector m_{med}. The shaded area corresponds to the closed mass values for the pseudovector (*a*) and vector (*b*) carrier. The results are obtained from Run-2 data in the combined channel of the production of a pair of jets and a pair of leptons

on the value of the ultraviolet cut-off scale for the four-fermion contact interaction model and the Arkani-Hamed–Dimopoulos–Dvali model of flat extra spatial dimensions. Also, for the first time, the universality of lepton interactions in the region up to 3 TeV was tested and confirmed. In addition, a series of calculations of electroweak and QCD radiative corrections for the processes of production of pairs of high-energy muons in the Drell–Yan process was performed.

MoU-agreed plans to upgrade and test the CMS detectors, particularly the High Granularity Calorimeter (HGCal) and upgrade of the forward muon station ME1/1, are progressing well [79–82].

In the **NA62** experiment at SPS (CERN) with the participation of JINR physicists, as part of the search for New Physics in rare kaon decays, 17 candidates for the ultra-rare decay of a charged kaon $K^+ \to \pi^+ \nu\bar{\nu}$ were discovered with an expected background of 7 events. This allowed us to make the world's best estimate of the relative probability of the decay $\mathrm{BR}(K^+ \to \pi^+ \nu\bar{\nu}) = (11.0^{+0.4}_{-3.5} \pm 0.3_{\mathrm{syst}}) \cdot 10^{-11}$, which is consistent with the prediction of the Standard Model.

JINR physicists also completed a study of the radiative decay $K^+ \to \pi^0 e^+ \nu\gamma$ using statistics from $1.3 \cdot 10^5$ candidates with a background of less than 1%, collected in 2017–2018. Measurements of the relative probability of this decay in three limited kinematic regions were made with relative accuracy within 1%, improving existing results by more than a factor of two. The asymmetry of this decay, which may be associated with T violation, was studied, but

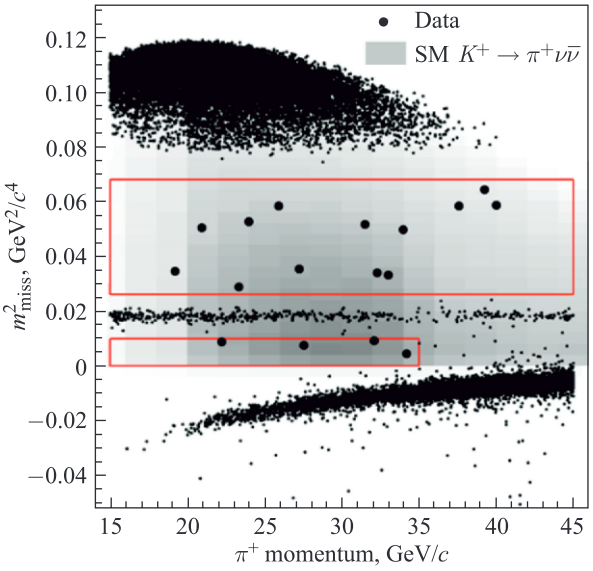

Candidate events for ultra-rare decay (in the box) and background events in the variables of the measured momentum of the charged pion and the square of the missing mass associated with the neutrino

no evidence of its existence was found within the achieved accuracy [83, 84].

JINR's team in the **NA64** experiment (CERN) is actively involved in upgrading the installation and conducting data acquisition sessions at the SPS accelerator with a beam of muons with an energy of 160 GeV and electrons with an energy of 100 GeV. The search for light dark matter and its mediator, the dark photon, continues. Using the statistics of

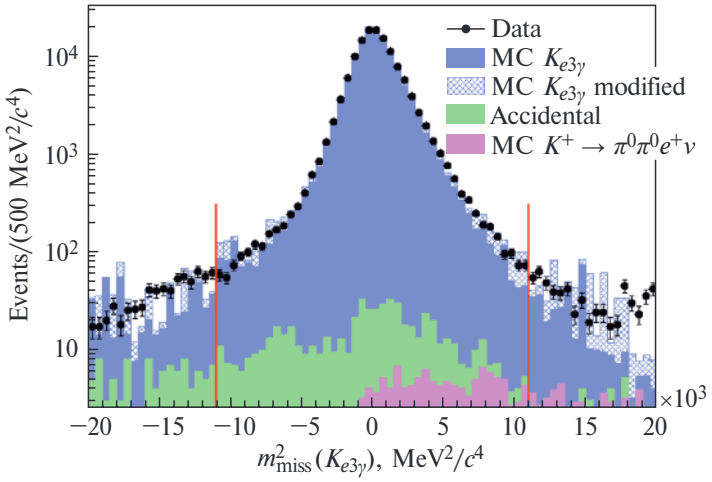

Distribution of the squared missing mass of combinations of registered particles $\pi^0 e^+ \nu\gamma$ for selected experimental events (points), as well as for the expected signal and background (histogram)

$3.4 \cdot 10^{11}$ eot, a search was carried out for the first time for the light Z' boson arising in expansion models of the Standard Model associated with the breaking of baryon−lepton symmetry. The mechanism of dark bremsstrahlung in the reaction of scattering of 100 GeV electrons on a nuclear target $eZ \to eZZ'$ is responsible for the generation of Z'. The result of the analysis, at a 90% confidence level, excluded this mechanism of Z'-boson formation in the mass range from 1 keV to 1 GeV, significantly supplementing the previously existing restrictions obtained in a series of neutrino experiments.

The statistics of $9.37 \cdot 10^{11}$ eot interactions of electrons with an energy of 100 GeV with an active target was collected during NA64 operation in 2016−2022. The most interesting region of parameters of models of scalar and fermionic thermal dark matter with sub-Gev mass (LDM), produced by a mediator — a new vector boson — dark photon A', was studied for the first time. No dark matter formation signals were detected, which made it possible to establish more accurate limits on the interactions of A' with photons for the mass region $m_{A'} \leqslant 0.35$ GeV, as well as to exclude scenarios of scalar and Majorana LDM in the region of parameters of the interaction constant $\chi - A'$, limited from above $\alpha_D \leqslant 0.1$, and the mass region of dark matter particles of $0.001 \leqslant m_\chi \leqslant 0.1$ GeV under the condition $3m_\chi \leqslant m_{A'}$ [85, 86].

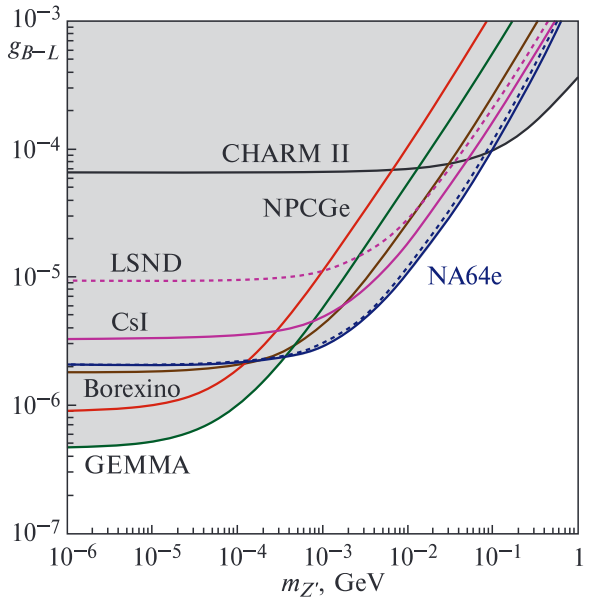

NA64 result for exclusion at 90% confidence level of the region of existence of Z' in the $B-L$ symmetry breaking model depending on the coupling constant g_{B-L} and mass $m_{Z'}$ is compared with the results of the neutrino experiments TEXONO, GEMMA (reactor), Borexino (solar neutrinos), LSND and CHARM II (accelerator experiments)

Within the **BESIII** project, the tests of CP symmetry in entangled $\Xi^0 - \bar{\Xi}^0$ pairs were carried out. The $J/\psi \to \Xi^0 - \bar{\Xi}^0$ process and subsequent decays are investigated using $(10087 \pm 44) \cdot 10^6$ J/ψ events collected at the BESIII experiment. The decay parameters α_Ξ, ϕ_Ξ of Ξ^0 and $\bar{\Xi}^0$ are simultaneously measured with unprecedented accuracies. The most precise values for CP asymmetry observables A_{CP}^{Ξ} and $\Delta\phi_{CP}^{\Xi}$ of Ξ^0 decay are obtained. For the first time, the weak and strong phase differences $\xi_P - \xi_S$ and $\delta_P - \delta_S$ are determined, which are the most precise results for any weakly decaying baryon [87].

The implementation of the SHE Factory experimental programme began at the end of 2020. In 2020–2023, experiments were conducted with ^{48}Ca beams in the following reactions: $^{232}\mathrm{Th} + {}^{48}\mathrm{Ca} \rightarrow {}^{280}\mathrm{Ds}^*$, $^{238}\mathrm{U} + {}^{40}\mathrm{Ar} \rightarrow {}^{278}\mathrm{Ds}^*$, $^{238}\mathrm{U} + {}^{48}\mathrm{Ca} \rightarrow {}^{286}\mathrm{Cn}^*$, $^{242}\mathrm{Pu} + {}^{48}\mathrm{Ca} \rightarrow {}^{290}\mathrm{Fl}^*$, $^{243}\mathrm{Am} + {}^{48}\mathrm{Ca} \rightarrow {}^{291}\mathrm{Mc}^*$. Around 250 events of superheavy nuclei formation were observed; the decay properties of 40 nuclei ranging from lawrencium ($Z = 103$) to moscovium ($Z = 115$) were studied. Six isotopes were synthesized and studied for the first time: ^{286}Mc, ^{264}Lr, ^{275}Ds, ^{276}Ds, ^{272}Hs, and ^{268}Sg.

In 2023, an experiment on the synthesis of the isotopes of element 116 in the $^{54}\mathrm{Cr} + {}^{238}\mathrm{U}$ reaction was conducted for the first time at the Superheavy Element Factory accelerator complex. The experiment was aimed at measuring the cross-section reduction factor upon passing from reactions with the ^{48}Ca beam to those with a heavier ^{54}Cr beam, as well as at maintaining the high current of the ^{54}Cr beam. Two synthesis events of a new isotope of element 116, ^{288}Lv, were registered. The experiment has continued in 2024 [10–12].

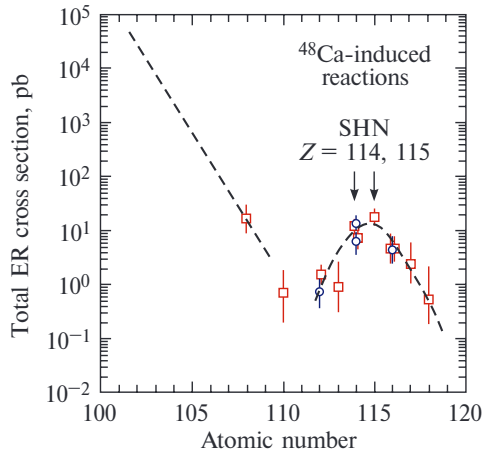

Behaviour of the production cross section of the heaviest nuclei in fusion reactions of ^{48}Ca with actinides

The deep underwater neutrino telescope **Baikal-GVD** is one of the three world's largest telescopes in terms of effective area and volume for observing natural neutrino fluxes and the largest one in the Northern Hemisphere.

From 2017 to 2023, 11 clusters of the Baikal telescope were installed; its working volume exceeded ≈ 0.5 km^3 in the task of recording events from high-energy neutrinos (over 100 TeV). The detector contains 12 clusters of deep-sea strings of recording and control equipment (3456 optical modules).

At the beginning of March 2021, the official commissioning of the Baikal-GVD detector with eight clusters took place.

Baikal expedition

Lake Baikal, 13 March 2021. Signing of the Memorandum of Understanding between the RF Ministry of Science and Higher Education and JINR on the development of the Baikal deep underwater neutrino telescope during the ceremonial launch of the Baikal-GVD telescope

Participants of the Baikal-GVD project working meeting at the ice camp at the site of the next expedition to deploy the deep-sea neutrino telescope. *Photo: © Irkutsk State University*

The first ten events were selected as astrophysical neutrino candidates after the analysis of the 2018–2020 data. The data were analyzed, and the first results of the search for events from neutrinos on the Baikal-GVD detector associated with the alerts of the Antarctic IceCube detector were published [88, 89].

In 2022, when analyzing the data obtained during the operation of the detector in the 2018–2021 configurations, 11 cascading events with an energy of over 15 TeV initiated by neutrinos of astrophysical nature were selected, which confirms at a confidence level of 3σ the results of the first observation

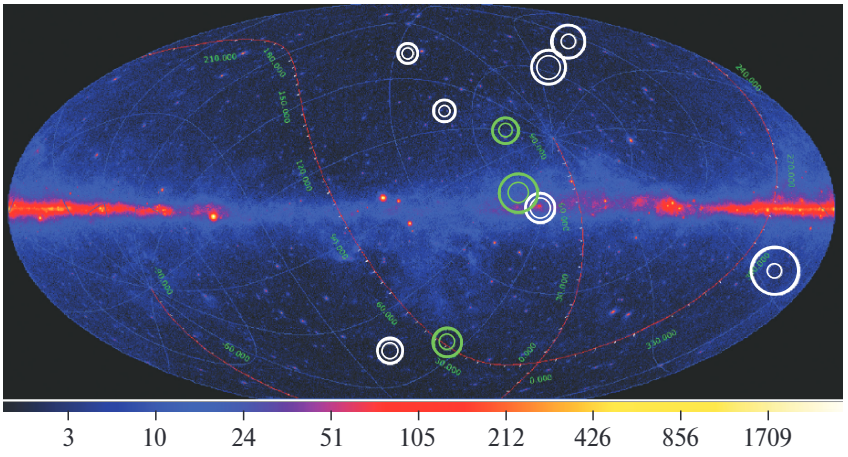

Position of the first ten candidates for astrophysical neutrino events in Baikal-GVD on a celestial map with FERMI-LAT sources in the galactic coordinate system. The inner and outer circles around the events correspond to the 50 and 90% detection probability

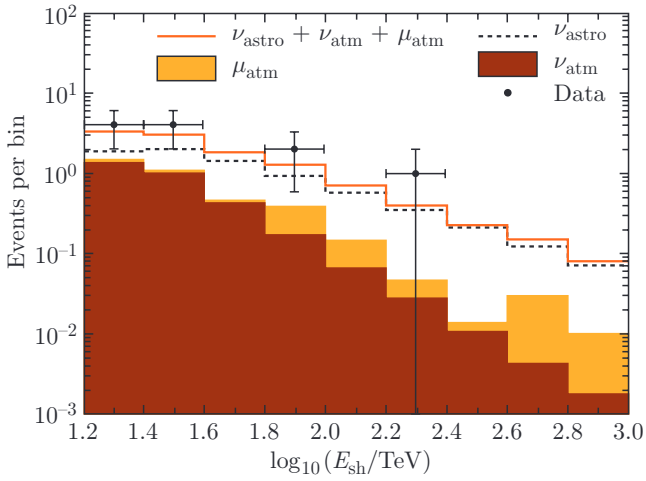

Energy distributions of experimental and theoretically expected events in the analysis of cascade events from under the horizon: black dots are the experimental events; the dotted histogram is the distribution of events expected from the diffuse neutrino flux of astrophysical nature with parameters obtained from the 2018–2021 Baikal-GVD data; stacked yellow and brown areas are background events from atmospheric muons and atmospheric neutrinos; the orange histogram is the total number of expected signal and background events

of the flux of high-energy astrophysical neutrinos on the Antarctic detector IceCube [90].

In 2023, when analyzing the data obtained during the detector's operation in the 2018–2022 configurations, correlations with radio-bright blazars of cascading events with energies exceeding 100 TeV were investigated.

Although no statistically significant effects were found on the current dataset, the analysis points to a number of possible associations with both extragalactic and galactic sources. In particular, the analysis

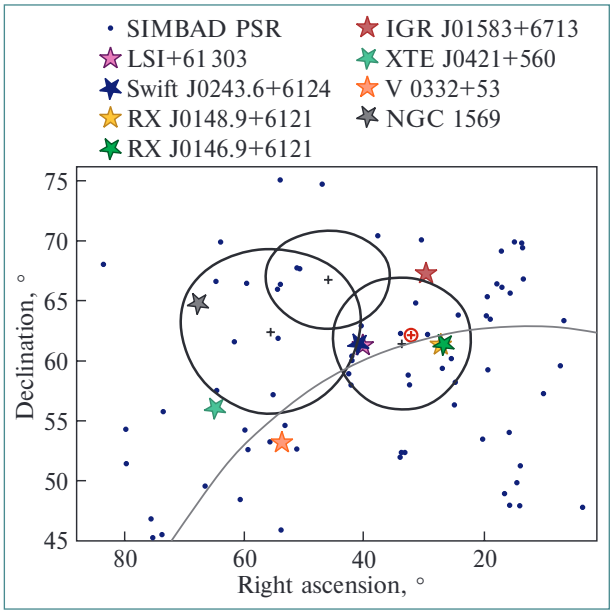

Three Baikal-GVD high-energy cascading events GVD190216CA, GVD190604CA and GVD210716CA near the galactic plane (gray line) and errors in determining their directions (black lines). The point of statistically most significant excess of the IceCube flux over the isotropic one in the Northern Hemisphere is shown as a red plus

of the observed triplet of neutrino candidates in the galactic plane is presented. Its potential connection with certain galactic sources has been investigated, and the coincidence of the directions of arrival of cascading events with several bright blazars has been considered [91].

Two experiments are being conducted at the Kalinin Nuclear Power Plant (KNPP) aimed at studying the fundamental properties of neutrinos: ***ν*GeN** and **DANSS**.

The *ν*GeN experimental facility is located under reactor No. 3 of the KNPP at a distance of just over 10 m from the centre of the reactor core. This makes it possible to operate with a gigantic neutrino flux of more than $5 \cdot 10^{13}$ cm$^{-2} \cdot$s^{-1}. The surrounding structural materials of the reactor provide good protection from cosmic radiation, corresponding to 50 m water equivalent. In 2021, the work on equipment optimization was completed and the planned measurements began. The energy resolution of the detector achieved under the conditions of the KNPP was 101.6(5) eV (FWHM). The possibility of detecting events with an energy above 250 eV with an efficiency of 80% was demonstrated.

The first results on the search for coherent neutrino scattering and other interactions were obtained. A comparison of the data collected while the reactor was on and off (154 and 39 d, respectively) has not yet revealed signs of the expected signal from coherent neutrino scattering. This made it possible to impose a limit on an important parameter of ionization losses in germanium (quenching) at the level of $k < 0.23$ (90% CL) [92, 93].

The DLNP employees, together with colleagues from ITEP (Moscow), created the DANSS neutrino detector, which does not contain flammable or caustic liquids and is suitable for placement near in-

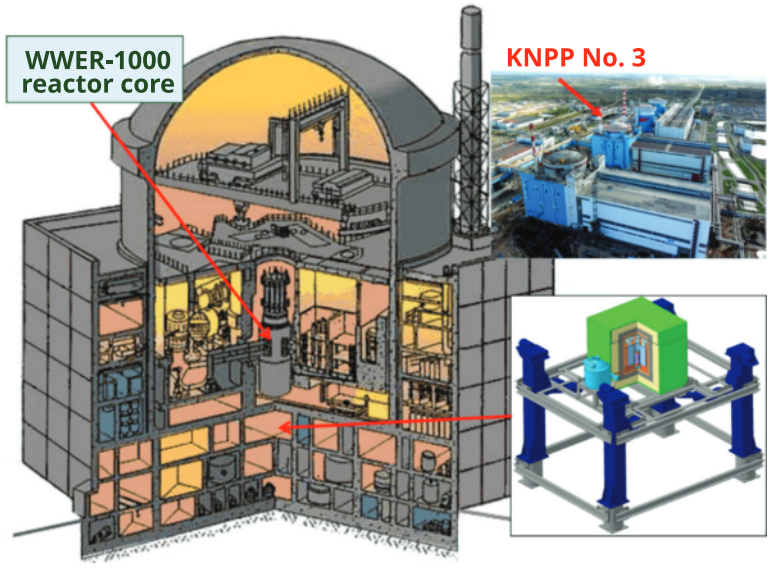

dustrial nuclear reactors. The DANSS detector has started to operate at unit 4 of the KNPP. It registers about 4000 neutrinos per day with a background less than 2–3% (both values are the world's best now). Due to a lifting gear, the detector is on line movable by 2 m, thus measuring the neutrino energy spectrum as a function of the distance. In addition to the reactor diagnostics, this feature allows investigating of short-range neutrino oscillations (i.e., periodic variation in the neutrino flux with distance) in the way independent of any questionable assumptions about the theoretical neutrino spectrum.

In 2019, an updated full-scale analysis of the 2016–2019 data was performed with improved estimation of all background sources and systematic errors. The world's best model-independent restriction on the existence of a sterile neutrino was obtained [94].

A new analysis of the data of the DANSS experiment for the period from 2016 to 2023 has included the absolute antineutrino count rate information (ratio 0.98 ± 0.04 to the predicted values using the Huber and Mueller model and a conservative estimation of the systematic uncertainty at 7%). For large ($\gtrsim 10$ eV^2) values of the parameter Δm^2_{41}, the values of $\sin^2 2\theta_{ee} > 0.26$ are excluded at the 90% confidence level. Also, the use of absolute values of the neutrino flux allowed us to exclude the best point $\Delta m^2_{41} = 7.3$ eV^2, $\sin^2 2\theta_{ee} = 0.36$, obtained in the Neutrino-4 experiment and almost the entire region of the acceptable parameters of the BEST experiment [95].

Within the **TAIGA** project, the mechanical part of the fourth Cherenkov telescope was manufactured at JINR, shipped and assembled at the test site. A prototype of a wide-angle lens Cherenkov

Atmospheric Cherenkov telescope TAIGA-IACT

telescope was also developed and manufactured at the test site. The lens with a diameter of 600 mm was manufactured at JINR. A signal from a source in the Crab Nebula with a reliability of 12.6σ was received.

The signal from the Crab Nebula was examined. Three methods were used and mutually verified: single (TAIGA-mono), stereo (TAIGA-stereo) and hybrid (TAIGA-hybrid) developed by the TAIGA collaboration. The latter is supposed to use data simultaneously detecting an event with a gamma-ray energy of more than 80 TeV by one telescope and several wide-angle detectors. The results are in good agreement with the data from other gamma observatories and make it possible to use the hybrid method in future studies of gamma rays with energy above 100 TeV using Cherenkov radiation. Observations and data collection from various gamma radiation sources continue [96].

Assembly of the largest liquid scintillator reactor antineutrino detector **JUNO** continues in China. To date, more than half of the planned 18 000 photomultiplier tubes (PMTs) with a diameter of 20 in. and 25 000 PMTs with a diameter of 3 in. have been installed. All these photomultipliers are provided with high-voltage power supply using specialized modules developed and manufactured by JINR, including their testing and commissioning.

In parallel, preparation for the assembly and installation of the Top Tracker (TT) is underway. The manufacturing plant begins to fulfill the order for the production of supporting structures developed by JINR. The detector data acquisition software, also developed by JINR, is currently being debugged on a TT prototype at IPHC (Strasbourg, France) [97].

In 2020–2022, the **NOvA** experiment performed data analysis with an increased exposure, which now amounts to $13.6 \cdot 10^{20}$ POT (protons on target) in a neutrino beam and $12.5 \cdot 10^{20}$ POT in an antineutrino beam. Interpretation of different oscillation channels allowed the parameters of this phenomenon to be refined: the best fit value is at the point with the normal ordering, in the upper octant of the angle θ_{23} with $\sin^2 2\theta_{23} = 0.57^{+0.03}_{-0.04}$, $\Delta m^2_{32} = (2.41 \pm \pm 0.07) \cdot 10^{-3}$ eV^2 and $\delta_{CP} = 0.82^{+0.24}_{-1.0}\pi$. Thus, the NOvA data prefer the combinations of the oscillation parameters leading to the symmetry between neutrinos and antineutrinos, while the opposite combinations (inverse ordering, $\delta_{CP} = \pi/2$ and normal ordering, $\delta_{CP} = 3\pi/2$) are rejected at the levels of $> 3\sigma$ and $> 2\sigma$, respectively [98, 99].

The **Borexino** detector recorded neutrinos from the Sun in the scattering reaction on electrons in a liquid organic scintillator with a total mass of 300 t. A key factor in the success of the Borexino project was the absence of radioactive impurities in the liquid scintillator.

In 2017, within the Borexino project, the results of the time variation studies of the beryllium neutrino flux were published. The best fit value for the period of the signal variation $T = (367 \pm 10)$ d could be considered as the first measurement of the astronomic year duration using solar neutrinos. A new model-independent limit on the effective moment of the solar neutrino $\mu_\nu^{\text{eff}} < 2.8 \cdot 10^{-11}\ \mu_B$ (90% CL) was obtained [100, 101].

In 2018, the international collaboration Borexino published in *Nature* the compendium of its results on neutrinos, accompanying the thermonuclear processes in the Sun. The most precise and complete results of the spectral analysis of accumulated so far data are presented by the collaboration. The uncertainty of the "beryllium" neutrino flux is reduced to 2.7%, two times better than existing theoretical prediction. For the first time, the robust signature of the "*pep*" reaction in the Sun is detected, confirming the presence of the corresponding process in the Sun. Neutrino flux from the boron-8 reaction is measured with a low energy threshold of 3.2 MeV, unreachable in other neutrino detectors. The high precision of the *pp*-neutrino flux measurement revealed further details of the thermonuclear processes in the Sun's core and confirmed the thermonuclear origin of the Sun's energy production. Through the comparison of these experimental data of very high quality and accuracy with the forecasts of the Standard Solar Model, Borexino demonstrates incontrovertibly the existence in the low-energy region of the oscillation between neutrinos of different flavour by the MSW (Mikheyev–Smirnov–Wolfenstein) effect. In particular, Borexino emphasizes in a completely autonomous way, using only its own data and without having to resort to results of other experiments, the peculiar transition between the two regimes of "vacuum" and "matter" that represents the signature of the MSW effect [102].

Within the framework of the **TANGRA** project, a facility has been developed and constructed at FLNP that makes it possible to measure angular correlations and yields of gamma rays in 14-MeV neutron reactions. The figure illustrates the configuration of the facility with 18 gamma-ray scintillation detectors based on BGO crystals. Measurements were carried out on light and medium nuclei; the energies of visible γ transitions formed in various neutron reactions with these nuclei and their partial cross sections were determined. The obtained data on the characteristic gamma rays are critically important for the development of non-destructive elemental analysis methods using portable tagged-neutron generators [103].

In the framework of the JINR–ITEP–PNPI collaboration, a series of experiments were carried out to measure the *T*-odd effect of rotation of a fissile nucleus in the angular distributions of prompt γ rays (ROT effect) in the fission of ^{235}U induced by polarized neutrons.

The observed effect, although formally *T*-odd, is explained not by a violation of time invariance, but by the dynamics of the fission process near the break point and provides a unique opportunity for direct experimental determination of the parameters of the theory describing the quantum mechanical properties of the fission process.

The angle of rotation of the nucleus was determined for three values of incident neutron energy: 0.025, 0.06 and 0.3 eV. For the first time, the effect

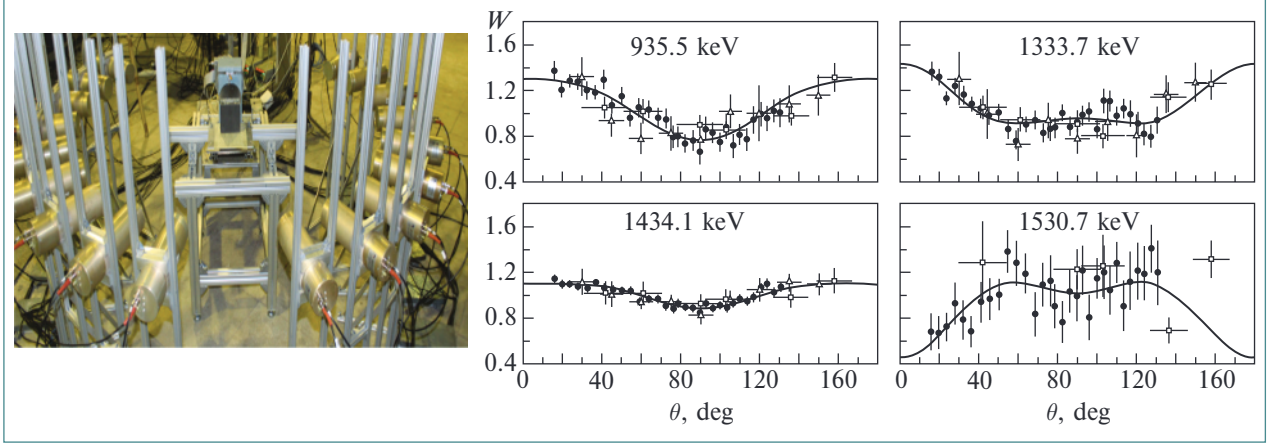

Left: TANGRA facility with 18 BGO scintillation detectors. Right: angular distributions of γ rays for transitions in ^{52}Cr. Solid curves are data approximation by Legendre polynomials

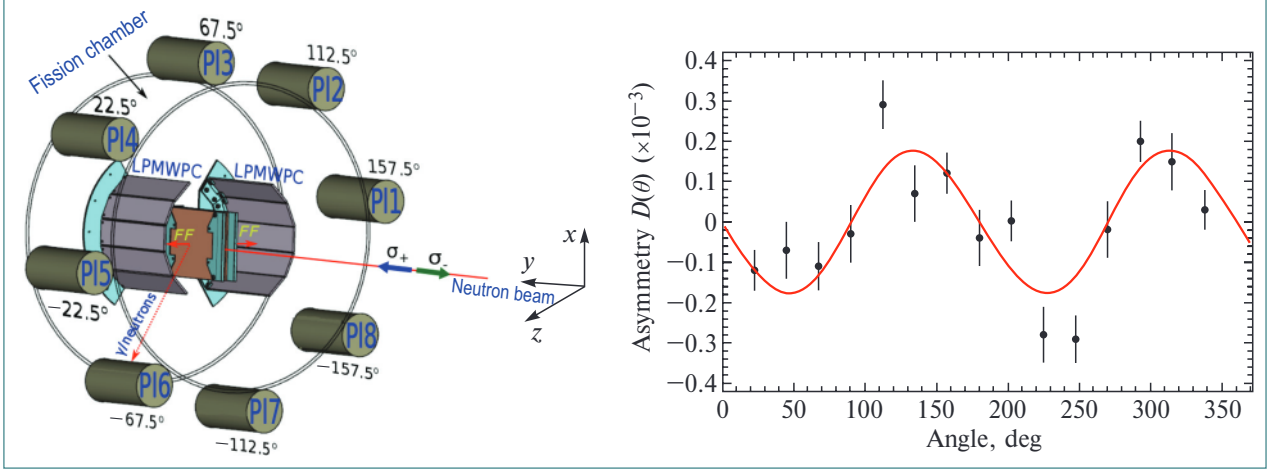

Left: scheme of the experimental facility. Right: asymmetry coefficient for γ rays as a function of the emission angle relative to the fission axis in the resonance of ^{235}U (0.3 eV)

was measured in the low-lying resonance of ^{235}U. It was shown that the sign of the observed effect does not change, but its magnitude for the first resonance of ^{235}U (0.3 eV) is 3 times less than that for thermal neutrons [104].

A series of studies were carried out to measure the cross section of the (n, α) reaction with fast neutrons on ^{35}Cl, ^{91}Zr, ^{40}Ca, ^{63}Cu, ^{58,60,61}Ni nuclei. The measurements were conducted with quasi-monoenergetic neutrons in the neutron energy range of 3.0–10.5 MeV at the EG-5 (FLNP JINR), EG-4.5 (Peking University) and the HI-13 (CIAE). The presented data on the reactions ^{60}Ni$(n, \alpha)^{57}$Fe (at E_n below 6 MeV) and ^{61}Ni$(n, \alpha)^{58}$Fe for neutrons in the MeV range were obtained for the first time. The obtained cross sections for the ^{60}Ni$(n, \alpha)^{57}$Fe and ^{61}Ni$(n, \alpha)^{58}$Fe reactions for the E_n range above 8.0 MeV, and ^{91}Zr$(n, \alpha)^{88}$Sr reaction in the MeV range were measured for the first time too. In addition, α-clustering factors were calculated by two methods, using the compound and "knock-on" mechanisms, which show that α clusters are formed after the interaction of neutrons with target nuclei.

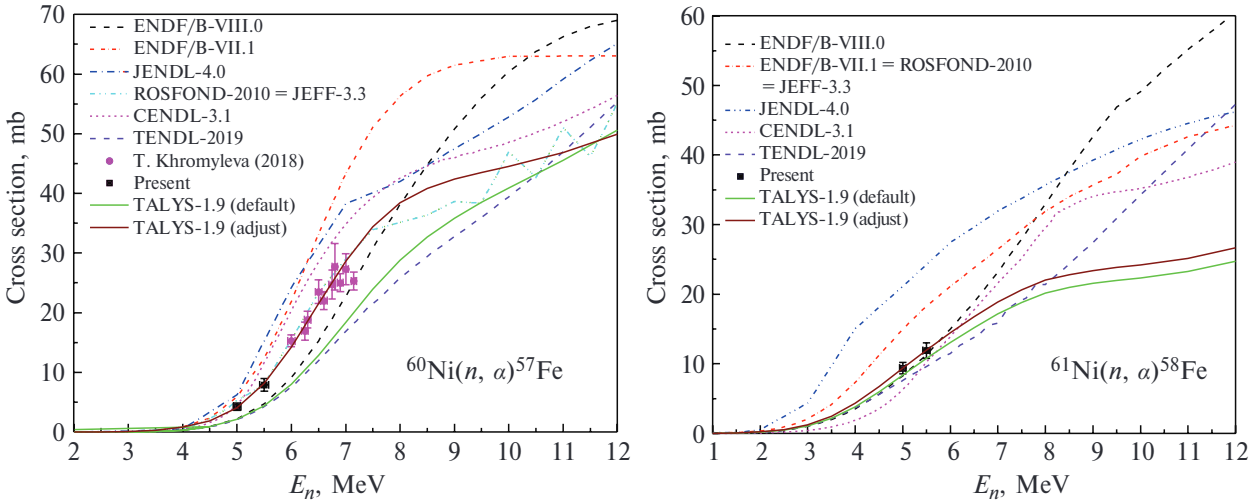

Cross sections for the reactions ^{60}Ni$(n, \alpha)^{57}$Fe (left) and ^{61}Ni$(n, \alpha)^{58}$Fe (right) in comparison with existing measurements, evaluations, and TALYS-1.9 calculations

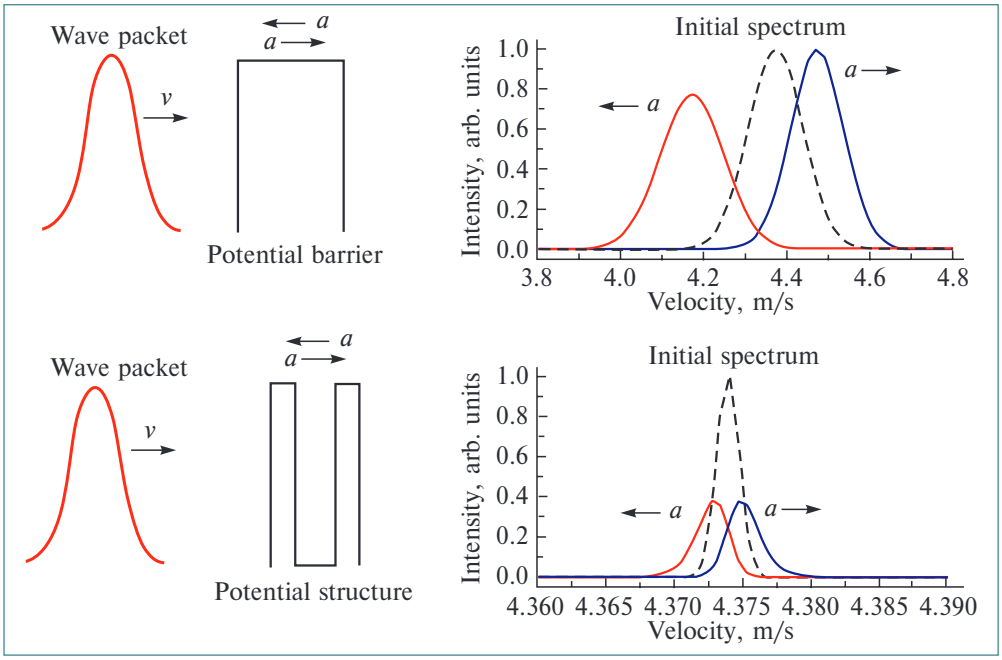

Results of studying the problem of interaction of a wave packet with a potential step and an interference filter that move with constant acceleration

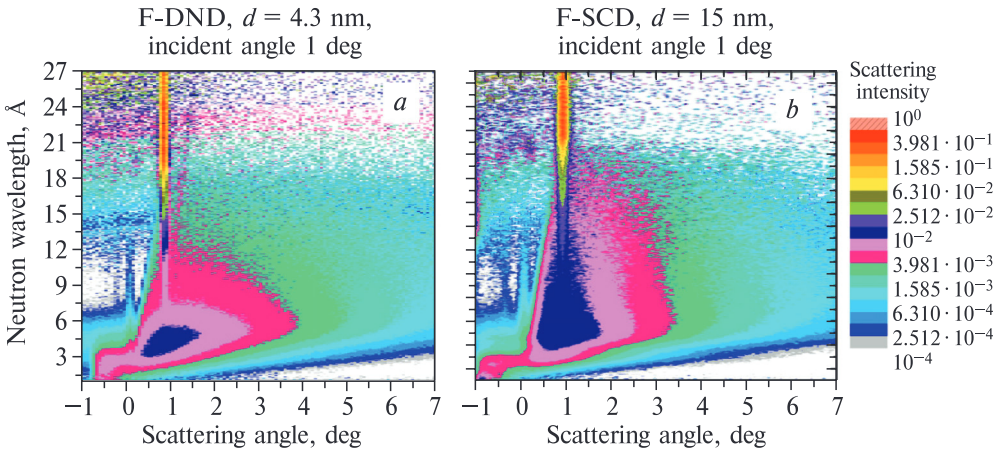

Probability of neutron scattering from the surface of powders of nanodiamonds of various sizes as a function of the neutron wavelength and scattering angle. Average size of nanoparticles in samples: *a*) 4.3 nm; *b*) 15.0 nm

The new results make it possible to refine theoretical models and, therefore, our understanding of the reaction mechanism [105].

Theoretical studies have been conducted to test the hypothesis of the existence of the acceleration effect in the following formulation: the result of the interaction of a particle with any object moving with acceleration should be a change in its energy and frequency, determined by the relation $\Delta\omega = ka\tau$, where k is the wave number, a is the acceleration of the object and τ is the interaction time. The results demonstrated a pronounced presence of the acceleration effect in all studied problems. In the case of resonance structures, the acceleration effect is proportional to the lifetime of the state inside the object. The results obtained confirm the hypothesis that the acceleration effect is a consequence of the existence of a nonzero interaction time in quantum mechanics [106].

The possibility of enhanced directional extraction of very cold neutrons (VCNs) from a source surrounded by a nanodiamond reflector was experimentally demonstrated. The gain factor for a narrow solid angle of extraction of VCNs with velocities of 57 and 75 m/s was 10. The gain factor for a wide solid angle was 33 for neutrons with a velocity of 47 m/s. This is equivalent to a multiple increase in the power of a nuclear research reactor. In practice, the obtained results can be used to develop an intense source of low-energy neutrons.

The effect of nanodiamond sizes on the efficiency of reflection of cold neutrons (CNs) at small grazing angles was studied. Measurements have shown that powder with a nanoparticle size of about 15 nm gives a higher albedo for neutrons with a wavelength of more than 4 Å and a lower albedo for neutrons wigh a wavelength of less than 4 Å compared to nanodiamonds with an average size of 4.3 nm. This phenomenon of quasi-specular reflection of CNs from nanopowders can be used to focus or transport CNs to research facilities in cases where other reflectors are destroyed in intense fields of ionizing radiation [107, 108].

In 2017–2021, the **IBR-2** reactor operation was organized in 7 or 8 cycles per year. Since October 2021, the nuclear facility has been switched to temporary shutdown mode for equipment replacement and obtaining a new license from Rostekhnadzor for the right to operate the IBR-2. The preparation of documents necessary for obtaining the license and their expert examination were carried out. After the license is issued, it is planned to resume the reactor operation for physics experiments.

In 2020, a second source of cold neutrons was put into trial operation in the direction of IBR-2 beamlines 1, 4, 5, 6, 9. To cool it, the Linde 1200 refrigerator with a cooling capacity of 1200 W at 10 K is used. The cold moderator provides continuous, stable operation for 11 days and gives a gain in the range of long-wavelength neutrons up to 9 (depending on the beamline and the region of the neutron spectrum) at a moderator material temperature of ~25 K [109].

Magnetic oxide is an unusual geometrically frustrated functional material with a tetragonally distorted spinel-type structure, demonstrating pronounced magnetocaloric, magnetoelastic and magnetodielectric effects, which, along with academic interest, also have practical significance. The crystal and magnetic structure of Mn_2O_3, Mn_3O_4 was studied using neutron diffraction in the pressure range up to 20 GPa and temperatures of 15–300 K. At pressures above 2 GPa, the suppression of low-temperature modulated phases and the stabilization of the ferrimagnetic phase were observed. The magnetic structure of the high-pressure orthorhombic phase at $P = 20$ GPa was determined. In this phase, at $T_N = 275$ K, a long-range AFM order is formed

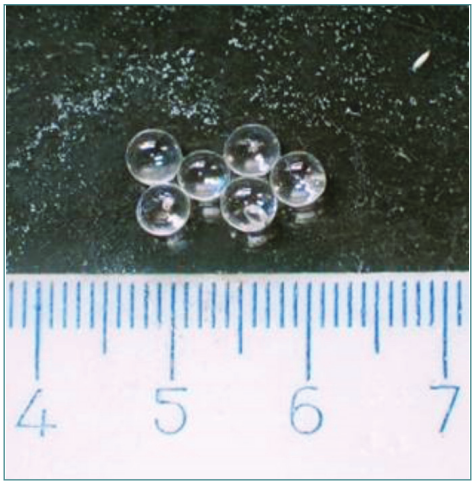

Mesitylene beads are the working substance of a cold retarder

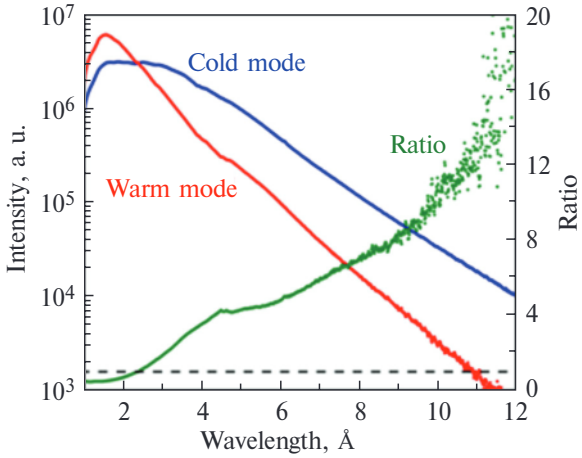

Neutron flux spectrum and gain factor on experimental beamline 5 for the cryogenic and thermal modes of operation of the CM-201 combined moderator

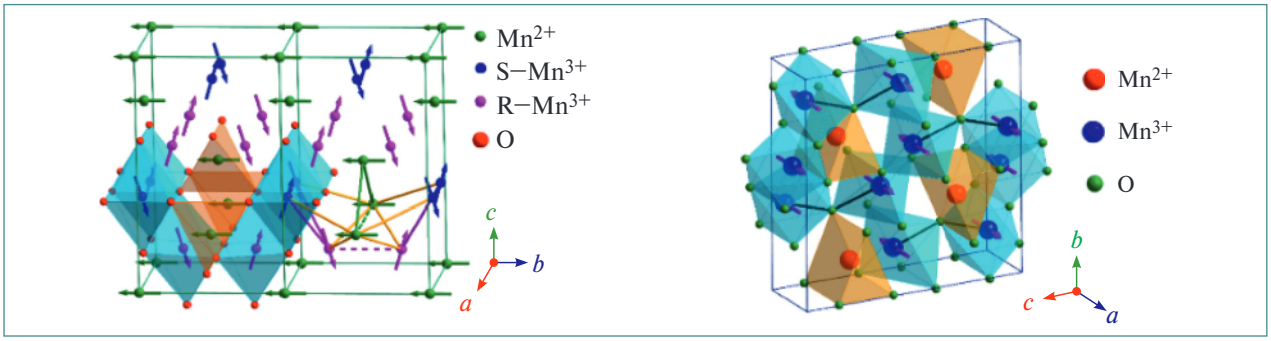

Schematic representation of the modulated magnetic structure occurring below $T_{N3} \sim 33$ K at ambient pressure and the geometry of competing magnetic interactions (left), as well as the magnetic structure of high-pressure orthorhombic phase (right)

with the propagation vector $k = (1/2, 0, 0)$ on the Mn^{3+} sublattice, while the Mn^{2+} sublattice remains magnetically disordered. Thus, the temperature of magnetic ordering under pressure increases by more than a factor of 6, which is a unique case among known magnetic materials [110, 111].

Layered van der Waals magnetic materials with magnetic lattice symmetry similar to graphene demonstrate that they retain magnetic order at sufficiently high temperatures even for a single atomic layer. Such materials have broad prospects in developing heterostructures for a new advanced generation of spintronics, nanoelectronics, information recording and storage devices.

Using neutron diffraction and Raman spectroscopy, the structural, magnetic and vibrational properties of a model representative of the family of CrX_3 van der Waals magnetic compounds — $CrBr_3$, were studied. The magnetic moments of Cr ions forming a graphene-like magnetic lattice in Br–Cr–Br layers are ordered ferromagnetically at a temperature $T_C = 37$ K. Anomalous behavior of structural characteristics was found in the vicinity of the ferromagnetic ordering temperature T_C. Below this temperature, the nature of thermal expansion changed from positive to negative [112].

In collaboration with the RAS Institute of Archeology, work was performed in one of the new areas — nondestructive research of the internal structure of cultural heritage items using neutron radiography and tomography. 3D models of fragments of a bracelet and a star-like radial colt from the Tver treasure (dated to the XIII–XIV centuries AD, found in 2014 in Tver) were reconstructed from neutron tomography data. Their analysis makes it possible to draw conclusions about the specific features of manufacturing technologies for such products in the given period of time. A comprehensive study of the internal structural organization and phase composition of a fragment of the Chelyabinsk meteorite was also carried out. The bulk mineral composition and spatial distribution of different components were determined [113, 114].

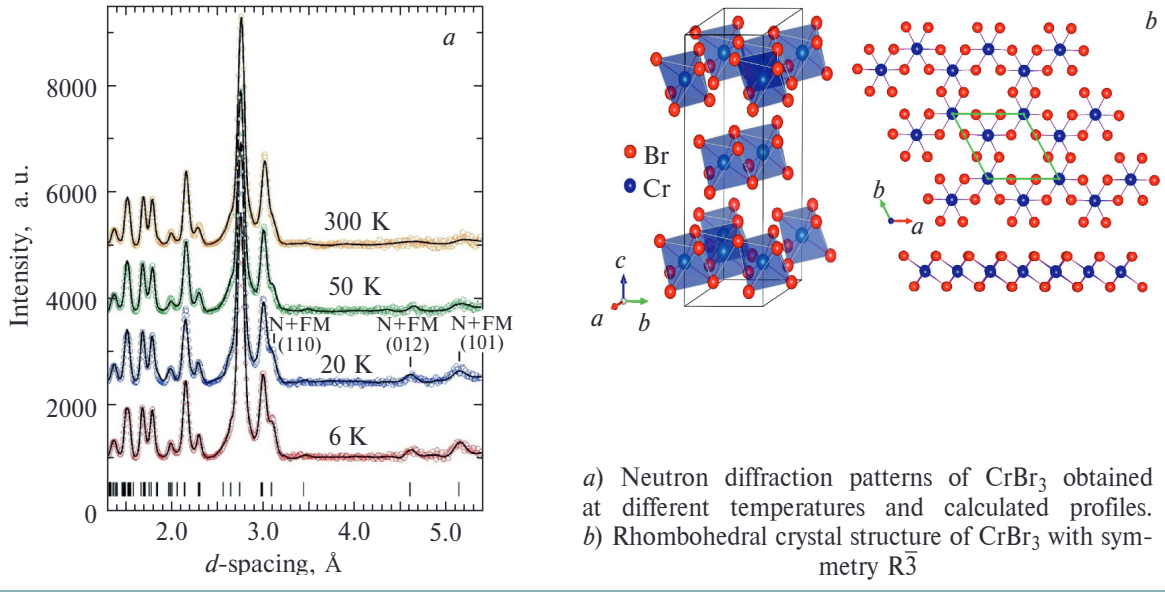

a) Neutron diffraction patterns of $CrBr_3$ obtained at different temperatures and calculated profiles. *b*) Rhombohedral crystal structure of $CrBr_3$ with symmetry $R\bar{3}$

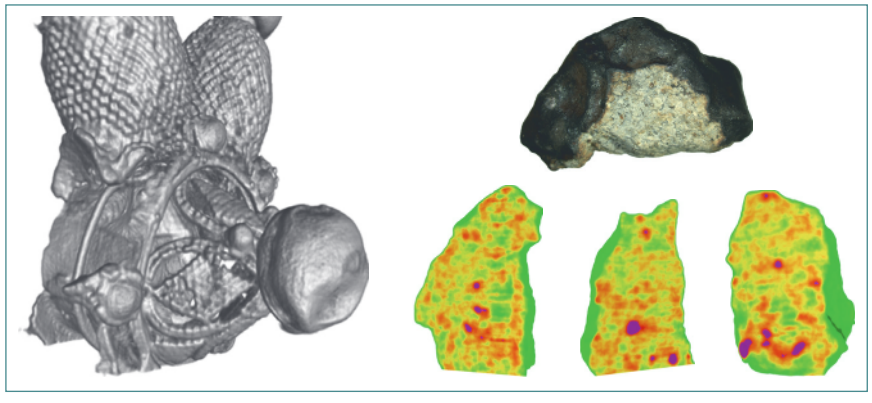

Left: Three-dimensional model of a fragment of the radial colt reconstructed from neutron tomography data. Right: A fragment of the Chelyabinsk meteorite and fragments of a 3D model of the internal organization of the studied sample. Pink areas correspond to metallic inclusions

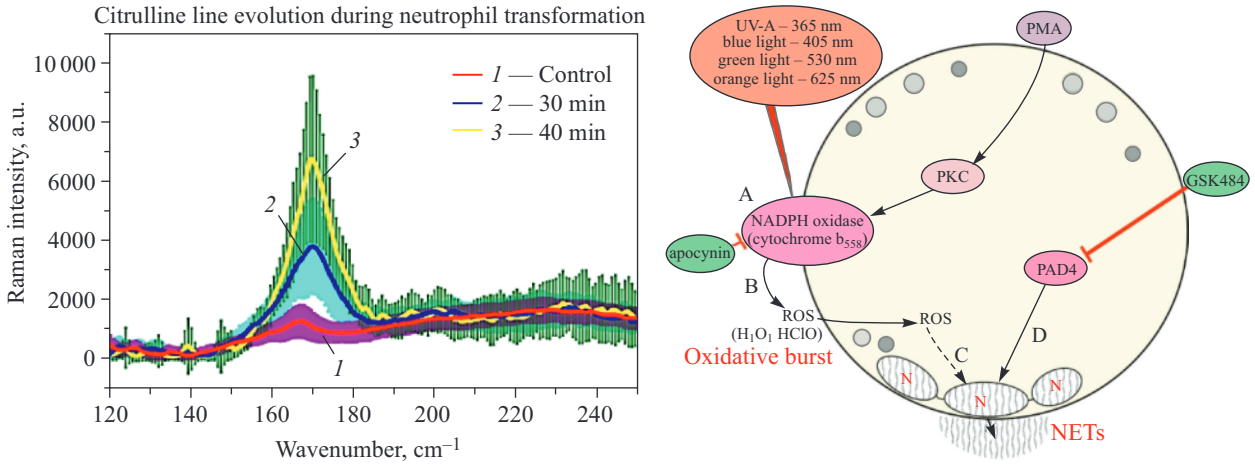

Left: Low-frequency region of the Raman spectrum of neutrophils: evolution (increase) of the intensity of the citrulline line, indicating pre-activation of NETosis. Right: Photo-induced NETosis signaling pathways

Raman spectroscopy was used to analyze neutrophils transformed during NETosis, which is a process of programmed neutrophil cell death.

Neutrophils are a type of leukocytes involved in the phagocytosis of pathogenic microorganisms (bacteria, fungi, protozoa). Activation of neutrophils induces NETosis, which is accompanied by the release of extracellular pathogens and minimizes harm to other cells. At the initial stage, under the action of special enzymes, a specific citrullination reaction takes place, by which we can judge the beginning of the NETosis activation process. Highly sensitive Raman spectroscopy made it possible to reveal the evolution (growth) of the citrulline peak in the low-frequency region of the spectrum within 30–40 min after the onset of cell activation, which can be classified as an early diagnosis of NETosis [115–117].

The interaction of model biological membranes with amyloid-beta peptide was studied using small-angle neutron scattering (SANS).

For the first time, the results showed a rearrangement of the overall membrane shape between spherical vesicles and flat nanodiscs in the presence of amyloid-beta peptides. This process clearly points to the destructive effect of the peptide. Interestingly, the observed mechanism could be directly related to the destruction of neuronal cells in Alzheimer's disease [118, 119].

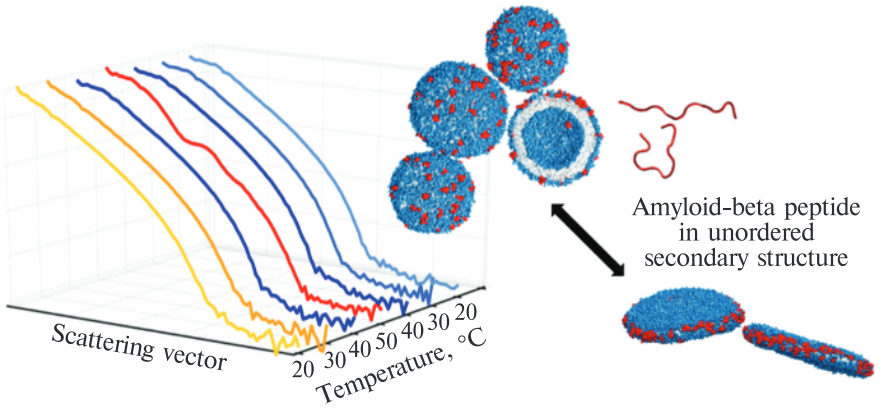

SANS curves demonstrating the destructive effect of amyloid-beta peptide on the model membrane by changing its shape from large vesicles to small vesicles and nanodiscs. The results of molecular dynamics simulations illustrate the morphological changes

DEVELOPMENT OF THE IBR-2 SPECTROMETER COMPLEX

In cooperation with the National Institute for Research and Development in Electrical Engineering (ICPE-CA, Bucharest, Romania), a cryomagnetic sample environment system for the DN-12 diffractometer of the IBR-2 reactor has been developed and constructed. The system consists of a magnet based on a high-temperature superconductor in a cryostat and a cryostat insert with a high-pressure chamber with a sample. The magnet is made in a Helmholtz pair configuration with a maximum magnetic field of 5 T.

The new device will significantly expand the possibilities for the study of condensed matter on the spectrometric base of the IBR-2 reactor. It makes it possible to independently vary the parameters on the sample under study during the neutron scattering experiment: the magnitude of the magnetic field, temperature, and pressure [120].

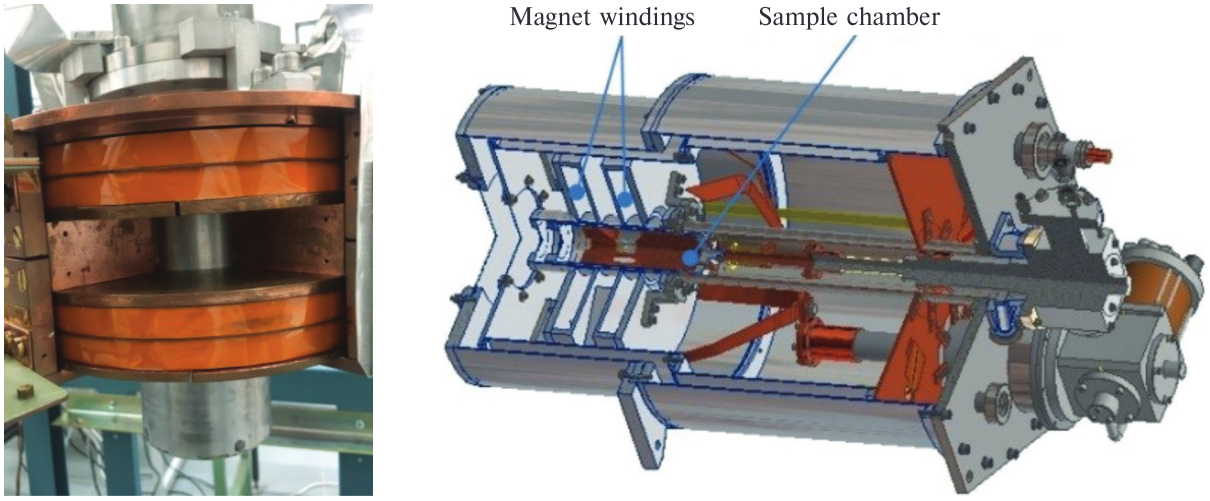

Left: External view of the cryomagnet implemented in the form of a Helmholtz pair, where a high-temperature superconductor tape 12 mm wide and 0.1 mm thick with a compensation layer of copper is used as a conductor. Right: 3D model of a cryomagnetic system based on the SRDK408S cryocooler

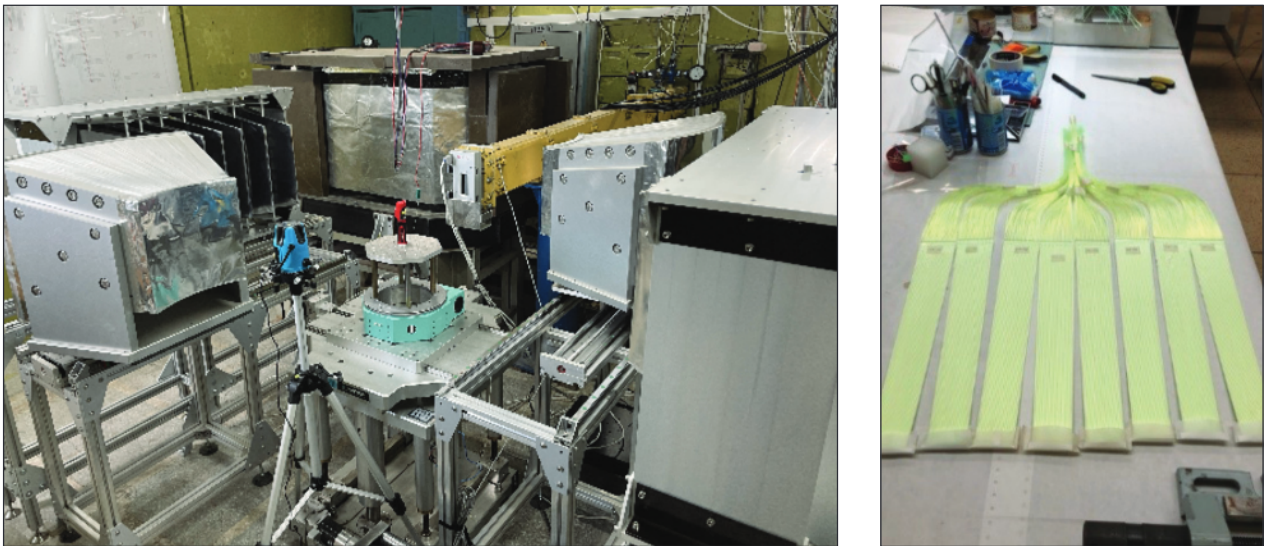

Left: ASTRA-M detector at the FSD spectrometer. Right: External view of individual elements of the ASTRA-M detector. The element is a (Ag)/^{6}LiF scintillator plate, which is shaped like a time-focusing surface with glued wavelength-shifting fibers that transmit the light flux from the neutron capture site to the photomultiplier

Works on the development of the ASTRA-M scintillation detector for Fourier stress diffractometer (FSD) were completed.

The main purpose of the spectrometer with the new ASTRA-M detector is the measurement of residual stresses in samples. The ASTRA-M detector implements a combined focusing method, when the entire range of observation by the scattering angle is divided into sectors, within each of which an independent detector is built corresponding to an individual time-focusing surface. The total covered solid angle is $\Omega = 0.55$ sr. High spatial resolution is achieved by reducing the size of the scattering volume due to the specific collimation [121].

Using charged particle beams of JINR accelerators, the mechanisms were clarified that determine differences in the lethal and mutagenic effectiveness of radiation with different physical characteristics. It has been established that under exposure to electromagnetic radiation and accelerated heavy charged particles, DNA damage of different quality is formed. Unlike photons, which induce single lesions, accelerated charged particles induce clustered DNA damage. The latter is difficult to repair by cells and determines the specifics of various radiation-induced effects. During the reporting seven-year period, research was aimed at studying the detailed structure of such damage and its repair in different systems.

Research on the Formation Mechanisms of Molecular Damage to the DNA Structure and Its Repair after Exposure to Heavy Charged Particles of Different Energies

The induction and repair were studied of DNA double-strand breaks (DNA DSBs) in mammalian and human cells after exposure to ionizing radiation with different physical characteristics. The kinetics was analyzed of the formation and elimination of radiation-induced foci (RIF) γH2AX/53BP1 in the nuclei of irradiated human fibroblasts and in mature neurons of a primary rat hippocampal culture.

The formation and repair of complex DNA DSBs involving modified bases were studied. It has been shown that with increasing radiation's LET, the RIF formation peak shifts to later times after irradiation, and the complexity of RIF clusters also increases [122].

In collaboration with Czech and German colleagues, a new method has been developed to analyze the fine structure of clustered DNA damage with ultra-high resolution. It is based on single-molecule localization microscopy. Using this method, the structure of clustered DNA DSBs was studied, and a comparative study was performed of their repair kinetics in human normal and tumor cells after irradiation with accelerated ^{15}N ions. The proposed approach allows obtaining new information about the nature of radioresistance of a number of tumors [123].

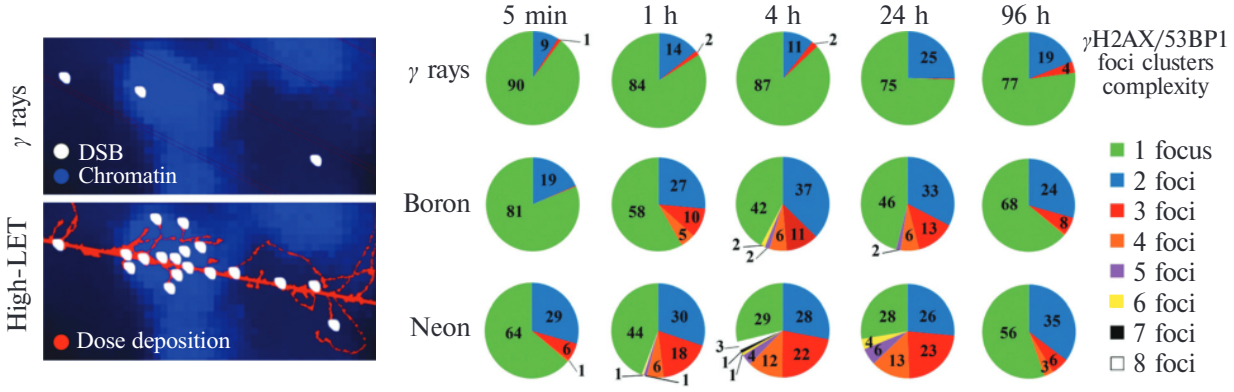

Formation of γH2AX/53BP1 foci clusters of various composition in nuclei of normal human skin fibroblasts after irradiation with ^{60}Co γ rays and ^{11}B and ^{20}Ne ions

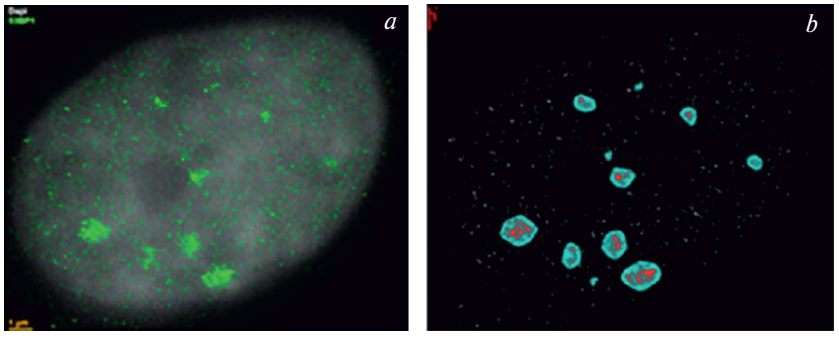

Visualization of the structure of 53BP1 repair protein clusters in nuclei of human U87 glioblastoma cells 24 h after exposure to 1.3 Gy of 13 MeV/nucleon ^{15}N ions. *a*) Microscope images; *b*) software post-processing

Fundamental Aspects of Increasing the Radiosensitivity of Tumor Cells under Proton Beam Exposure

A fundamentally new method for increasing the biological effectiveness of medical proton beams and gamma therapeutic units has been developed and patented. The method makes it possible to bring the biological effectiveness of proton irradiation closer to the effectiveness of irradiation with carbon ions. The approach is based on the use of 1-β-D-arabinofuranosylcytosine (AraC) — an officinal drug used in the treatment of hematopoietic system cancer. It has been established that when the drug is administered before irradiation of human cells with ionizing radiation, DNA single-strand breaks are transformed into lethal double-strand breaks [124, 125].

Specialists of LRB JINR and A. F. Tsyb Medical Radiological Research Centre studied the molecular and cellular mechanisms of the combined effect of AraC and proton radiation on the B16 murine melanoma *in vivo*. The control (non-irradiated) animals died on the 30th day as a result of tumor development. After combined exposure, the mean volume of tumors, compared with proton irradiation with no modifier, decreased 1.7–3.4-fold at different observation times ($p < 0.05$).

At the molecular level, it has been shown that the number of DNA double-strand breaks (DSBs) in tumor cells 2 days after completion of irradiation sessions significantly exceeds the DNA DSB level after radiation exposure without a modifier. It has been shown that the introduction of AraC enhances the antitumor effect of proton radiation through several mechanisms, including a decrease in the number of tumor stem cells, inhibition of cell proliferation, and angiogenesis in the tumor against the background of changes in the immune response in the primary focus and its infiltration by lymphocytes [126–129].

A metaphase analysis was performed of the formation of chromosomal aberrations in human Cal51 carcinoma cells and normal human peripheral blood lymphocytes after irradiation with photons and protons (150 MeV and Bragg peak). Using the prema-

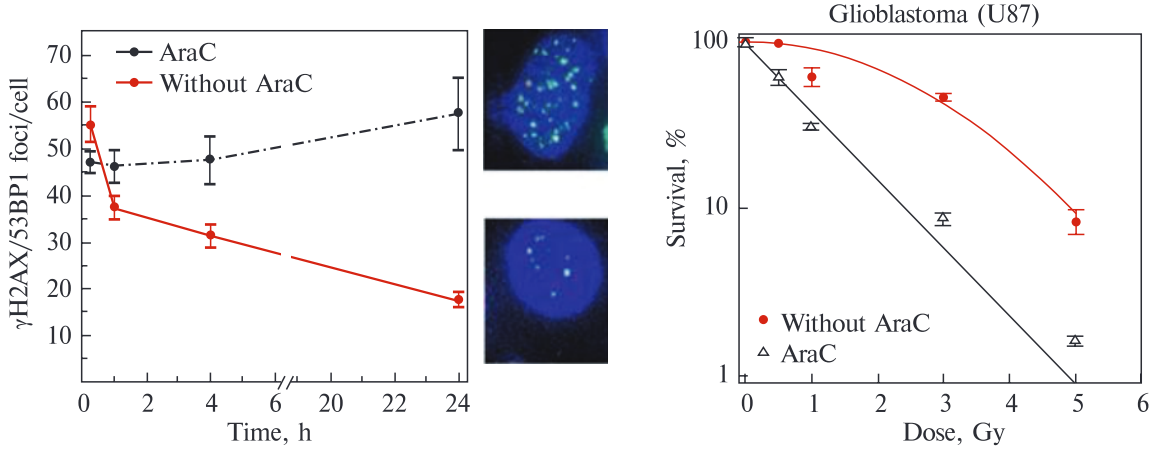

Formation and elimination kinetics of γH2AX/53BP1 foci in nuclei of human U87 glioblastoma cells (left) and survival curves (right) after combined exposure to AraC and 1.25 Gy of spread-out Bragg peak protons

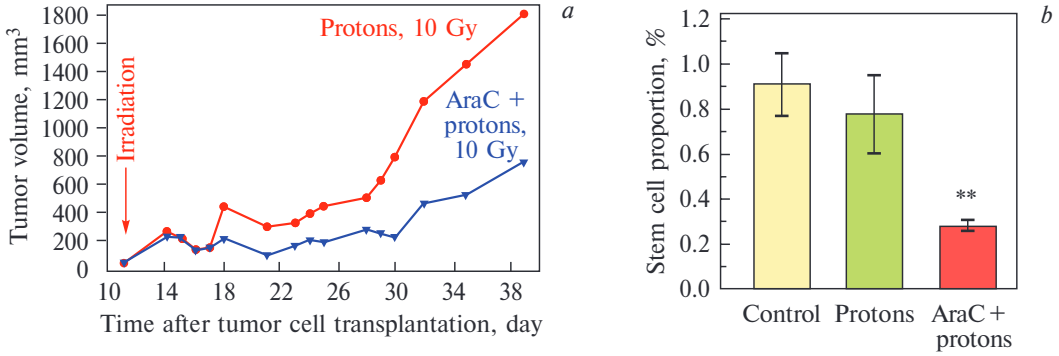

a) Inhibition of B16 melanoma tumor growth in mice after irradiation with protons and combined exposure to AraC and protons at a dose of 10 Gy. *b*) The proportion of tumor stem cells in the primary B16 melanoma focus 9 days after proton irradiation and combined exposure to AraC and protons

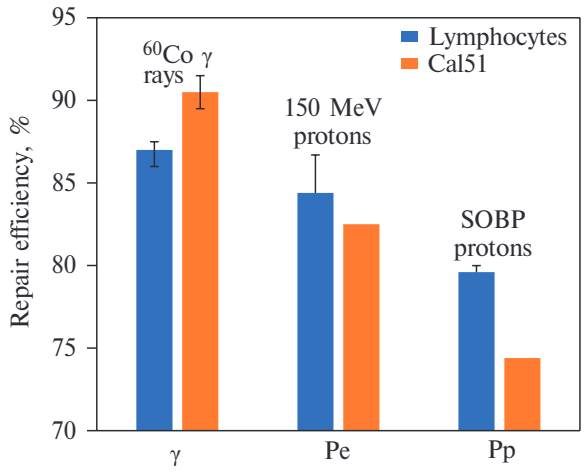

Efficiency of chromatin break repair in normal human lymphocytes and Cal51 carcinoma cells

ture chromatin condensation method, the proportion of successfully repaired chromatin breaks was assessed 12 h after irradiation. For γ-ray exposure, a more effective repair of chromatin breaks was observed in tumor cells compared with normal ones than for proton exposure. The results indicate the preference for the use of proton beams in radiation therapy for breast carcinoma [130].

Research on the Formation Mechanisms of Gene and Structural Mutations in Mammalian Cells after Exposure to Accelerated Heavy Charged Particles

Radiation-induced mutagenesis was studied in V79 Chinese hamster cells after exposure to accelerated ^{11}B, ^{20}Ne and ^{18}O ions with different LET and ^{60}Co γ rays. The maximum yield of mutant clones was observed at different times depending on the characteristics of ionizing radiation, the position of the maximum shifting toward later times with increasing LET. The dependence of the position of the maximum yield of the mutant fraction on LET can be well described by an exponential function. In mutants induced by ions, an increase in the level of deletions was observed with increasing LET (up to ~40%). In spontaneous mutants, clones with deletions accounted for no more than 10% [131, 132].

Research on the Radiation-Induced Disorders in Different Structures of the Rodent Brain

A comparative study was performed of behavioral disorders and morphological changes in the brain of adult female rats after 1 Gy irradiation with ^{60}Co γ rays and protons of various energies. Impairments of short-term memory and motor and exploratory activity of animals were observed. A comparative pathomorphological analysis of possible causes of behavioral disorders revealed early amyloidosis, autolysis of the ependymal layer, neurodegenerative changes in different brain structures, and the development of neuronal hypertrophy. It has been shown that the observed destructive changes increase with increasing the particles' LET, which was 0.2 keV/μm (γ rays), 0.5 keV/μm (170 MeV protons), and 0.97 keV/μm (70 MeV Bragg peak protons) [133].

The effect was studied of ^{60}Co γ rays at a dose of 2 Gy on behavioral reactions, immunohematological status, and morphology and functions of neurons in the central nervous system of seven-month-old ICR mice.

Using the open field test system, differences in the behavior of irradiated animals were revealed, expressed in an increase in the number of rearings and a change in the strategy of motor activity. After irradiation, the development of leukopenia and a decrease in the glioneuronal index in the brain parenchyma of mice were observed [134].

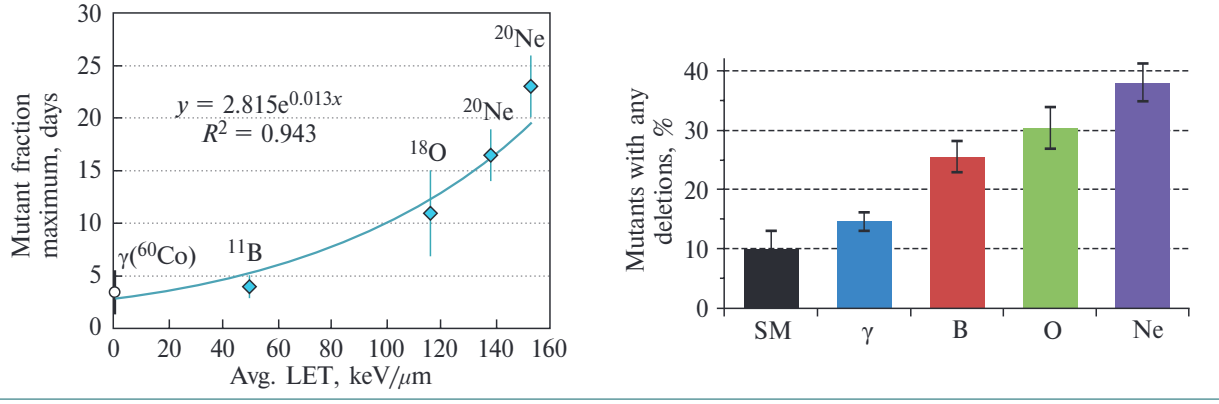

The maximum level of radiation-induced mutagenesis in Chinese hamster cells and structural changes in the *hprt* gene depending on the expression time and LET of accelerated ions

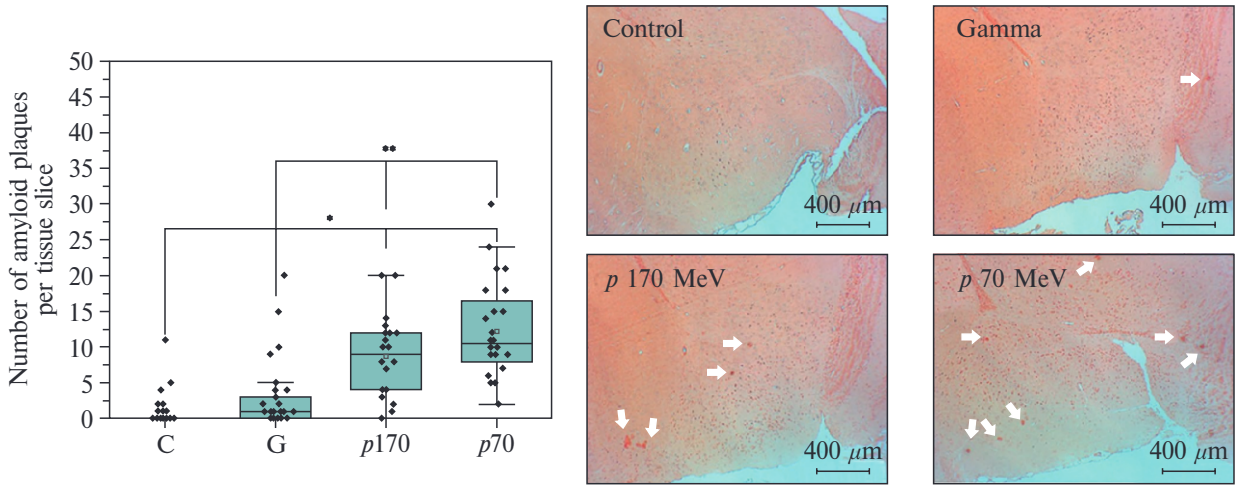

Amyloid plaques in the forebrain of rats 30 days after irradiation (marked by white arrows on the sections). C — controls; G — ^{60}Co γ rays; *p*170 — 170 MeV protons; *p*70 — 70 MeV protons

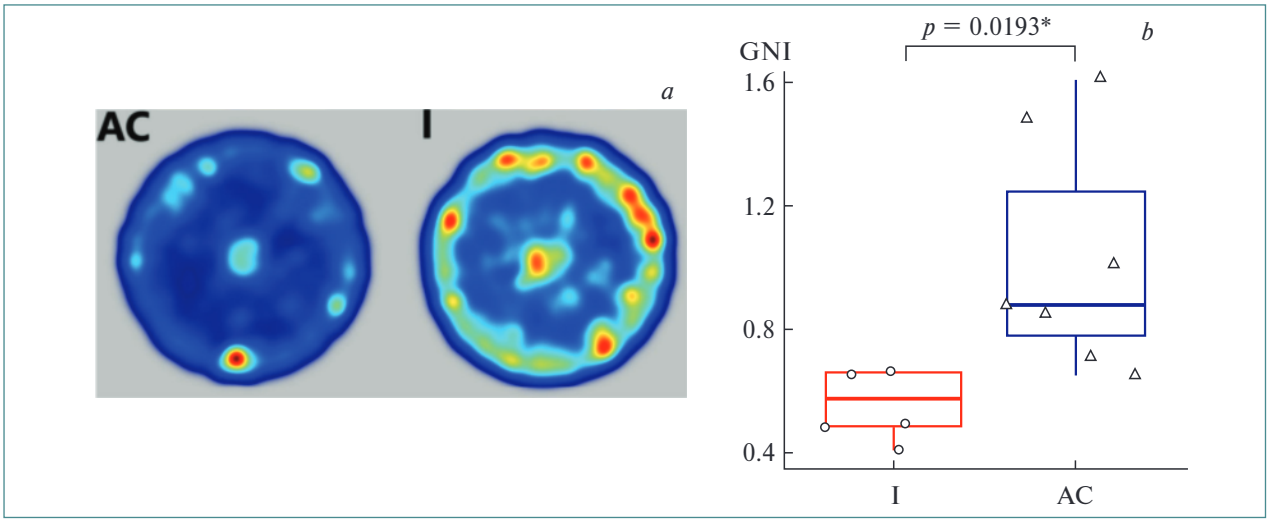

a) Thermal map of movement in the open field test. *b*) Glial neuronal index (GNI) of irradiated mice compared with aged control mice. Number of animals: I — irradiated ($n = 10$); AC — aged control ($n = 10$). Noldus EthoVision software

Mathematical Modeling of Molecular Mechanisms of Disorders in the Structure and Functions of the Central Nervous System after Exposure to Accelerated Heavy Charged Particles

An original modeling method has been proposed for microdosimetric calculations of radiation damage in neurons and their subcellular structures after exposure to accelerated charged particles. Based on the developed model, using the Geant4-DNA software, formation of radiation-induced DNA damage in hippocampal cells of the rodent brain was analyzed.

Based on data on DNA damage in the nuclei of nerve cells, survival rates of a radiosensitive population of cells of the subgranular zone of the hippocampus were calculated for accelerated heavy charged particle exposure [135, 136].

A mathematical model of the CA3 region of the hippocampus was developed using the NEURON software. Based on this model, the occurrence has been calculated of synchronous neural oscillations that contribute to the formation of the γ and θ rhythms, which play an important role in the mechanisms of memory and learning. Using the example of the ionotropic glutamate receptor NMDA, which plays the key role in the regulation of synaptic plasticity, learning, and the formation of various types of memory, with the NAMD software, molecular dynamics modeling was performed of the activation process of the full atomic structure

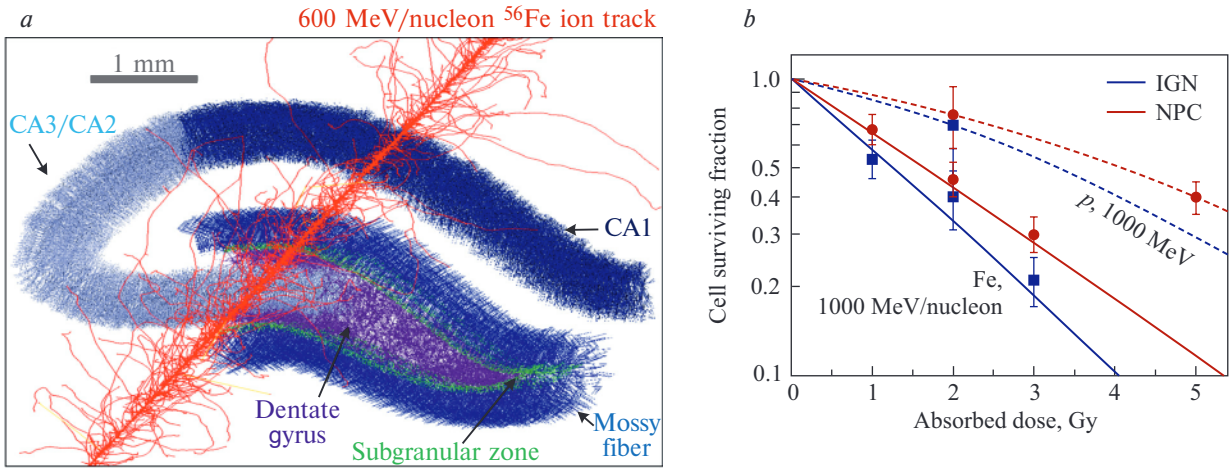

a) Monte Carlo simulation of 600 MeV/nucleon ^{56}Fe ion track structure in a three-dimensional model of the rat hippocampus. *b*) Calculation of the survival of neural progenitor cells (NPC, red lines, • — experiment) and immature granular neurons (IGN, blue lines, ▪ — experiment) after irradiation with protons (dashed lines) and iron ions (solid lines) with an energy of 1 GeV/nucleon

of the NMDA receptor. The influence is considered of single- and double-point mutations, as well as structural mutations (deletions), on the structure of the ion channel and on the functioning of the neural network as a whole. The proposed model approach allows evaluation of the effect of mutations in the genes of hippocampal neurons on synaptic receptors. This approach was tested on the experimentally known effects of mutations in the transmembrane domain leading to epileptic disorders. By the activity character of the neural network and the corresponding electroencephalogram, it is possible to assess the macroscopic effect of a particular mutation type [137].

Radiation Research

In order to develop experimental methods for assessing the radiation risk of space flights under terrestrial conditions, a unique simulator of the radiation field inside the habitable module of a spacecraft in deep space has been proposed and patented. It reproduces in the correct ratio all components of the radiation field inside the spacecraft, averaged over solar activity [138–140].

A number of studies have been conducted to assess the radiation risk to astronauts during long-term interplanetary flights and to develop methods of experimental space radiobiology. Detailed calculations of the spectra of all components of the radiation field

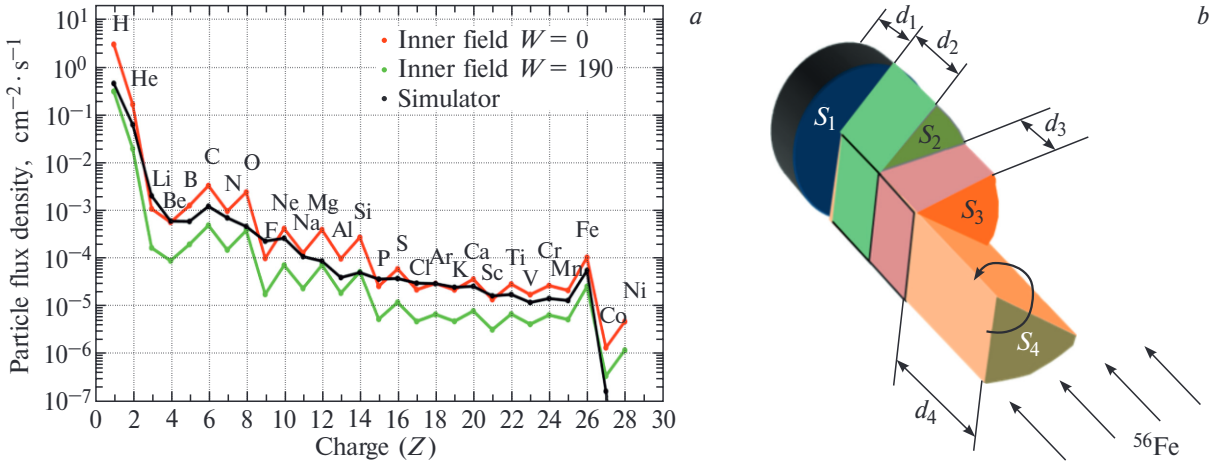

a) Comparison of the calculated charge distributions of particles in the internal radiation field of a spacecraft at the minimum and maximum solar activity and the calculated charge distribution of particles in the field behind the simulator. *b*) Schematic view of the simulator converter

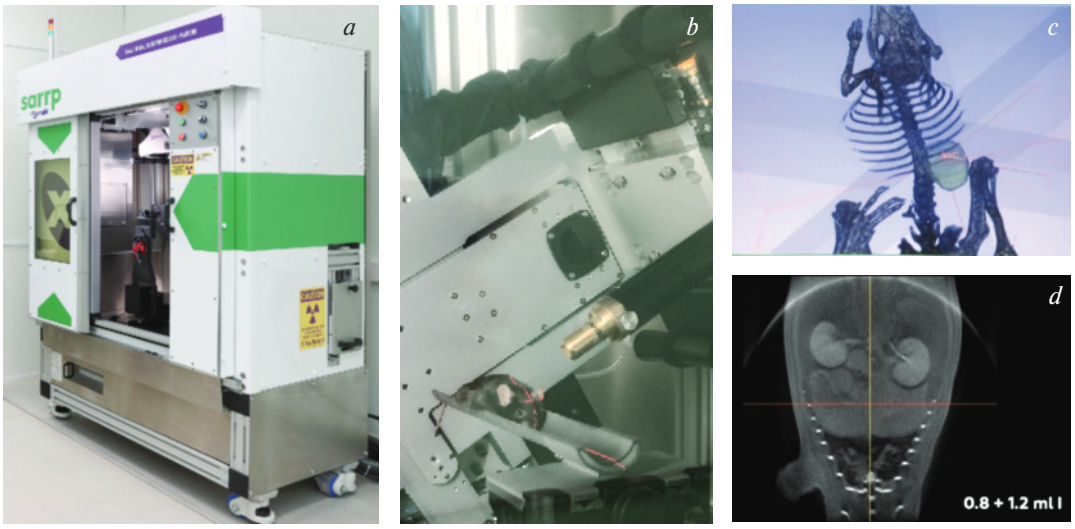

SARRP facility. General view (*a*), irradiation of a mouse during an experiment (*b*), irradiation planning system (*c*), computed tomography of the internal organs of a mouse with a contrast agent (*d*)

inside the habitable module of the spacecraft from galactic cosmic radiation were carried out for minimum and maximum solar activity. The calculations were verified using the only available experimental data from the RAD and Liulin-MO instruments and showed good agreement with experiment. The adjusted fluence — effective dose conversion factors were calculated for all components of the radiation field inside the spacecraft [141, 142].

A monograph has been published, which examines the main specifics of the formation of ionizing radiation fields at high-energy proton and heavy ion accelerators; the activation of equipment, refrigerants, air, and shielding; and the development of radiation monitoring tools [143].

Two X-ray facilities were put into operation: a compact CellRad irradiator (Precision X-ray Inc., the U.S.) for work with cell cultures and a multifunctional SARRP (Small Animal Radiation Research Platform) complex (Xstrahl Ltd., the U.K.) for radiobiological studies on small laboratory animals with the possibility of X-ray tomography and highly conformal irradiation.

Astrobiological Research

In collaboration with colleagues from Italy and the Czech Republic, the formation was studied of complex prebiotic compounds, including nucleic bases, after irradiation of simple organic compounds with protons in the presence of meteorite matter as a catalyst. A new mechanism has been proposed that promotes the formation and processing of insoluble organic matter in meteorites and during prebiotic processes [144–146].

A series of studies of fossilized microorganisms (microfossils) in meteorites has been carried out using scanning electron microscopy and energy-dispersive X-ray microanalysis. The first illustrated atlas of microfossils from the Orgueil meteorite has been released [147].

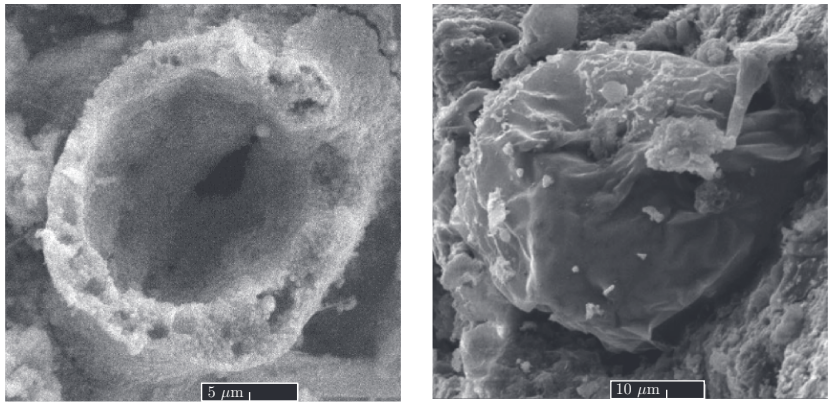

Images of fossilized microorganisms from the Orgueil meteorite

At **Linac-200**, an extensive user programme is being created to be used for:
— beam tests and calibration of detectors for the MPD and SPD experiments (electromagnetic calorimeters, straw detectors, vertex detectors), elements of the NICA collider beam diagnostic system and detectors for other experiments;
— development of an accelerator source of terahertz radiation with a tunable spectrum for radiobiological research (LRB);
— irradiation of biomaterials and detectors for space experiments (DLNP, IBMP);
— study of photonuclear reactions (FLNR, DLNP, BLTP, MSU, University of Novi Sad (Serbia));
— radiation materials science (Sarov, Tomsk University).

The accelerator hall contains the 5th and the 6th stations of the facility with energies up to 400 MeV. Work is underway to create an automated control system of Linac-200.

Compact Precision Laser Inclinometer (**CPLI**) has established itself as a high-precision, reliable instrument for recording the angular oscillations of the Earth's surface. The achieved instrumental accuracy is 10^{-9} rad.

During 2022, six new-type CPLIs were created. Their placement in scientific centres of Russia and abroad has begun.

Two CPLIs are installed in the MPD detector hall of the future NICA collider. For several months, monitoring of angular microseisms from industrial noise and natural phenomena was carried out. The largest microseisms reach amplitudes of 4 mkrad. Possible ways to suppress industrial interference to stabilize the collider beam focus are the introduction of feedback into the control system of the collider magneto-optics and/or the use of piezo stackers [148].

TARDISS (Cell Genetics). In 2021, the group of researchers from DLNP performed Stage II of the experiment at the Baksan Neutrino Observatory (BNO) of the Institute for Nuclear Research of the Russian Academy of Sciences (INR RAS) on the study of ultradeep microbial communities inhabiting

Linac-200

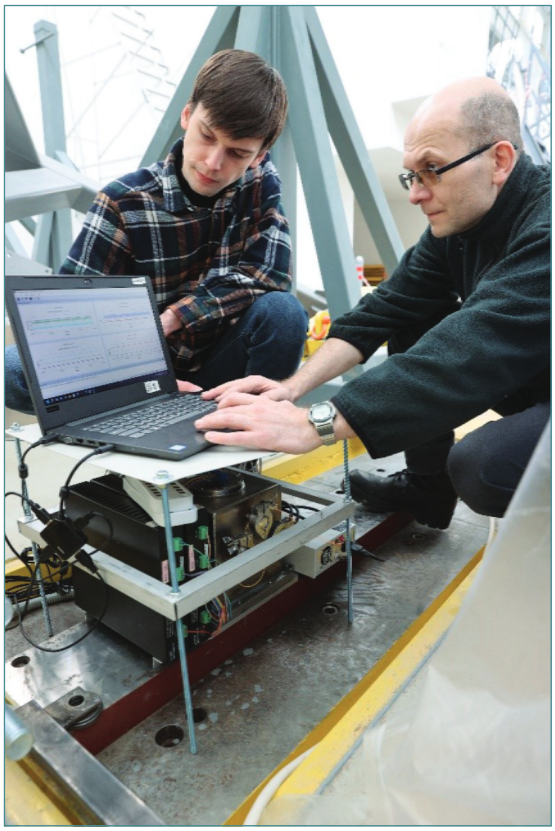

Installation of a compact laser inclinometer in the MPD NICA hall

the extreme environment near the Elbrus magma chamber. Water, soil and inorganic sediments were sampled in an underground hot spring at a distance of 4200 m away from the cross-passage entrance.

Joint experiments of JINR and INR RAS were carried out to study the effect of low-radiation background on model biological objects. For the first time, all *D. melanogaster* genes that changed their expression in conditions of low-background laboratory were identified using RNA sequencing. Analysis of the data indicates that there is no effect of a decrease in the radiation background on a complex model organism [149].

Within the framework of the international UN programme "Atmospheric deposition of heavy metals in Europe — assessments based on the analysis of moss biomonitors", work was carried out to assess air pollution in 12 JINR Member States: Armenia, Azerbaijan, Belarus, Bulgaria, Georgia, Kazakhstan, Moldova, Mongolia, Romania, Russia, Slovakia, and Vietnam. The data presented in the Atlas of atmospheric deposition of heavy metals "Mosses as biomonitors of air pollution" on the simultaneous collection of biomonitor mosses over large areas make it possible to assess both spatial and temporal trends in the concentrations of heavy metals, as well as to identify areas with high levels of pollution as a result of local and transboundary transport of metals [150].

Within the framework of the current collaboration between the Academy of Scientific Research and Technology (ASRT, Egypt) and JINR, work was conducted to give a comprehensive picture on the assessment of the ecological situation in Egypt using soil and sediments samples from the Nile River and its Delta, the coastal areas of the Mediterranean and Red Seas. The characterization of the samples was given using two analytical techniques:

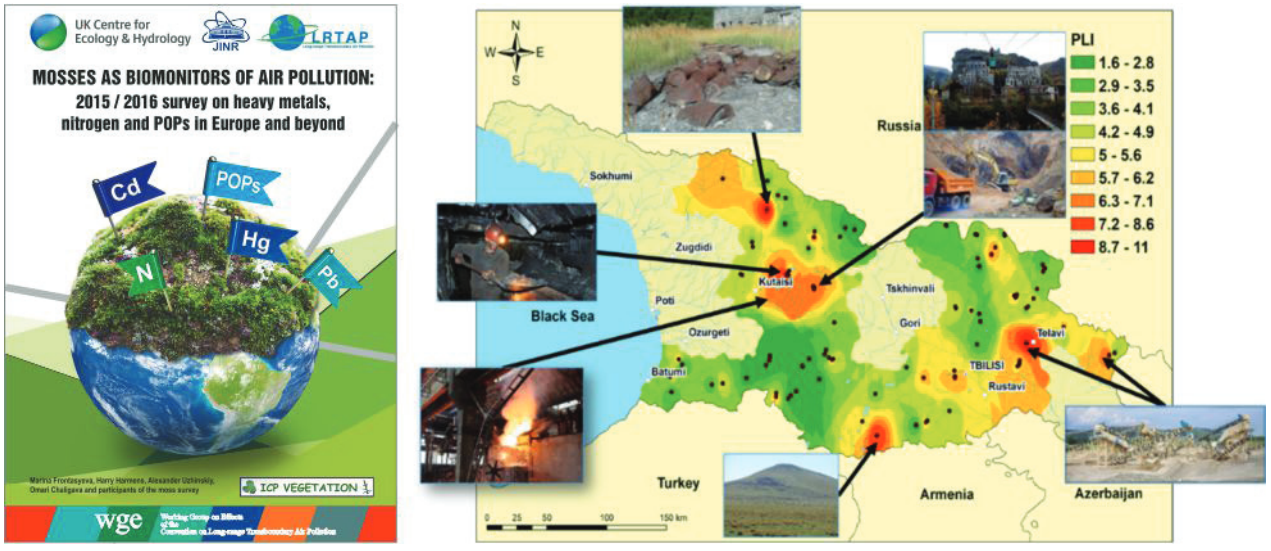

Left: Atlas of atmospheric deposition of heavy metals. Right: Spatial distribution of the air pollution load index (PLI) in Georgia

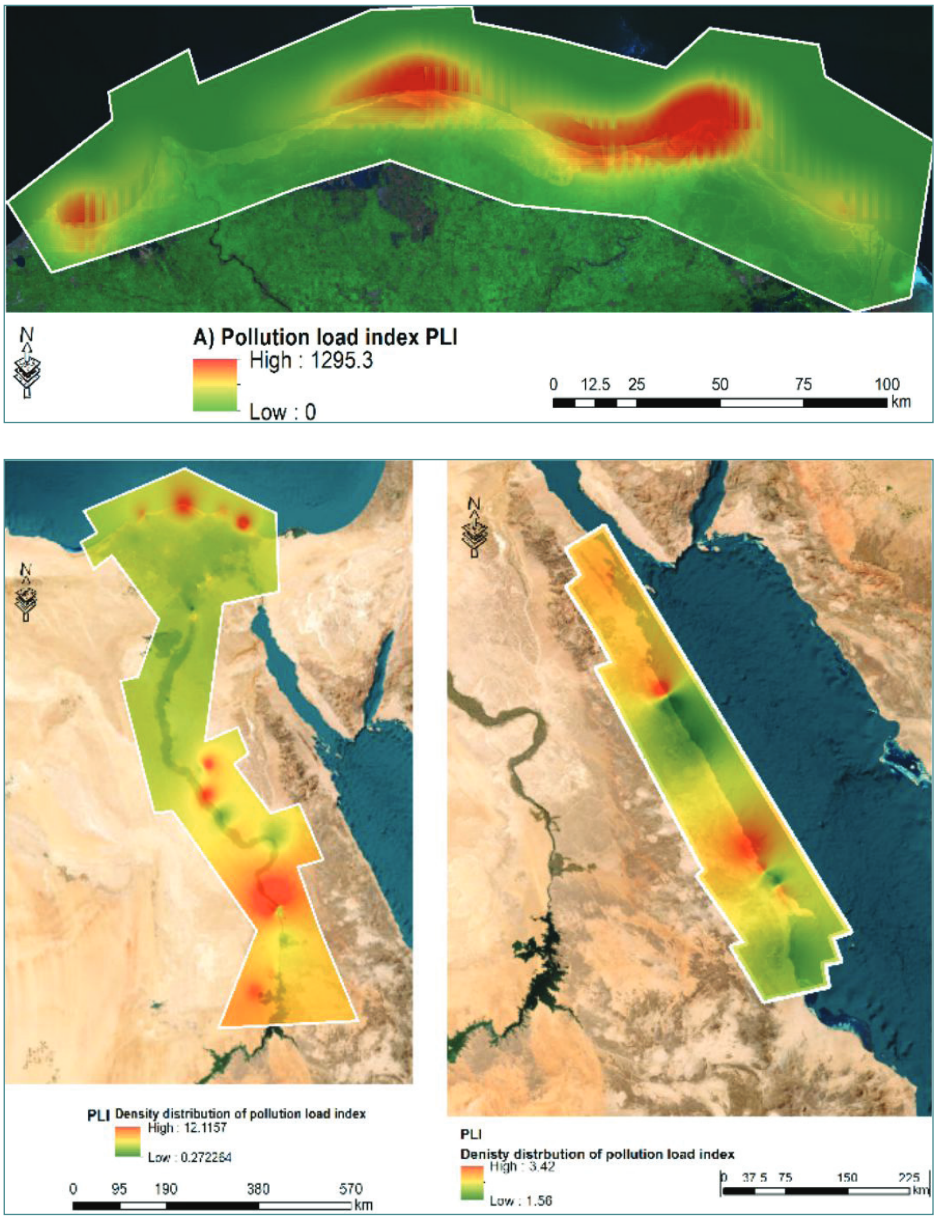

Spatial distribution of pollution load index along the coastal areas of the Mediterranean Sea, the Nile River and its Delta

neutron activation analysis (NAA) and inductively coupled plasma mass spectrometer (ICP-MS).

The characterization of the samples in terms of pollution revealed that this is not uniform and that some sites are relatively more polluted than others, but overall do not pose a significant risk to humans and the environment. Nevertheless, continuous monitoring is highly recommended in view of possible future changes [151, 152].

One of MLIT's major directions in the Seven-Year Plan for the Development of JINR for 2017–2023 was the planned development of a world-class Multifunctional Information and Computing Complex (MICC) at the Institute. It encompassed the following: the development and enhancement of the JINR telecommunication and network infrastructure; the modernization of the MICC engineering infrastructure; the modernization, development and creation of new MICC components for data storage, processing and analysis; the development of the IT infrastructure of the NICA project; the enhancement of the performance and volume of the data storage systems of the grid components, i.e., Tier1 and Tier2; the enlargement of the cloud infrastructure resources and establishment of an integrated cloud environment for the JINR Member States; the expansion of the HybriLIT heterogeneous computing complex. All indicators of the Seven-Year Plan were attained [153, 154].

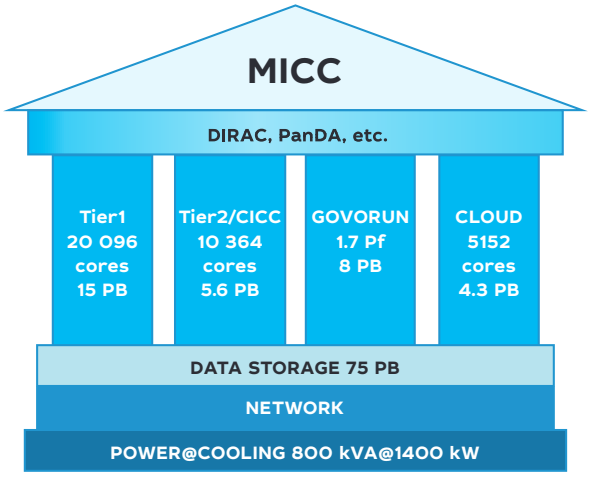

JINR Multifunctional Information and Computing Complex

JINR Network Infrastructure. The JINR network infrastructure reached a new technological level. The bandwidth of the Moscow–JINR telecommunication channel was increased from 100 Gb/s to 3×100 Gb/s, the capacity of the Institute's backbone was enhanced from 10 Gb/s to 2×100 Gb/s, and a distributed computing cluster network was built between the DLNP and VBLHEP sites with a bandwidth of up to 400 Gb/s, which meets the requirements of the NICA megaproject.

MICC Engineering Infrastructure. In accordance with the MICC project, work to modernize the morally and technically outdated engineering infrastructure of MLIT was performed. A complex of engineering systems was created, it comprises uninterruptible power supplies and two diesel generator units, representing a guaranteed power supply system that ensures the complete energy independence of the information and computing system, as well as of the network infrastructure, from the external power supply network. The modernized MICC climate control system is a complex of interconnected equipment with various air and liquid cooling schemes, with the help of which the required temperature conditions, ensuring the MICC functioning in 24×365 mode, are created [155].

JINR Grid Environment (Tier1 and Tier2 Sites). The JINR grid infrastructure is represented by the Tier1 centre for the CMS experiment at the LHC and the Tier2 centre for processing data of the NICA, LHC, BES, BIOMED, NOvA, ILC experiments, etc. Both JINR grid sites ensured 100% availability and reliability of the services.

The Tier1 processing system for CMS was expanded as planned from 3600 to 20096 cores, cur-

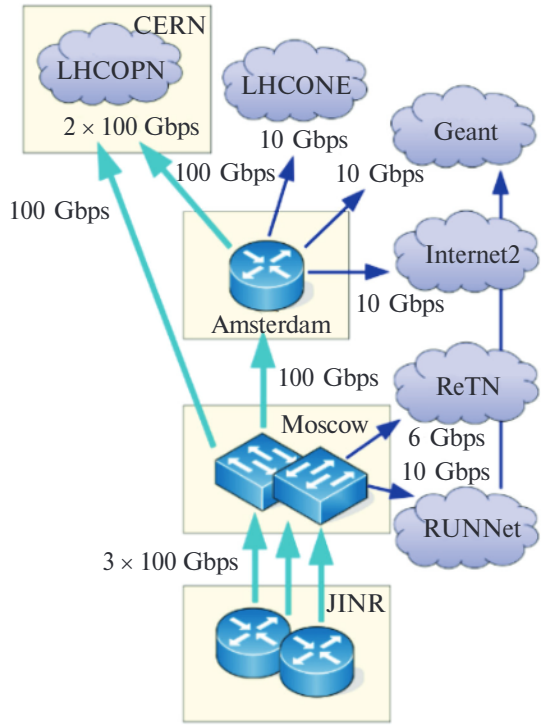

JINR network infrastructure

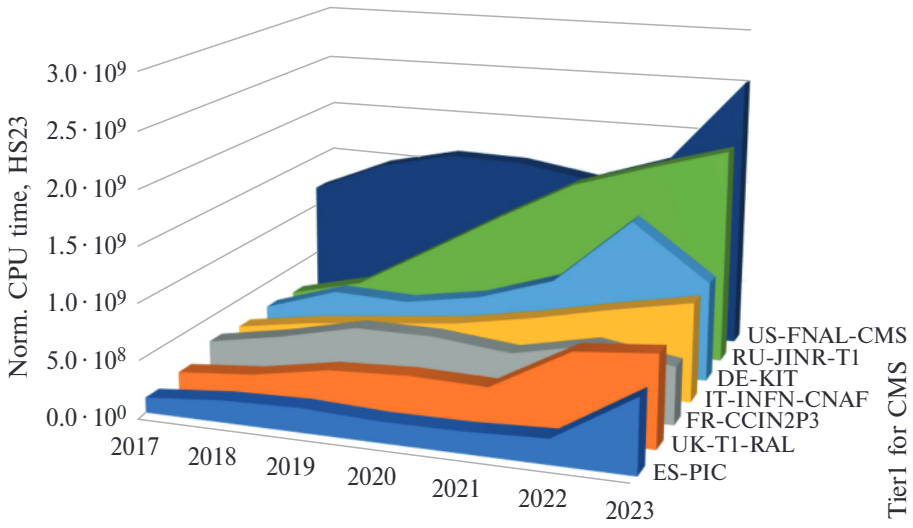

Contribution of the world Tier1 centres to CMS experimental data processing for 2017–2023: distribution by the normalized CPU time in HS23 hours

rently delivering the 32 382.54 HS06 performance. The storage system was enlarged. The total usable capacity of disk servers was increased from 4 to 15 PB and from 5.4 to 51 PB for the IBM TS3500 and IBM TS4500 tape libraries. In terms of performance, Tier1 occupies one of the leading places among the other Tier1 centres for the CMS experiment. Since 2021, the resources of the Tier1 centre are also used to model and process data of the NICA experiments.

The computing resources of the Tier2 centre were expanded as planned from 2470 to 10 364 cores, providing the 66 788.4 HS06 performance. The total usable capacity of disk servers is 5.6 PB. The JINR Tier2 website is the best in the Russian consortium RDIG (Russian Data Intensive Grid). From 2017 to 2023, the contribution of JINR Tier2 to RDIG's productivity enhanced from 42 to 90%.

The EOS distributed storage system (the so-called "data lake") was successfully integrated into the MICC structure and is employed for storing and accessing large amounts of information. There is 23.3 PB of storage space available for EOS users. The participants of the NICA experiments, of the neutrino programme and other users store data on EOS according to quotas [156].

Cloud Infrastructure. The resources of the cloud infrastructure were enlarged from 330 to 5152 CPU cores and from 840 GB to 61.5 TB of total RAM. The total amount of disk space in the ceph-based software-defined storage was increased to 4.3 PB. The expansion of cloud infrastructure resources was financed within the NOvA/DUNE, JUNO, Baikal-GVD experiments (DLNP), the scientific groups of which are the main users of the cloud infrastructure.

During the reporting period, work to integrate the cloud structures of the JINR Member States into the DIRAC-based distributed platform was actively performed.

The cloud infrastructures of the Institute of Nuclear Physics of Kazakhstan, the Research Institute for Nuclear Problems of Belarusian State University, Plekhanov Russian University of Economics, Khetagurov North Ossetian State University, the Institute for Nuclear Research and Nuclear Energy of the Bulgarian Academy of Sciences, the Institute of Nuclear Physics of the Academy of Sciences of Uzbekistan, the Institute of Physics of the National Academy of Sciences of Azerbaijan, the Egyptian Academy of Scientific Research and Technology, Sofia University "St. Kliment Ohridski" were integrated (at present, in the last three organizations, technical work is underway, job launch has been suspended). A technical solution to create a cloud infrastructure for the Georgian Technical University is being elaborated. During the coronavirus pandemic in 2020–2022, DICE resources free from their core activity were utilized to conduct research on the SARS-CoV-2 virus within the Folding@Home platform [157, 158].

Heterogeneous Infrastructure. The Govorun supercomputer was created in 2018 on top of the experience gained during the operation of the HybriLIT heterogeneous cluster, which is part of the JINR MICC. HybriLIT has shown its relevance in solving tasks of lattice QCD, radiation biology, applied research, etc. The continuous growth in the number

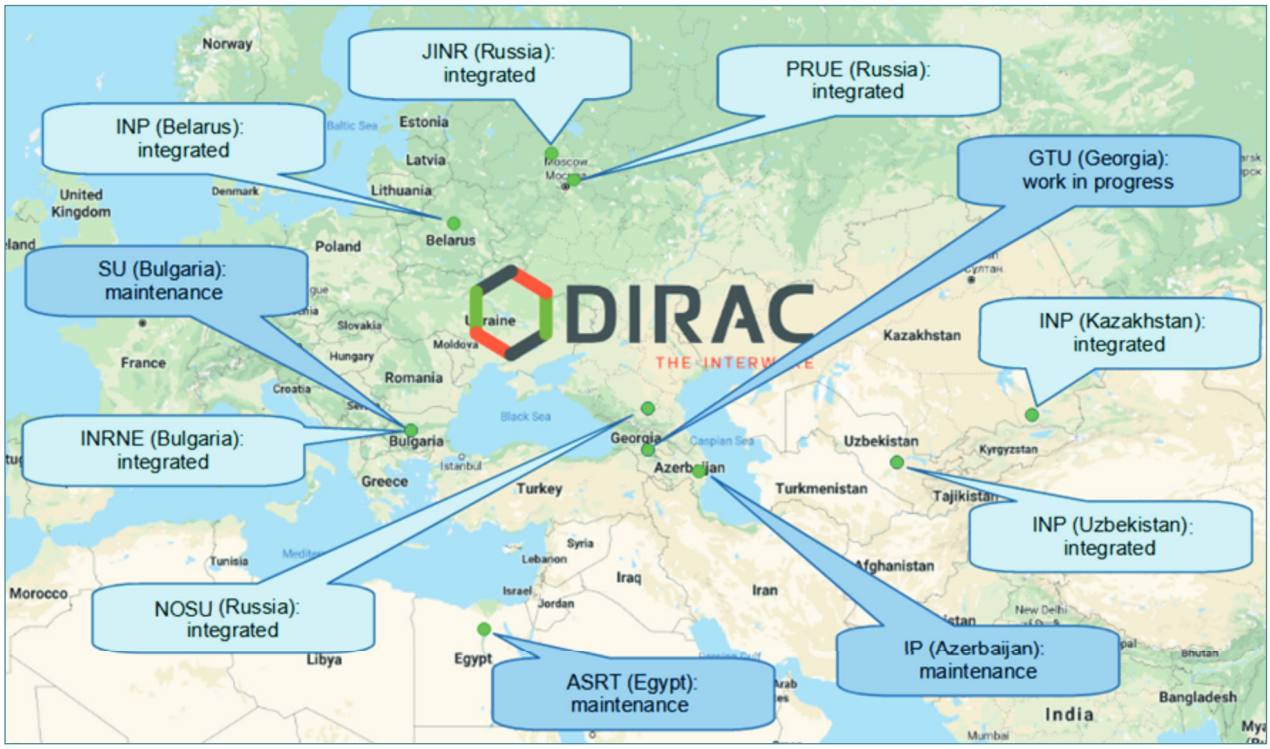

Clouds of organizations integrated into the JINR distributed information and computing environment (DICE)

of users and the expansion of the range of tasks to be solved entailed not only a significant enhancement in the computing capabilities of the cluster, but also the development and implementation of novel technologies, which resulted in the creation of a new computing system, the Govorun supercomputer. The Govorun supercomputer was built as a high-performance, scalable liquid-cooled system with a hyperconverged and software-defined architecture.

The Govorun supercomputer has unique properties in terms of the flexibility of customizing the user task, ensuring the most efficient use of the computing resources of the supercomputer. The Govorun supercomputer encompasses a GPU component, a CPU component and a hierarchical data process-

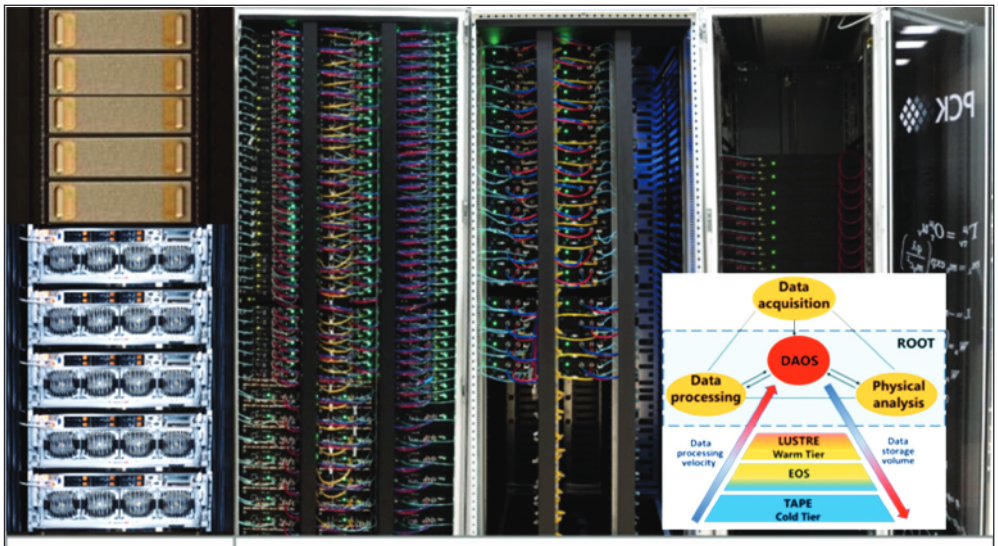

GPU accelerator	Hyperconverged CPU and distributed storage nodes

Govorun supercomputer

ing and storage system with a read/write speed of 300 Gb/s, which is an extremely convenient tool for processing large data arrays, including for the NICA megaproject. According to the speed of accessing data, the storage system is divided into layers, namely, very hot data, the most demanded data, to which it is currently required to provide the fastest access, hot data and warm data. Each layer of the developed system can be used both independently and as part of data processing workflows. For the high-speed data processing and storage system, the Govorun supercomputer received the prestigious Russian DC Awards 2020 in "the Best IT Solution for Data Centres" nomination.

Since its presentation, the overall performance of the Govorun supercomputer has enhanced from 0.5 to 1.7 PFlops for double precision operations, and the total capacity of the hierarchical storage has increased from 288 TB to 8.6 PB.

In 2020, the development and implementation of an ecosystem for machine/deep learning and high-performance computing (ML/DL/HPC ecosystem) in the HybriLIT platform were completed. The ecosystem is actively used to create algorithms on top of neural network approaches for solving applied tasks.

Since 2021, an information and computing system (ICS) to solve tasks related to the computations of electronic shells of superheavy elements has been intensively developed on the HybriLIT platform. The ICS embraces the computing resources of the Govorun supercomputer and a set of IT solutions and software required for modeling electronic shells. To calculate the electronic properties of superheavy elements, intensive computing using the AMS and DIRAC software was performed on this system. In addition, to develop quantum algorithms, a testing polygon for quantum computing with installed quantum computing simulators, namely, Cirq, Qiskit, PennyLane, capable of operating on various computing architectures, was deployed in the ICS.

At the end of 2021, a scalable research infrastructure of a new level was created on the basis of combining the supercomputers of JINR, JSCC RAS and SPbPU. It allows the participants to enlarge their local computing power, to provide access to the means for storing and processing large data volumes, to distributed data storages (data hubs), as well as to utilize each other's capacities in the case of peak loads. Such an infrastructure is also in demand for the tasks of the NICA megascience project.

The resources of the Govorun supercomputer are employed by scientific groups from all Laboratories of the Institute. The total number of Govorun supercomputer users is currently 312, of which 255 are JINR staff members, and 57 are from the Member States. Access to the resources of the Govorun su-

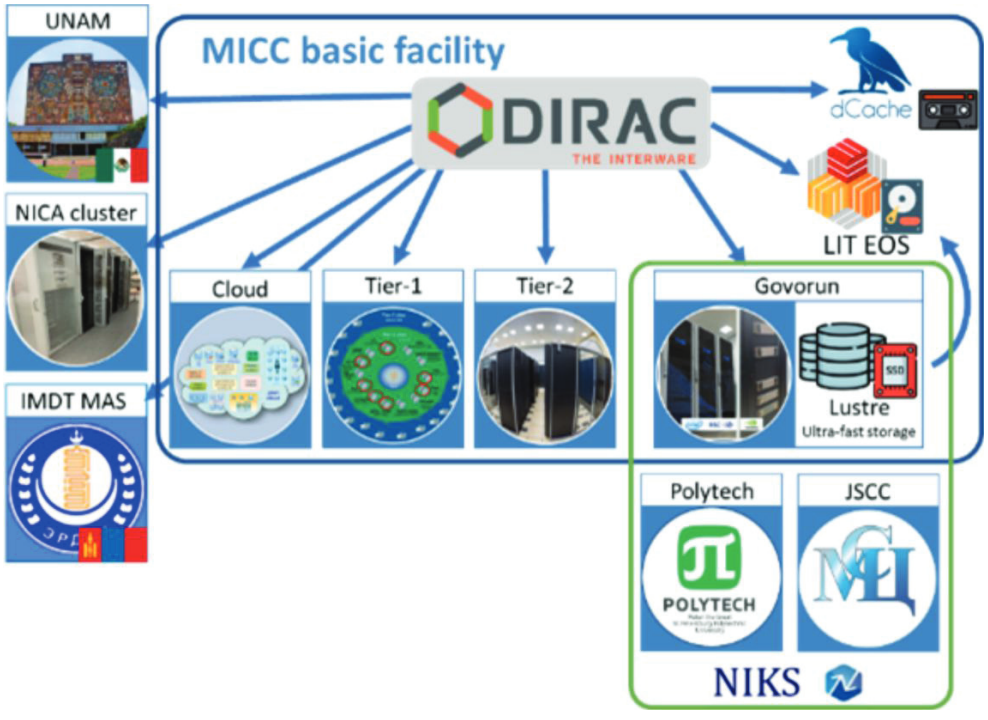

Scheme for the integration of geographically distributed heterogeneous resources based on the DIRAC Interware

percomputer is provided only to those users who are directly involved in the implementation of the JINR Topical Plan. The results obtained using the resources of the HybriLIT platform, including the Govorun supercomputer, the education and testing polygon and the ML/DL/HPC ecosystem [159–162], are reflected in over 300 user papers, two of them are in the Nature Physics journal.

Integration of Computing Resources. Within the implementation of the Seven-Year Plan, using the DIRAC (Distributed Infrastructure with Remote Agent Control) Interware, the computing resources of Tier1/Tier2, the Govorun supercomputer, the cloud environments of JINR and its Member States' organizations, the NICA cluster, the cluster of the National Autonomous University of Mexico (UNAM), the cluster of the Institute of Mathematics and Digital Technology of the Mongolian Academy of Sciences (IMDT MAS), the National Research Computer Network of Russia and storage resources, namely, dCache, EOS and the Lustre ultrafast data storage system, were combined.

The main users of the distributed platform are the scientific groups of the MPD, SPD, BM@N, Baikal-GVD experiments. The 8th BM@N physics run was the first time at JINR when the entire computing infrastructure, integrated by the DIRAC platform, was used for the complete reconstruction of raw experimental data [163, 164].

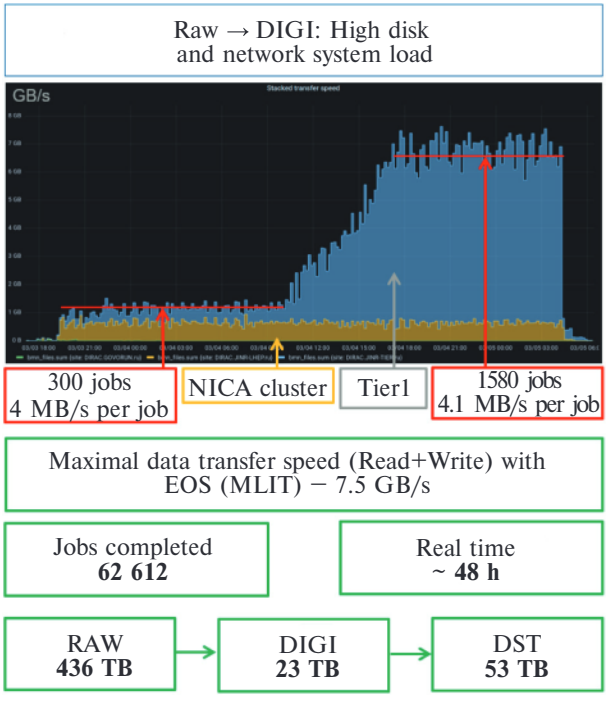

Data processing intensity within the 8th run of the BM@N experiment using DIRAC

Monitoring and Accounting System. To ensure the reliable functioning of the MICC, a multilevel monitoring and accounting system, which operates in 24×365 mode, was created and is expanding.

The system performs more than 16000 checks for over 1800 elements involved in the monitoring. The developed complex monitoring system of the MICC enables to receive information from different components of the computing complex: the engineering infrastructure, the network, compute nodes, job launch systems, data storage elements, grid services, which guarantees a high level of reliability of the MICC [165].

MICC monitoring system

JINR Digital EcoSystem. Since 2022, work to create the Digital JINR platform, i.e., the JINR Digital EcoSystem, has been underway. Its major objective is to provide a single environment for the creation and development of digital services, their integration with each other and the analysis of information on all aspects of JINR's activity. The Digital EcoSystem encompasses a wide range of services, from resources for users of basic facilities to arranging business trips, vouchers, ordering certificates, etc. The main groups of services are administrative (area of responsibility of the JINR Development of Digital Services Department) and scientific. Access to the system is based on the JINR Single Sign-On (SSO) authentication service via a single access point of the Digital EcoSystem [166].

Methods, Algorithms and Software for Modeling Physical Systems, Mathematical Processing and Analysis of Experimental Data. One of the important activities of MLIT within the implementation of the Seven-Year Plan was to provide mathematical, al-

Single access point interface of the Digital EcoSystem

gorithmic and software support for experimental and theoretical studies underway at JINR, in many of which computing resources are an essential tool for producing significant scientific results. A summary of some prominent results is presented below.

For the first time, it became possible to algorithmize the classical problem posed by the outstanding Norwegian mathematician Sophus Lie in 1883 and verify by point transformations the linearizability of nonlinear ordinary differential equations resolved with respect to the highest order derivative. The developed algorithm enables not only to determine whether a given equation is linearizable, but also to obtain a system of differential equations for the linearizing transformation, the solution of which gives an explicit form of such a transformation. At the International Symposium on Symbolic and Algebraic Computation (ISSAC 2017, Kaiserslautern, Germany, July 25–28, 2017), the work was recognized as the best presented and was awarded a prize from the American Association for Computing Machinery.

In April 2020, the scientific paper of an international research group, in which staff members of MLIT (O. Chuluunbaatar) and BLTP (Yu. Popov) participated within JINR international cooperation, was published in Nature Physics. A kinematically complete experimental measurement of the characteristics of Compton scattering at free atoms, using the highly efficient method of COLd Target Recoil Ion Momentum Spectroscopy (COLTRIMS), was conducted. A theoretical description of the phenomenon is based on the calculations carried out on the Govorun supercomputer.

The KANTBP 3.1 program for calculating the energy values, reflection and transmission matrices, and the corresponding wave functions in the adiabatic coupled-channel approach was developed and published in the CPC Program Library. The advantage of this program compared to the widely used CCFULL program for calculating the cross section for heavy-ion fusion and fission reactions is the careful processing of the boundary conditions for solving the system of coupled Schrödinger equations, which allows maintaining a high accuracy of calculations that take into account a large number of coupled channels. The theoretical cross sections obtained with the help of the KANTBP 3.1 program well describe experimental data for different heavy-ion fusion and fission reactions.

In the course of research conducted jointly with FLNP within the UNECE International Cooperative Program (ICP) Vegetation for monitoring and predicting air pollution processes in Europe and Asia, a cloud platform for managing monitoring data was developed at JINR. To ensure the reliable storage, analysis, processing and collective use of monitoring data, modern methods of software management, statistics and machine learning were applied, which also enabled to use satellite image data

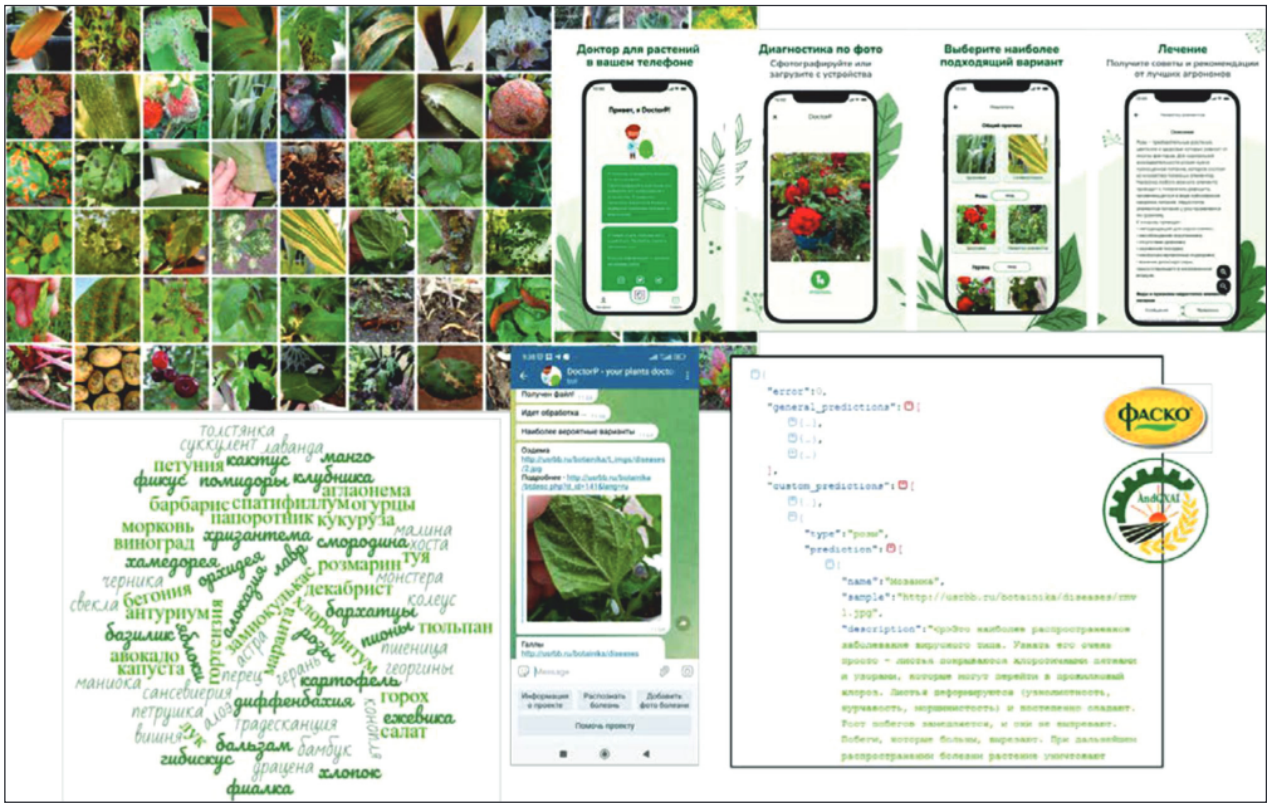

Examples of DoctorP platform interfaces

to predict atmospheric pollution by certain heavy metals in a number of European regions.

A platform and a mobile application (DoctorP) for detecting plant diseases and pests were elaborated. Both a general model capable of detecting 68 disease classes and specialized models for 30 ornamental and agricultural crops are available. The database contains over 6000 images. To obtain a prediction and treatment recommendations from experienced agronomists, one just needs to send a photo showing the problem. The platform can be accessed by third-party applications and services. Garden Retail Service (formerly Fasko) and the Andijan Institute of Agriculture and Agrotechnology (Uzbekistan) already took advantage of this opportunity.

A hardware and software platform was developed on top of quantum fuzzy controllers built into the control circuit to solve the task of controlling the pressure and flow of liquid nitrogen of superconducting magnets of the cryogenic system of the NICA accelerator complex. The multilevel control system embraces the existing lower executive level, based on the Tango Controls system, and a new level at which control actions are formed using a quantum fuzzy controller. At the same time, optimal control quality parameters, such as temperature, nitrogen consumption, speed, the required pressure level and minimal complexity of the control implementation, are provided. The operability and effectiveness of the developed intelligent system for the remote control of the technological process of cooling a superconducting magnet with a guaranteed achievement of a stable superconductivity zone were experimentally demonstrated. The design of quantum fuzzy controllers is based on quantum information technologies and is performed using the QSCIT (Quantum Soft Computational Intelligence Toolkit) software developed by MLIT specialists.

Since 2020, on the basis of the ML/DL/HPC ecosystem, a joint project between MLIT and LRB on the creation of an information system (IS) for analyzing behavioral and pathomorphological changes in the central nervous system when studying the effects of ionizing radiation and other factors on biological objects has been developing. Algorithms for experimental data processing on top of machine and deep learning methods and computer vision are implemented in the developed system. The IS embraces reliable modern tools of authentication and hierarchical data access control, a data storage system, as well as components for convenient work and the visualization of data analysis results.

Within the ML/DL/HPC ecosystem, using the example of solving a specific problem of investigating the magnetization dynamics in a Josephson ϕ^0 junction, a methodology for developing software

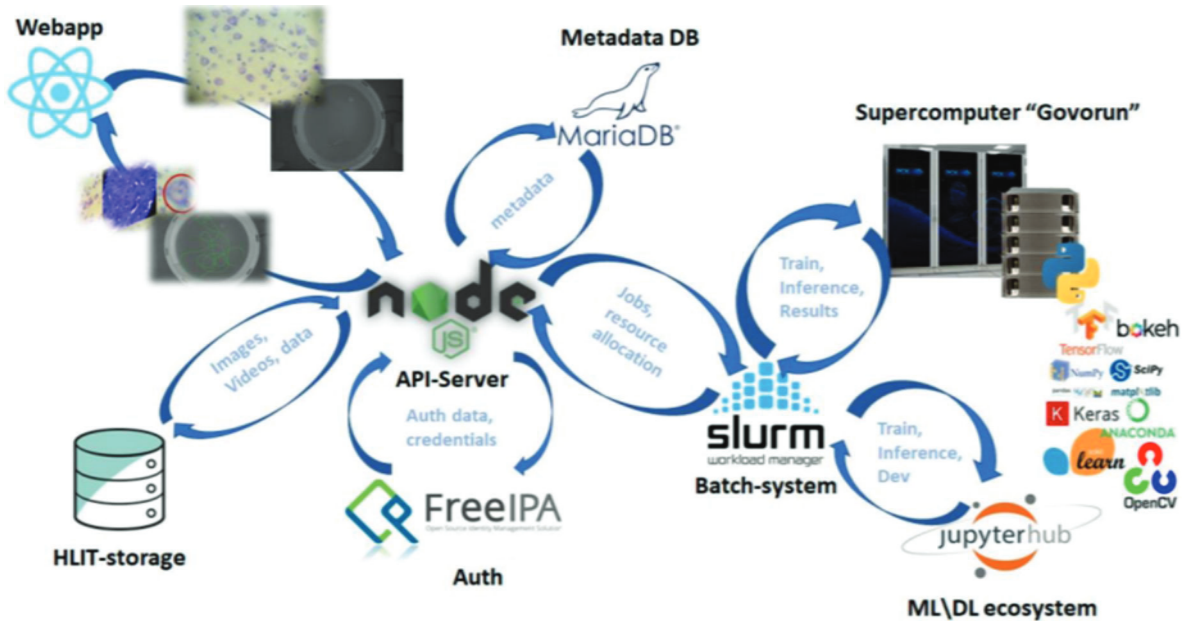

Architecture of the information system for radiation biology tasks

modules based on JupyterHub, which enable not only to perform computations, but also to visualize the results of the investigation and to accompany them with required formulas and explanations, was presented. A parallel implementation of the algorithm for carrying out computing for various values of model parameters on top of the Joblib Python library as well as modules with integration of Matlab code into Jupyter Notebook, which enable efficient applied computations for image analysis, were developed.

In 2017–2023, more than 1300 scientific papers within research conducted by MLIT staff members and over 700 articles within international collaborations were published, about 800 reports were delivered at international and Russian conferences. All studies conducted correspond to the expected results stated in the Plan [167–174].

The UC organizes an educational process for students from the basic departments of Moscow State University, MEPhI, MIPT, Dubna State University, St. Petersburg State University, and Kazan (Volga Region) Federal University (K(P)FU). Around 500 undergraduate and graduate students from universities of the JINR Member States annually complete internships and practical training at JINR.

JINR basic department was established at K(P)FU in 2017. Four graduates from the MSc study programme of the department were employed as research assistants at FLNP, VBLHEP and FLNR JINR. Two graduates, who completed their postgraduate studies in 2023, were hired at FLNP JINR as junior research assistants.

The UC organizes a delivery of candidate examinations for JINR employees attached to the MIPT Basic Department "Fundamental and Applied Problems of Microworld Physics". Since 2018, 44 people have passed PhD qualification exams at the department. During 2017–2023, 52 people were assigned to JINR to prepare dissertations for the scientific degree of Candidate of Sciences without mastering postgraduate training programmes.

INTEREST Online Programme. INTEREST (INTErnational REmote Student Training) is a year-round online programme launched in September 2020. It allows students to get acquainted with the main fields of research at the Institute, facilitates the search for a scientific supervisor for qualification work, as well as participation in onsite internships at JINR. The number of programme participants from 37 countries reached 331. During each wave of the

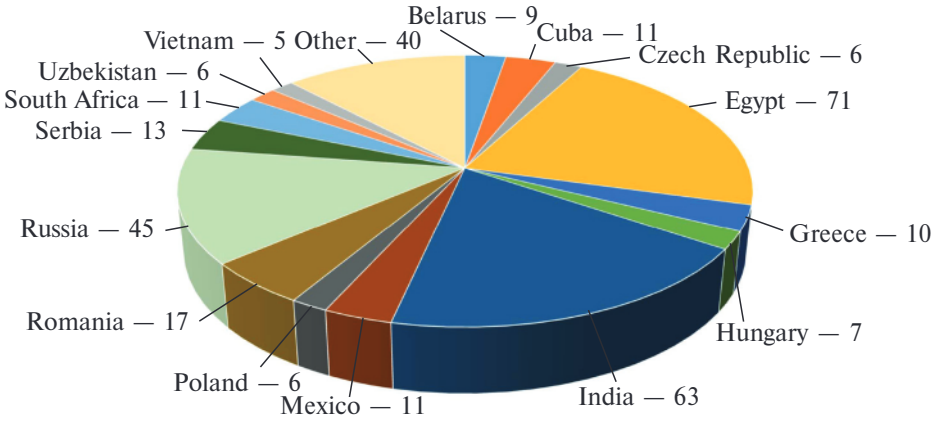

The number of participants of the INTEREST programme

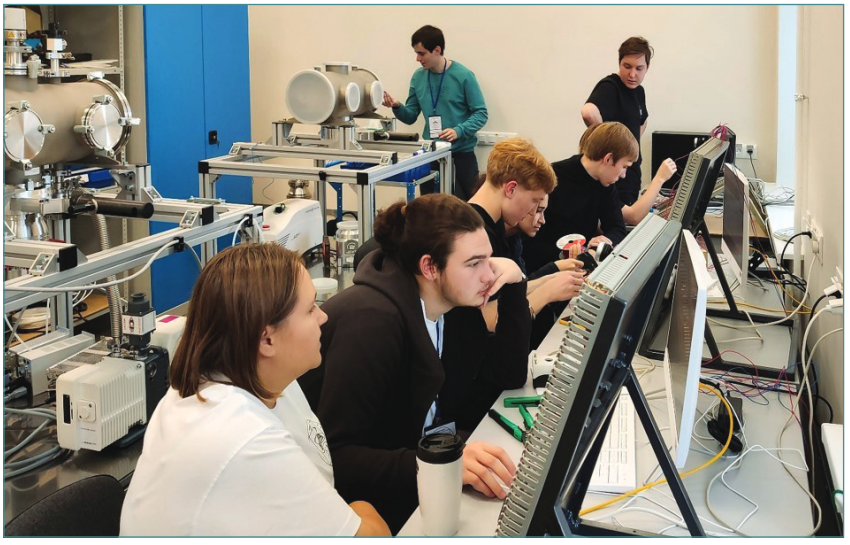

The Engineering Workshop on vacuum engineering and automation for UC students

programme, for 4–6 weeks the participants remotely work on the projects proposed by the Institute's experts. In addition to the implementation of the projects, lectures and online excursions are also offered to the participants, which helps them get to know the Institute's Laboratories better.

START Programme. In 2022, JINR Summer Student Programme was rebranded into the START programme — STudent Advanced Research Training. The online training programme runs all year round. Students from all over the world specializing in natural sciences, engineering and IT, completing the 3rd year of a Bachelor's and Master's degree programme, as well as 1st-year PhD students are allowed to participate in the programme. From 2017 to 2023, 296 people from 25 countries took part in the START programme. The programme also enables JINR experts to find young specialists who are invited to complete their full-time internship at the Institute for a period of 6–8 weeks.

International Student Practice. International Student Practice in the JINR fields of research means three-week full-time programmes launched in 2004. Since 2007, the practices have been organized as several stages a year. 508 students participated in the stages of the international student practices from 2017 to 2023. An eventful cultural and educational programme is prepared for the students, although mainly the time of each stage is spent on carrying out scientific projects under the supervision of JINR specialists.

Vocational Guidance Activities. Every year, together with the representatives of the Institute's Lab-

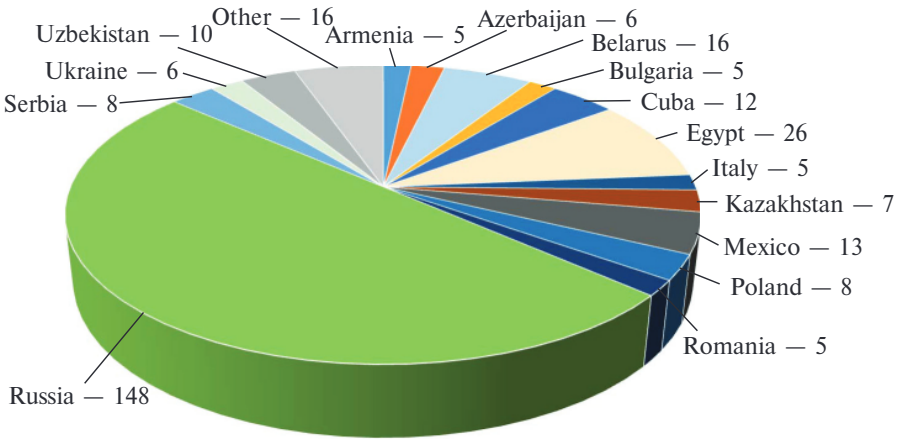

The number of participants of the START programme for 2017–2023

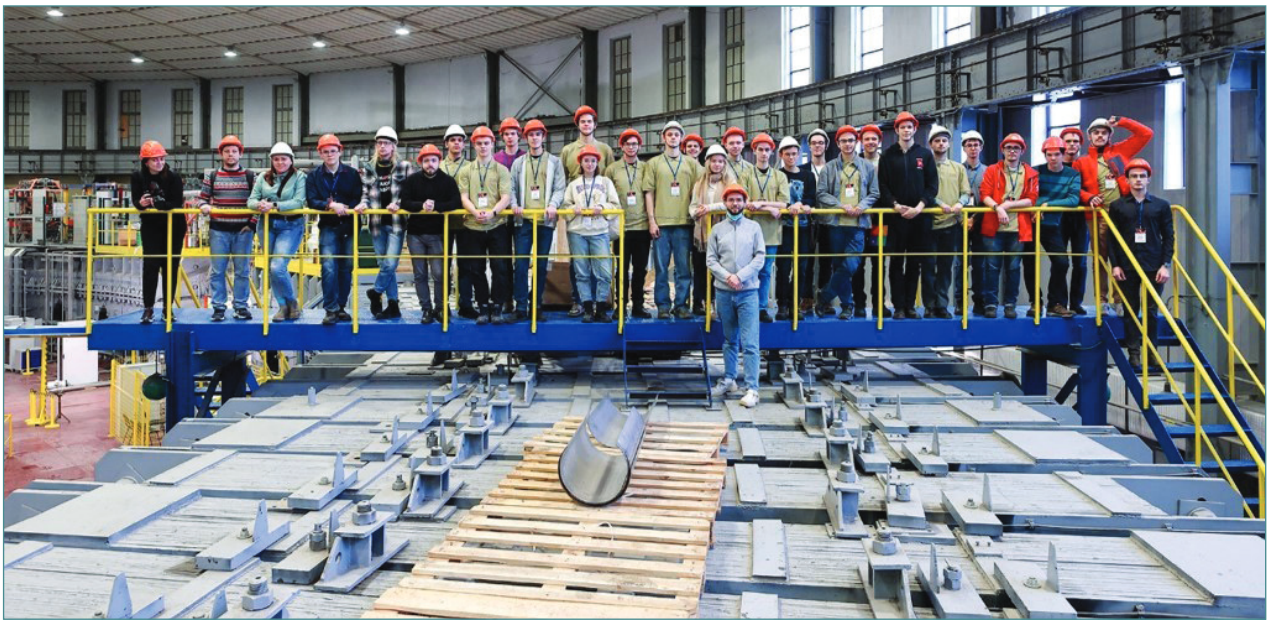

Participants of the START student programme on an excursion at VBLHEP JINR

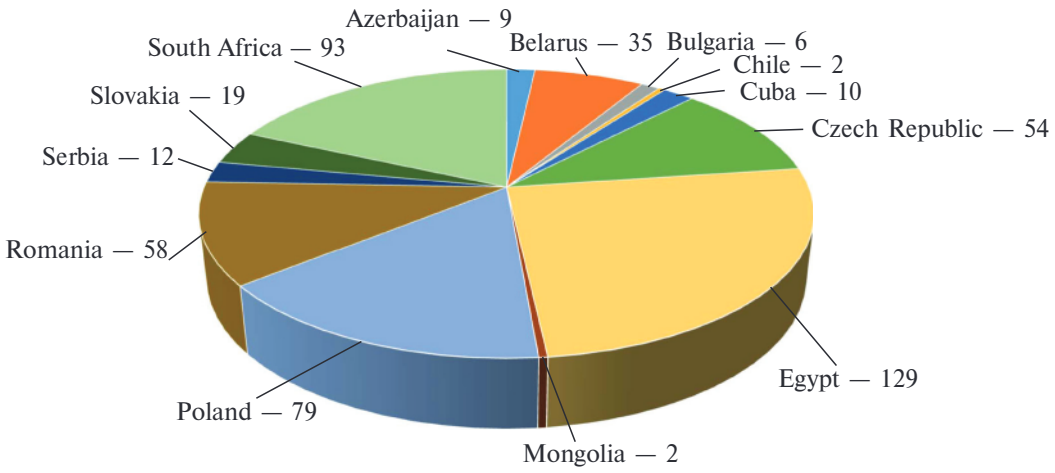

The number of participants of the International Student Practice in the period from 2017 to 2023

The second stage of the UC International Student Practice for young specialists from RSA

oratories, the University Centre organizes and participates in vocational guidance activities and events. They are aimed at applicants and students as potential future JINR employees to present the Institute's main fields of research. Online and onsite activities include Russian science festivals, organizing exhibitions, lectures, excursions, master classes and physical demonstrations at various events, as well as at the JINR Information Centres. Among them:

- All-Russian Science Festival "NAUKA 0+" in Moscow at the Expocentre Exhibition Centre and Moscow State University. Programmes presented by JINR consisted of lectures, master classes, demonstration of models of the Institute's main facilities and stands with information about research projects;
- "Geek Picnic" Festival of Science, Technology and Art in the Muzeon Art Park;
- "Technosreda" Festival on September 25–26, 2021;
- 19th World Festival of Youth and Students in Sochi, 2017;
- 2nd Congress of Young Scientists in Sochi, 2022;
- International Dark Matter Day, 2019;

JINR stand and a group of UC employees at the "NAUKA 0+" Festival in Moscow

- "Nanograd" Forum of School League Programme in Saint Petersburg, 2022;
- Physics Workshop "Element 105", Summer School;
- Day of JINR Basic Departments at Dubna State University;
- Career Days at MSU, MIPT, MEPhI, SPbU, and Dubna State University.

"JINR Main Facilities" Exposition. An interactive exposition "JINR Main Facilities" made by the staff members of the University Centre was devoted to celebrating the 65th anniversary of the foundation of JINR.

Interactive models' stands are the best way to be introduced to the main facilities of the Institute, such as a cyclotron, a collider with a particle detector, the IBR-2 pulsed reactor, the Baikal-GVD deep underwater neutrino telescope, etc.

Workshops for Students. JINR University Centre and the JINR Basic Department at MIPT "Fundamental and Applied Problems of Microworld Physics" organized schools on the physics of quark-glu-

Intensive Physics School for MIPT students, organized by UC JINR

on matter both in spring and autumn 2023. The schools were attended by 65 students of 1st–4th year studying elementary particle physics.

The summer scientific school "Physics and Technology of Accelerators" was organized by JINR in collaboration with Tomsk Polytechnic University in July 2023 for students of 3rd–4th year from technical universities of the JINR Member States majoring in engineering physics.

JINR Schools for Teachers. 200 teachers from 37 regions of the Russian Federation and seven JINR Member States took part in International Schools for Physics Teachers organized at JINR and CERN from 2017 to 2023.

Since 2017, three International Schools for Physics Teachers were held at CERN and seven Schools were organized at JINR (including two Schools for regions of the Russian Federation, namely, Primorye and Kamchatka). The Scientific Schools for Physics Teachers have been organized since 2009, such format is becoming increasingly popular.

The programmes of the Schools at JINR include introductory lectures and excursions to the Institute's Laboratories, workshops, visits to Dubna State University, the Library named after D. I. Blokhintsev, the Lyceum named after V. G. Kadyshevsky, as well as round-table discussions on school education issues and exchange of teaching experience.

Interaction with School Students. The UC organizes events for schoolchildren, teachers and the general public aimed at popularizing scientific knowledge and developing interest in natural and exact sciences, physics and mathematics. The UC annually holds the following events: "Days of Physics" Festival, CyberDubna Robotics Tournament, competitions in the design and programming of robots, Technical Hackathon, and the International Computer School.

Since 2021, there have been organized scientific schools for students of the Children's University under the Egyptian Academy of Scientific Research and Technology. Thirteen students participated in the most recent one, which took place in September 2023. They were selected out of almost 500 candidates. In total, 39 people became participants in the school over 2021–2023.

In 2022, more than 600 school students of 7–11 grades took part in the cycle "Lessons of Real Nuclear Physics", a joint project of the Educational Centre "Sirius" and JINR. Students were distributed in 90 science and technology studios of "Lessons of the Present" based on educational organizations in 41 regions of Russia.

Students participating in the UC Engineering Workshop on an excursion at FLNR JINR

Engineering Workshops. The scientific and engineering group was organized in 2016 as a subdivision of the UC to train students and engineering and technical specialists from the JINR Member States at operating and newly created modern physical facilities.

A key feature of the workshop is working with real equipment. So far there have been developed workshops on automation, vacuum technology, electronics, and microwave technology; a new workshop on Medipix was added in 2019. A workshop on dosimetry is in development.

Development and Creation of Educational Programmes. In 2023, the first stage of the project to create an open information and educational environment at JINR was completed. As part of this project, employees of the department of development of educational programmes at the UC prepared student training courses focused on JINR research fields, created information systems to support fun-

International Workshop "Open information and educational environment to support fundamental and applied interdisciplinary research at JINR"

damental research in the Laboratories. In addition, multimedia exhibitions, including the mobile ones, are organized. This allows sharing experiences with the Member and Partner States universities. The major project of the Institute, "Virtual Laboratory", is successfully developing. It introduces students and young scientists to real experimental equipment and the processing of real experimental data.

Visits. The UC organizes introductory programmes for schoolchildren, students and teachers. During the stage of planning the programmes for visits to the Institute's Laboratories, the level of training and learning profile of the guests are taken into account carefully.

Collaboration with Educational Organizations of Dubna. Physics and Mathematics Open Classroom

Egyptian schoolchildren at the Physics and Mathematics Lyceum named after Academician V. G. Kadyshevsky

based at school No. 9, UC Physics Workshop, and Yandex Lyceum based at school No. 6 are organized and run in Dubna with the support of JINR. Physics and Mathematics Open Classroom organizes classes in physics and mathematics for students of 6–8 grades, and classes in experimental physics — for 10th grade students. Physics and Mathematics Open Olympiads are held annually.

Teaching Manuals for School. UC specialists prepared a set of school textbooks for advanced study of physics in grades 7–9. The set includes a textbook, a book of problems, a workbook, as well as virtual workshops and methodological support. The textbooks were published by the Prosveshchenie Publishing House in 2023 and approved by the Commission of the Ministry of Education of the Russian Federation. Textbooks for high school students are currently in progress.

Further Professional and Qualification Training. To improve certification procedures for employees of organizations supervised by Rostekhnadzor, the Federal Service for Environmental, Technological and Nuclear Supervision created a Unified Testing Portal in the field of industrial safety, safety of hydraulic structures, and safety in the electric power industry. To compile with the new regulation, a specialized computer class was established at the University Centre in 2021 to test the personnel responsible for the proper condition and safe operation of equipment.

The UC successfully runs English language courses, as well as Russian language courses for foreign specialists. From 2017 to 2020, the UC also provided training in French and German. In 2020, upon request, a specific purpose English course was organized for the staff members of the Design Engineering Department of DLNP who are involved in the international collaborations between JINR and CERN. In 2021, English language courses were also organized for employees of various JINR departments.

REFERENCES

1. *Butenko A. et al.* NICA Accelerator Complex at JINR // Proc. of the 10th Intern. Part. Accel. Conf. (IPAC2019), Melbourne, Australia, 2019.
2. *Bazanov M. et al.* Light-Ion Linear Accelerator for the NICA Project // Phys. Part. Nucl. Lett. 2020. V. 17, No. 4. P. 481–487.
3. *Butenko A., Khodzhibagiyan H., Kostromin S., Meshkov I., Sidorin A., Syresin E., Trubnikov G., Tuzikov A.* The NICA Complex Injection Facility // Proc. of the 27th Russ. Part. Accel. Conf. (RuPAC2021), Alushta, 2021. JACoW Publ.
4. *Butenko A. et al.* First Experiments with Accelerated Ion Beams in the Booster of the NICA Accelerator Complex // Proc. of the 12th Intern. Part. Accel. Conf. (IPAC2021), Campinas, Brazil, May 24–28, 2021.
5. *Syresin E. et al.* NICA Ion Collider and Plans of Its First Operations // Proc. of the 13th Intern. Part. Accel. Conf. (IPAC2022), Bangkok, Thailand, June 12–17, 2022.
6. *Bryzgunov M. I., Bubley A. V., Lebedev V. A., Meshkov I. N., Osipov K. G., Parkhomchuk V. V., Prokofichev Yu. V., Reva V. B., Sergeev A. S., Semenov S. V., Timonin R. V., Shpakov V. S.* First Experiments on Electronic Cooling of Ions in the NICA Booster // Proc. of the XXVIII Russ. Part. Accel. Conf. (RuPAC2023), Novosibirsk, Russia, Sept. 11–15, 2023.
7. *Gulbekian G. G., Dmitriev S. N., Itkis M. G., Oganessian Yu. Ts., Gikal B. N., Kalagin I. V., Semin V. A., Bogomolov S. L., Buzmakov V. A., Ivanenko I. A., Kazarinov N. Yu., Osipov N. F., Pashchenko S. V., Sokolov V. A., Pchelkin N. N., Prokhorov S. V., Khabarov M. V., Gikal K. B.* Launch of the DC-280 Cyclotron — the Basic Installation of the FLNR JINR Superheavy Elements Factory // Phys. Part. Nucl. Lett. 2019. V. 50, No. 6. P. 653.
8. *Oganessian Yu. Ts. et al.* // Nucl. Instr. Meth. A. 2022. V. 1033. P. 166640.
9. *Yavor M. I., Gall N. R., Muradymov M. Z. et al.* // J. Instrum. 2022. V. 17. P. 11033.
10. *Oganessian Yu. Ts., Utyonkov V. K., Ibadullayev D. et al.* // Phys. Rev. C. 2022. V. 106. P. 024612.
11. *Oganessian Yu. Ts., Utyonkov V. K., Kovrizhnykh N. D. et al.* // Phys. Rev. C. 2022. V. 106. P. L031301.
12. *Oganessian Yu. Ts., Utyonkov V. K., Shumeiko M. V. et al.* // Phys. Rev. C. 2023. V. 108. P. 024611.
13. *Fomichev A. S. et al.* // Eur. Phys. J. A. 2018. V. 54. P. 97.
14. *Kaminski G. et al.* // Nucl. Instr. Meth. B. 2020. V. 463. P. 504.
15. *Bezbakh A. A. et al.* // Phys. Rev. Lett. 2020. V. 124. P. 022502.
16. *Kazakov D. I., Borlakov A. T., Tolkachev D. M., Vlasenko D. E.* // Phys. Rev. D. 2018. V. 97. P. 125008.
17. *Kazakov D. I.* // Phys. Lett. B. 2018. V. 786. P. 327.
18. *Bednyakov A., Pikelner A.* Four-Loop Gauge and Three-Loop Yukawa Beta Functions in a General Renormalizable Theory // Phys. Rev. Lett. 2021. V. 127, No. 4. P. 041801.
19. *Bednyakov A., Pikelner A.* Six-Loop Beta Functions in General Scalar Theory // J. High Energy Phys. 2021. V. 04. P. 233.
20. *Zhi-Da Bai, Korobov V. I., Zong-Chao Yan, Ting-Yun Shi, Zhen-Xiang Zhong* // Phys. Rev. Lett. 2022. V. 128. P. 183001.
21. *Kazakov D. I., Tolkachev D. M., Iakhibbaev R. M.* // J. High Energy Phys. 2023. V. 4. P. 128; J. Cosmol. Astropart. Phys. 2023. V. 9. P. 49.
22. *Astrakhantsev N., Braguta V., Kotov A.* Temperature Dependence of Shear Viscosity of $SU(3)$-Gluodynamics within Lattice Simulation // J. High Energy Phys. 2017. V. 04. P. 101.
23. *Astrakhantsev N. Yu., Braguta V. V., Kotov A. Yu.* Temperature Dependence of the Bulk Viscosity within Lattice Simulation of $SU(3)$-Gluodynamics // Phys. Rev. D. 2018. V. 98, No. 5. P. 054515.
24. *Astrakhantsev N., Braguta V. V., D'Elia M., Kotov A. Yu., Nikolaev A. A., Sanfilippo F.* Lattice Study of the Electromagnetic Conductivity of the Quark-Gluon Plasma in an External Magnetic Field // Phys. Rev. D. 2020. V. 102, No. 5. P. 054516.
25. *Bornyakov V. G., Braguta V. V., Ilgenfritz E.-M., Kotov A. Yu., Molochkov A. V.* Observation of Deconfinement in a Cold Dense Quark Medium // J. High Energy Phys. 2018. V. 03. P. 161.
26. *Astrakhantsev N. Yu., Bornyakov V. G., Braguta V. V., Ilgenfritz E.-M., Kotov A. Yu.* Lattice Study of Static Quark–Antiquark Interactions in Dense Quark Matter // J. High Energy Phys. 2019. V. 05. P. 171.
27. *Bornyakov V. G., Braguta V. V., Nikolaev A. A., Rogalyov R. N.* Effects of Dense Quark Matter on

Gluon Propagators in Lattice QC_2D // Phys. Rev. D. 2020. V. 102. P. 114511.

28. *Astrakhantsev N., Braguta V. V., Ilgenfritz E.-M., Kotov A. Yu., Nikolaev A. A.* Lattice Study of Thermodynamic Properties of Dense QC_2D // Phys. Rev. D. 2020. V. 102, No. 7. P. 074507.
29. *Braguta V. V., Kudrov I. E., Roenko A. A., Sychev D. A., Chernodub M. N.* Lattice Study of the Equation of State of a Rotating Gluon Plasma // JETP Lett. 2023. V. 117, No. 9. P. 639–644.
30. *Braguta V. V., Kotov A. Yu., Kuznedelev D. D., Roenko A. A.* Influence of Relativistic Rotation on the Confinement–Deconfinement Transition in Gluodynamics // Phys. Rev. D. 2021. V. 103, No. 9. P. 094515.
31. *Braguta V. V., Kotov A. Yu., Kuznedelev D. D., Roenko A. A.* Study of the Confinement/Deconfinement Phase Transition in Rotating Lattice *SU*(3)-Gluodynamics // Pisma Zh. Eksp. Teor. Fiz. 2020. V. 112, No. 1. P. 9–16; JETP Lett. 2020. V. 112, No. 1. P. 6–12.
32. *Ivanov Yu. B., Russkikh V. N., Toneev V. D.* // Phys. Rev. C. 2006. V. 73. P. 044904.
33. *Ivanov Yu. B., Soldatov A. A.* // Phys. Rev. C. 2018. V. 97. P. 024908.
34. *Ivanov Yu. B., Soldatov A. A.* // Phys. Rev. C. 2018. V. 98. P. 014906.
35. *Kozhevnikova M., Ivanov Yu. B.* // Phys. Rev. C. 2023. V. 107. P. 024903.
36. *Khvorostukhin A. S., Kolomeitsev E. E., Toneev V. D.* // Eur. Phys. J. A. 2021. V. 57. P. 294.
37. *Ivanov Yu. B., Soldatov A. A.* // Phys. Rev. C. 2018. V. 97. P. 044915.
38. *Ivanov Yu. B.* // Phys. Rev. C. 2021. V. 103. L031903.
39. *Tsegelnik N., Kolomeitsev E. E., Voronyuk V.* // Phys. Rev. C. 2023. V. 107. P. 034906.
40. *Tsegelnik N., Kolomeitsev E. E., Voronyuk V.* // Particles. 2023. V. 6. P. 373.
41. *Kolomeitsev E. E., Voskresensky D. N.* // Nucl. Phys. A. 2018. V. 973. P. 89–103.
42. *Kolomeitsev E. E., Voskresensky D. N., Borisov M. E.* // Eur. Phys. J. A. 2021. V. 57. P. 145.
43. *Voskresensky D. N.* // Prog. Part. Nucl. Phys. 2023. V. 130. P. 104030.
44. *Maslov K., Yasutake N., Ayriyan A., Blaschke D., Grigorian H., Maruyama T., Tatsumi T., Voskresensky D. N.* // Phys. Rev. C. 2019. V. 100. P. 025802.
45. *Röpke G., Voskresensky D. N., Kryukov I. A., Blaschke D.* // Nucl. Phys. A. 2018. V. 970. P. 224.
46. *Hong J., Adamian G. G., Antonenko N. V.* Ways to Produce New Superheavy Isotopes with $Z = 111–117$ in Charged Particle Evaporation Channels // Phys. Lett. B. 2017. V. 764. P. 42–48.
47. *Hong J., Adamian G. G., Antonenko N. V.* Possibilities of Production of Transfermium Nuclei in Complete Fusion Reactions with Radioactive Beams // Phys. Rev. C. 2017. V. 96. P. 014609.
48. *Dzhioev A. A., Langanke K., Martinez-Pinedo G., Vdovin A. I., Stoyanov Ch.* // Phys. Rev. C. 2020. V. 101. P. 025805.
49. *Severyukhin A. P., Arsenyev N. N., Pietralla N.* First Calculation of the $\gamma\gamma$-Decay Width of a Nuclear $2+1$ State: The Case of ^{48}Ca // Phys. Rev. C. 2021. V. 104. P. 024310.
50. *Shirikova N. Yu., Sushkov A. V., Malov L. A., Kolganova E. A., Jolos R. V.* // Phys. Rev. C. 2022. V. 105. P. 024309.
51. *Nasirov A. K., Kayumov B. M., Ganiev O. K., Yuldasheva G. A.* // Phys. Lett. B. 2023. V. 842. P. 137976.
52. *Ivantsov I., Ferraz A., Kochetov E.* Itinerant-Localized Model of Strongly Correlated Electrons: Fermi-Surface Reconstruction // Phys. Rev. B. 2017. V. 96. P. 195161.
53. *Nashaat M., Botha A. E., Shukrinov Yu. M.* // Phys. Rev. B. 2018. V. 97. P. 224514.
54. *Yamaletdinov R. D., Katkov V. L., Nikiforov Y. A., Okotrub A. V., Osipov V. A.* // Adv. Theory Simul. 2020. V. 3. P. 1900199.
55. *Hoang Ngoc Cam, Nguyen Thanh Phuc, Osipov V. A.* // npj 2D Mater. Appl. 2022. V. 6. P. 22.
56. *Astrakhantsev N. Yu., Braguta V. V., Katsnelson M. I., Nikolaev A. A., Ulybyshev M. V.* Quantum Monte Carlo Study of Electrostatic Potential in Graphene // Phys. Rev. B. 2018. V. 97, No. 3. P. 035102.
57. *Braguta V. V., Katsnelson M. I., Kotov A. Yu., Trunin A. M.* Catalysis of Dynamical Chiral Symmetry Breaking by Chiral Chemical Potential in Dirac Semimetals // Phys. Rev. B. 2019. V. 100, No. 8. P. 085117.
58. *Braguta V. V., Katsnelson M. I., Kotov A. Yu.* Lattice Field Theory Simulations of Dirac Semimetals // Ann. Phys. 2018. V. 391. P. 278–292.
59. *Boyda D. L., Braguta V. V., Katsnelson M. I., Kotov A. Yu.* Lattice Quantum Monte Carlo Study of Chiral Magnetic Effect in Dirac Semimetals // Ann. Phys. 2018. V. 396. P. 78–86.
60. *Obukhov Yu. N., Silenko A. J., Teryaev O. V.* General Treatment of Quantum and Classical Spinning Particles in External Fields // Phys. Rev. D. 2017. V. 96. P. 105005.
61. *Fedoruk S., Ivanov E., Lechtenfeld O., Sidorov S.* // J. High Energy Phys. 2018. V. 1804. P. 043; arXiv:1801.00206 [hep-th].

62. *Dorey P., Romanczukiewicz T., Shnir Ya.* // Phys. Lett. B. 2020. V. 806. P. 135497.
63. *Povolotsky A. M.* Exact Densities of Loops in $O(1)$ Dense Loop Model and of Clusters in Critical Percolation on a Cylinder // J. Phys. A: Math. Theor. 2021. V. 5422. P. LT01.
64. *Isaev A. P., Krivonos S. O.* Split Casimir Operator for Simple Lie Algebras, Solutions of Yang–Baxter Equations and Vogel Parameters // J. Math. Phys. 2021. V. 62, No. 8. P. 083503.
65. *Fursaev D. V., Pirozhenko I. G.* // Phys. Rev. D. 2023. V. 107. P. 025018; arXiv:2309.01272 [gr-qc]. 2023.
66. *Fursaev D. V., Davydov E. A., Pirozhenko I. G., Tainov V. A.* arXiv:2311.01863 [gr-qc]. 2023.
67. *Kapishin M. (for the BM@N Collab.).* Studies of Baryonic Matter at BM@N (JINR) // 27th Intern. Conf. on Ultrarelativistic Nucleus–Nucleus Collisions (Quark Matter 2018), Venezia, Italy, May 14–19, 2018.
68. *Pokatashkin G. et al.* Hyperons at the BM@N Experiment: First Results // 24th Intern. Baldin Seminar, Dubna, Sept. 17–22, 2018.
69. *Kapishin M. (for the BM@N Collab.).* First BM@N Results // Proc. of the 18th Intern. Conf. "Strangeness in Quark Matter" (SQM-2019), Bari, Italy, 2019.
70. *Patsyuk M. et al.* Unperturbed Inverse Kinematics Nucleon Knockout Measurements with a 48 GeV/c Carbon Beam // Nat. Phys. 2021. V. 17. P. 693.
71. *STAR Collab.* // Nature. 2017. V. 548. P. 62.
72. *Aghasyan M. et al.* Search for Muoproduction of X(3872) at COMPASS and Indication of a New State // Phys. Lett. B. 2018. V. 783. P. 334.
73. *Malinina L. (for the ALICE Collab.).* Femtoscopic Correlations of Identical Charged Particles in pp-Collisions at LHC Energies with Event-Shape Selection // 5th Intern. Conf. on Part. Phys. and Astrophys. (ICPPA-2020), Moscow, Oct. 7, 2020.
74. *Aaboud M. et al. (ATLAS Collab.).* Measurement of VH, $H \to b\bar{b}$ Production as a Function of the Vector-Boson Transverse Momentum in 13 TeV pp Collisions with the ATLAS Detector // J. High Energy Phys. 2019. V. 05. P. 141.
75. *Aaboud M. et al. (ATLAS Collab.).* Measurements of the Production Cross-Section for a Z Boson in Association with b-Jets in Proton–Proton Collisions at $\sqrt{s} = 13$ TeV with the ATLAS Detector // J. High Energy Phys. 2020. V. 07. P. 44.
76. *Aaboud M. et al. (ATLAS Collab.).* Measurements of WH and ZH Production in the $H \to b\bar{b}$ and Decay Channel in pp Collisions at 13 TeV with the ATLAS Detector // J. Instrum. 2021. V. 16. P. 07029.
77. *Eletskikh I. et al.* ATLAS Results on Exotic Hadronic Resonances // Proc. of the 11th Intern. Conf. on New Frontiers in Physics (ICNFP2022), OAC, Kolymbari, Crete, Greece, 30 Aug. – 11 Sept. 2022. ATLAS-CONF-2022-040.
78. *Karpov S., Karpova Z. et al.* Search for Quantum Black Hole Production in Lepton + Jet Final States Using Proton–Proton Collisions at $\sqrt{s} = 13$ TeV with the ATLAS Detector. arXiv:2307.14967 (submitted to Phys. Rev. D).
79. *Sirunyan A. M. et al. (CMS Collab.).* Search for Resonant and Nonresonant New Phenomena in High-Mass Dilepton Final States at 13 TeV // J. High Energy Phys. 2021. V. 7. P. 208.
80. *Zhizhin I. A., Lanyov A. V., Shmatov S. V.* Searches for New Physics in the Dilepton Channel with the CMS Detector at the Large Hadron Collider // Phys. At. Nucl. 2021. V. 84, No. 2. P. 184–189; Yad. Fiz. 2021. V. 84, No. 2. P. 143–148.
81. *Savina M. V., Seitova D.* Program of Searches with the CMS Detector for Signals from Multidimensional Low-Energy Gravity at the Large Hadron Collider // Phys. At. Nucl. 2021. V. 84, No. 2. P. 190–196; Yad. Fiz. 2021. V. 84, No. 2. P. 149–155.
82. *Tumasyan A. et al. (CMS Collab.).* Search for Heavy Resonances and Quantum Black Holes in $e\mu$, $e\tau$, and $\mu\tau$. Final States in Proton–Proton Collisions at 13 TeV // J. High Energy Phys. 2023. V. 5. P. 227.
83. *Marchevski R. (for the NA62 Collab.).* New Result on the Search for the $K^+ \to \pi^+\nu\nu$ Decay at the NA62 Experiment at CERN // 40th Intern. Conf. on High Energy Physics (ICHEP-2020), Prague, 28 July – 7 Aug. 2020.
84. *Gil E. C. et al. (NA62 Collab.).* A Study of the $K^+ \to \pi^0 e^+ \nu\gamma$ Decay // J. High Energy Phys. 2023. V. 9. P. 40.
85. *Andreev Yu. M. et al. (NA64 Collab.).* Search for a New B–L Z' Gauge Boson with the NA64 Experiment at CERN // Phys. Rev. Lett. 2022. V. 129, No. 16. P. 161801.
86. *Andreev Yu. M. et al. (NA64 Collab.).* Search for Light Dark Matter with NA64 at CERN // Phys. Rev. Lett. 2023. V. 131. P. 161801.
87. *Ablikim M. et al. (BESIII Collab.).* Tests of CP Symmetry in Entangled Ξ^0–Ξ^0 Pairs // Phys. Rev. D. 2023. V. 108. P. L031106.
88. *Allakhverdyan V. A. et al.* Neutrino Telescope in Lake Baikal: Present and Nearest Future // PoS ICRC2021. 2021. 002; doi: 10.22323/1.395.0002.
89. *Avrorin A. V. et al.* Deep-Underwater Cherenkov Detector in Lake Baikal // J. Exp. Theor. Phys. 2022. V. 161, No. 4. P. 476–496 (in Russian).

90. *Allakhverdyan V.A. et al. (Baikal-GVD Collab.)*. Diffuse Neutrino Flux Measurements with the Baikal-GVD Neutrino Telescope // Phys. Rev. D. 2023. V.107, No. 4. P.042005; e-Print:2211.09447 [astro-ph.HE].
91. *Allakhverdyan V.A. et al. (Baikal-GVD Collab.)*. Search for Directional Associations between Baikal Gigaton Volume Detector Neutrino-Induced Cascades and High-Energy Astrophysical Sources // Mon. Not. Roy. Astron. Soc. 2023. V.526, No.1. P.942–951; e-Print:2307.07327.
92. *Lubashevskiy A.* Search for the Coherent Elastic Neutrino-Nucleus Scattering and Other Rare Processes in νGeN Experiment at Kalinin Nuclear Power Plant // 29th Intern. Workshops on Weak Interactions and Neutrinos (WIN 2023), Zhuhai, China, June 3–8, 2023.
93. *Lubashevskiy A.V.* Results of the νGeN Experiment on the Search for Coherent Scattering of Reactor Antineutrinos and Other Rare Processes // 73rd Intern. Conf. on Nucl. Phys. "Nucleus-2023: Fundamental Problems and Applications", Sarov, Russia, Oct. 9–13, 2023.
94. *DANSS Collab*. Search for Sterile Neutrinos at the DANSS Experiment // Phys. Lett. B. 2018. V.787. P.56–63.
95. *Skrobova N.* Measurements of the Absolute Reactor Antineutrino Energy Spectrum Dependence on the Fuel Composition // Phys. At. Nucl. 2023. V.86. P.544–550.
96. *Sveshnikova L.G. et al.* Status of the TAIGA Experiment: Gamma Astronomy // Phys. At. Nucl. 2023. V.86, No.9. P.1–7; doi: 10.1134/S1063778823090247.
97. *Abusleme A. et al. (JUNO Collab.)*. The JUNO Experiment Top Tracker // Nucl. Instr. Meth. A. 2023. V.1057. P.168680.
98. *Acero M.A. et al. (NOvA Collab.)*. Adjusting Neutrino Interaction Models and Evaluating Uncertainties Using NOvA Near Detector Data // Phys. Rev. Lett. 2019. V.123, No.15. P.151803.
99. *Acero M.A. et al. (NOvA Collab.)*. Improved Measurement of Neutrino Oscillation Parameters by the NOvA Experiment // Phys. Rev. D. 2022. V.106, No.3. P.032004.
100. *Agostini M. et al. (Borexino Collab.)*. Seasonal Modulation of the ^{7}Be Solar Neutrino Rate in Borexino // Astropart. Phys. 2017. V.92. P.21.
101. *Agostini M. et al. (Borexino Collab.)*. Limiting Neutrino Magnetic Moments with Borexino Phase-II Solar Neutrino Data // Phys. Rev. D. 2017. V.96. P.091103(R).
102. *Borexino Collab*. Comprehensive Measurement of *pp*-Chain Solar Neutrinos // Nature. 2018. V.562. P.505–510.
103. *Grozdanov D.N. et al.* // Phys. At. Nucl. 2020. V.83, No.3. P.384–390.
104. *Berikov D. et al.* // Phys. Rev. C. 2021. V.104, No. 2. P.024607; doi: 10.1103/PhysRevC.104.024607.
105. *Jiang Haoyu et al.* // Chin. Phys. C. 2020. V.44, No.11.
106. *Zakharov M.A., Kulin G.V., Frank A.I.* // Eur. Phys. J. D. 2021. V.75. P.47.
107. *Chernyavsky S. et al.* // Rev. Sci. Instrum. 2022. V.93. P.123302; doi: 10.1063/5.0124833.
108. *Bosak A. et al.* // Materials. 2023. V.16. P.703; doi: 10.3390/ma16020703.
109. *Bulavin M.V. et al.* // J. Surf. Invest.: X-ray, Synchrotron Neutron Techn. 2022. V.16, No.1. P.1–6; doi: 10.1134/S1027451022010037.
110. *Cong J. et al.* // Nat. Commun. 2018. V.9. P.2996.
111. *Kozlenko D.P. et al.* // Phys. Rev. B. 2022. V.105. P.094430.
112. *Kozlenko D.P. et al.* // npj Quantum Mater. 2021. V.6. P.19.
113. *Kichanov S.E. et al.* // JINR News. 2017. No.1. P.20–23.
114. *Kichanov S.E. et al.* // Springer Nat. Appl. Sci. 2019. V.1. P.1563.
115. *Bandarenka H. et al.* // ChemNanoMat. 2020. V.7, No. 2. P.141–149; doi: 10.1002/cnma.202000521.
116. *Arzumanyan G. et al.* // J. Raman Spectrosc. 2020. V.1. P.10; doi.org/10.1002/jrs.5844.
117. *Arzumanyan G. et al.* // Int. J. Mol. Sci. 2023. V.24; doi.org/10.3390/ijms24065770.
118. *Ivankov O.I. et al.* // Sci. Rep. 2021. V.11. P.21990:1–9.
119. *Kurakin S.A. et al.* // BBA — Biomembranes. 2024. V.1866. P.184237:1–11.
120. *Dobrin I. et al.* // IEEE Trans. Appl. Supercond. 2016. V.26, No.3. P.1–4; doi: 10.1109/tasc.2016.2520086.
121. *Belushkin A.V. et al.* // Instrum. Exp. Tech. 2022. V.65, No.4. P.539–550; doi: 10.1134/S0020441222050025.
122. *Jezkova L. et al.* // Nanoscale. 2018. V.10. P.1162.
123. *Hausmann M. et al.* // Front. Phys. 2020. V.8. P.578662.
124. A Method for Increasing the DNA Double-Strand Break Formation Frequency in Human Cells after Ionizing Radiation Exposure in the Presence of Radiomodifiers / Krasavin E.A., Boreyko A.V., Kulikova E.A., Bulanova T.S., Timoshenko G.N., Chausov V.N. Patent RU 2699670, Russia's Federal Service for Intellectual Property (Rospatent). Publ. 09.09.2019. Bull. No.25 (in Russian).

125. *Chausov V.N. et al.* // Phys. Part. Nucl. Lett. 2018. V.15, No.6. P.700–710.

126. A Method for Increasing the Effectiveness of Ionizing Radiation on Melanoma / Zamulaeva I.A., Boreyko A.V., Bugay A.N., Kaprin A.D., Koryakin S.N., Krasavin E.A., Matchuk O.N., Mosina V.A., Selivanova E.I., Chausov V.N. Patent RU 2774032, Russia's Federal Service for Intellectual Property (Rospatent). Publ. 14.06.2022. Bull. No.17 (in Russian).

127. A Method for Increasing the Effectiveness of Proton Therapy on Melanoma Stem Cells / Matchuk O.N., Boreyko A.V., Bugay A.N., Zamulaeva I.A., Kaprin A.D., Koryakin S.N., Krasavin E.A., Mosina V.A., Selivanova E.I., Solovyov A.N., Chausov V.N., Yakimova A.O. Patent RU 2798733, Russia's Federal Service for Intellectual Property (Rospatent). Publ. 23.06.2023. Bull. No.18 (in Russian).

128. *Boreyko A.V. et al.* Combined Action of DNA Synthesis Inhibitors and Accelerated Protons on Malignant Tumor Cells // Part. Nucl., Lett. 2023. V.20, No.4. P.698–708 (in Russian).

129. *Zamulaeva I.A. et al.* Radiobiological Effects of the Combined Action of 1-β-D-Arabinofuranosylcytosine and Proton Radiation on B16 Melanoma *In Vivo* // Phys. Part. Nucl. Lett. 2023. V.20, No.1. P.63–75.

130. *Kowalska A., Nasonova E., Kutsalo P., Czerski K.* Chromosomal Radiosensitivity of Human Breast Carcinoma Cells and Blood Lymphocytes Following Photon and Proton Exposures // Radiat. Environ. Biophys. 2023. V.62. P.151–160.

131. *Bláha P. et al.* // Mutat. Res. 2017. V.803–805. P.35–41.

132. *Bláha P. et al.* // Front. Phys. 2021. V.8. P.584326.

133. *Severyukhin Yu.S. et al.* Comparative Analysis of Behavioral Reactions and Morphological Changes in the Rat Brain after Exposure to Ionizing Radiation with Different Physical Characteristics // Cell. Mol. Neurobiol. 2022. V.43. P.339–353.

134. *Kolesnikova I.A. et al.* The Effects of Whole Body Gamma Irradiation on Mice, Age-Related Behavioral, and Pathophysiological Changes // Cell. Mol. Neurobiol. 2023. V.43, No. 7. P.3723–3741.

135. *Batmunkh M. et al.* Optimized Neuron Models for Estimation of Charged Particle Energy Deposition in Hippocampus // Phys. Med. 2019. V.57. P.88–94.

136. *Bayarchimeg L. et al.* Evaluation of Radiation-Induced Effects in Membrane Ion Channels and Receptors // Phys. Part. Nucl. Lett. 2019. V.16. P.54–62.

137. *Batova A.S. et al.* Effect of Mutant NMDA Receptors on the Oscillations in a Model of Hippocampus // J. Bioinform. Comput. Biol. 2019. V.17, No.1. P.1940003.

138. *Gordeev I.S., Timoshenko G.N.* A New Type of Ground-Based Simulator of Radiation Field inside a Spacecraft in Deep Space // Life Sci. Space Res. 2021. V.30. P.66–71.

139. A Device for Modeling Mixed Radiation Fields at High-Energy Heavy Ion Beams for Experimental Radiobiological Research / Timoshenko G.N., Gordeev I.S. Patent RU 2761376, Russia's Federal Service for Intellectual Property (Rospatent). Publ. 07.12.2021. Bull. No. 34 (in Russian).

140. *Gordeev I.S.* State Certificate of Computer Program Registration No.2023667527, Russia's Federal Service for Intellectual Property (Rospatent). Appl. 07.08.2023. Publ. 15.08.2023. Appl. No.2023666479 (in Russian).

141. *Timoshenko G.N., Belvedersky M.I.* Fluence-to-Effective Dose Conversion Coefficients for Male Astronauts // J. Radiol. Prot. 2019. V.39, No.2. P.511–521.

142. *Timoshenko G.N., Gordeev I.S.* Simulation of Radiation Field inside Interplanetary Spacecraft // J. Astrophys. Astron. 2020. V.41. P. 5.

143. *Timoshenko G.N.* Radiation Protection of High-Energy Accelerators. Dubna: JINR, 2022. 111 p. (in Russian).

144. *Saladino R. et al.* Meteorite Assisted Phosphorylation of Adenosine under Proton Irradiation Conditions // Chem. Eur. J. 2019. V.25. P.3181–3189; doi/full/10.1002/syst.201900039.

145. *Bizzarri B.M. et al.* High-Energy Proton-Beam-Induced Polymerization/Oxygenation of Hydroxynaphthalenes on Meteorites and Nitrogen Transfer from Urea: Modeling Insoluble Organic Matter? // Chem. Eur. J. 2020. V.26. P.14919–14928.

146. *Bizzarri B.M. et al.* Meteorite-Catalyzed Intermolecular Trans-Glycosylation Produces Nucleosides under Proton Beam Irradiation // RSC Adv. 2021. V.11, No.31. P.19258–19264.

147. *Rozanov A.Yu. et al.* The Orgueil Meteorite (an Atlas of Microfossils) / Ed. A.Yu.Rozanov. Moscow: RAS Paleontol. Inst., 2020. 130 p.

148. *Budagov Yu.A., Glagolev V.V., Lyablin M.V. et al.* Positionally Sensitive Spot Registration of a Single-Mode Laser Beam Using the Method of Dividing Plates // Phys. Part. Nucl. Lett. 2022. V.19, No.6. P.585–615 (in Russian).

149. *Zarubin M. et al.* First Transcriptome Profiling of *D.Melanogaster* after Development in a Deep Underground Low Radiation Background Laboratory. https://journals.plos.org/plosone/article/authors?id=10.1371/journal.pone.0255066.

150. *Frontasyeva M. et al.* Mosses as Biomonitors of Air Pollution: 2015/2016 Survey on Heavy Metals, Nitrogen and POPs in Europe and Beyond. Dubna: JINR, 2020. 136 p.

151. *Badawy W.M., Dmitriev A.Y., El Samman H., El-Taher A., Blokhin M.G., Rammah Y.S., Madkour H.A., Salama S., Budnitskiy S.Y.* Elemental Composition and Metal Pollution in Egyptian Red Sea Mangrove Sediments: Characterization and Origin // Mar. Pollut. Bull. 2024. V.198. P.115830; https://doi.org/10.1016/j.marpolbul.2023.115830.

152. *Badawy W., Elsenbawy A., Dmitriev A., El Samman H., Shcheglov A., El-Gamal A., Kamel N.H.M., Mekewi M.* Characterization of Major and Trace Elements in Coastal Sediments along the Egyptian Mediterranean Sea // Mar. Pollut. Bull. 2022. V.177. P.113526; https://doi.org/10.1016/j.marpolbul.2022.113526.

153. https://micc.jinr.ru/ — Multifunctional Information and Computing Complex.

154. *Baginyan A. et al.* Current Status of the MICC: An Overview // CEUR Workshop Proc. 2021. V.3041. P.1–6.

155. *Baginyan A. et al.* JINR Network Infrastructure for Megascience Projects // 2020 Intern. Sci. and Techn. Conf. Modern Computer Network Technologies (MoNeTeC), Moscow, Russia, 2020. P.1–5; doi: 10.1109/MoNeTeC49726.2020.9258004.

156. *Baginyan A. et al.* JINR Grid Infrastructure: Status and Plans // Proc. of the 10th Intern. Conf. "Distributed Computing and Grid Technologies in Science and Education" (GRID'2023), Dubna, Russia, July 3–7, 2023. Phys. Part. Nucl. (submitted).

157. *Balashov N. et al.* Changes and Challenges at the JINR and Its Member States Cloud Infrastructures // Proc. of the 10th Intern. Conf. "Distributed Computing and Grid Technologies in Science and Education" (GRID'2023), Dubna, Russia, July 3–7, 2023. Phys. Part. Nucl. (submitted).

158. https://dice.jinr.ru/ — DICE: Distributed Information and Computing Environment.

159. http://hlit.jinr.ru/ — HybriLIT Heterogeneous Platform.

160. *Belyakov D. et al.* "Govorun" Supercomputer for JINR Tasks // CEUR Workshop Proc. 2020. V.2772. P.1–12.

161. *Podgainy D.V. et al.* IT Solutions for JINR Tasks on the "Govorun" Supercomputer // CEUR Workshop Proc. 2021. V.3041. P.612–618.

162. *Butenko Yu. et al.* ML/DL/HPC Ecosystem of the HybriLIT Heterogeneous Platform (MLIT JINR): New Opportunities for Applied Research // PoS DLCP2022. 2022. P.027.

163. *Korenkov V., Pelevanyuk I., Tsaregorodtsev A.* Integration of the JINR Hybrid Computing Resources with the DIRAC Interware for Data Intensive Applications // Commun. Comp. Inform. Sci. 2020. V.1223. P.31–46; doi:10.1007/978-3-030-51913-1_3.

164. *Gertsenberger K., Pelevanyuk I.* BM@N Run 8 Data Production on a Distributed Infrastructure with DIRAC // Proc. of the XXVII Intern. Sci. Conf. of Young Scientists and Specialists (AYSS-2023), Dubna, Russia, 30 Oct.–3 Nov. 2023. Phys. Part. Nucl. Lett. 2024. V.21, No.4.

165. *Kashunin I.A., Mitsyn V.V., Strizh T.A.* Operating Principles of the Accounting System for JINR's Grid Sites // Phys. Part. Nucl. Lett. 2022. V.19, No.6(245). P.660–668 (in Russian).

166. https://digital.jinr.ru — JINR Digital EcoSystem.

167. *Lyakhov D.A., Gerdt V.P., Michels D.L.* Algorithmic Verification of Linearizability for Ordinary Differential Equations // Proc. of Intern. Symp. on Symbolic and Algebraic Computation (ISSAC 2017). ACM Press. 2017. P.285–292.

168. *Kircher M. et al.* Kinematically Complete Experimental Study of Compton Scattering at Helium Atoms near the Threshold // Nat. Phys. 2020. V.16. P.756–760.

169. *Chuluunbaatar O. et al.* KANTBP 3.1: A Program for Computing Energy Levels, Reflection and Transmission Matrices, and Corresponding Wave Functions in the Coupled-Channel and Adiabatic Approaches // Comput. Phys. Commun. 2022. V.278. P.108397:1–14.

170. *Uzhinskiy A.* Intelligent Environmental Monitoring Platform // Open Systems. DBMS. 2021. No.2. P.21–23 (in Russian).

171. *Uzhinskiy A.* Advanced Technologies and Artificial Intelligence in Agriculture // Appl. Math. 2023. V.3, No.4. P.799–813.

172. *Butenko A.V. et al.* Intelligent System for Remote Control of Liquid Nitrogen Pressure and Flow in the Cryogenic System of Superconducting Magnets: Hardware and Software Platform // Phys. Part. Nucl. Lett. 2023. V.20, No.2(247). P.183–199 (in Russian).

173. *Kolesnikova I.A. et al.* Information System for Radiobiological Studies // CEUR Workshop Proc. 2020. V.2743. P.1–6.

174. *Rahmonov I.R., Rahmonova A.R., Streltsova O.I., Zuev M.I.* Python Toolkit for the Simulation of the Josephson Junction Dynamics under the Influence of External Radiation. http://studhub.jinr.ru:8080/jjbook.

Selected Scientific Results Obtained in 2017–2023 at the Joint Institute for Nuclear Research [Elec-
S43 tronic edition]. — Dubna: JINR, 2024. — 71 p.

ISBN 978-5-9530-0623-1

Responsible for the preparation of the Report:
S. Nedelko
B. Starchenko
Yu. Shimanskaya

The Report was prepared by
A. Andreev
A. Cheplakov
D. Chudoba
O. Derenovskaya
E. Fedorova
A. Karpov
I. Koshlan
I. Simonenko

Translation by
E. Asanova
T. Avdeeva
I. Kronshtadtova
S. Negovelov
E. Pashka
M. Potapov
G. Sandukovskaya
S. Savinykh
A. Udovichenko
E. Voytishina

Photos by
I. Lapenko
E. Puzynina

Edited by
V. V. Bulatova, E. I. Kravchenko
Design by *I. G. Andreeva, V. A. Zhbankova*

Publishing Department
Joint Institute for Nuclear Research
Dubna, Moscow Region

Contents